Contents

Preface

These notes are adapted primarily from: *Development of Concepts of Physics*, by Arnold B. Arons (Reading, MA: Addison-Wesley, 1965); *Lectures on Quantum Mechanics*, by Gordon Baym (Reading, Massachusetts; The Benjamin/Cummings Publishing Company, 1969); *Quantum Physics of Atoms, Molecules, Solids, Nuclei, and Particles*, by Robert Eisberg and Robert Resnick (New York: John Wiley & Sons, 1985); *Introduction to Subatomic Physics*, by Frank Filthaut (course notes); *Introduction to Elementary Particles*, by David Griffiths (Weinheim: Wiley-VCH, 2008); *Quarks & Leptons: An Introductory Course in Modern Particle Physics*, by Francis Halzen and Alan D. Martin (New York: John Wiley & Sons, 1984); *Introduction to Accelerator Physics*, by Kjell Johnsen, in "92nd International School of Physics 'Enrico Fermi': Elementary particles", Varenna, Italy, 26 Jun - 6 Jul 1984, pp.470-502; *Introduction to High Energy Physics*, by Donald H. Perkins (Reading, MA: Addison-Wesley, 1982); *Introduction to Atomic and Nuclear Physics*, by Henry Semat (New York: Rinehard & Company, Inc., 1954). Errors are mine.

Chapter 1

Introduction

The modern concept of the atom began to take form at the end of the 18th century and early 19th century with the Law of Definite Proportions, proposed by J. L. Proust, followed shortly thereafter by John Dalton's focus on relative masses, which lead to the Rule of Greatest Simplicity and the Law of Multiple Proportions. These propositions were supplemented in the 19th century by the Law of Combining (Gas) Volumes and Avogadro's hypothesis of the equality of molecule counts in equal volumes of gases at equal temperature and pressure. With Faraday's Law of Electrolysis, the calculation of chemical reactions that followed from the earlier developments was verified, and the stage was set for Mendeléev and Meyer's synthesis of the Periodic Table of Elements.

These developments remained for the most part guided by the ancient notion that atoms were the ultimate, indivisible, elementary objects of which everything is composed. The multitude and periodicity of the elements made this expectation unlikely, and, of course, we now know that that atoms are composed of electrons and a nucleus. The nucleus is in turn composed of nucleons, which themselves are composed of quarks.

It is these constituents and their interactions that we will study in this course. The decade 1895 - 1905 is often designated the first of modern physics due to the discoveries of X-rays, radioactivity, the electron, the quantum nature of electromagnetic waves and sub-atomic particles, and special relativity. These discoveries and the phenomena themselves are all somehow related to electromagnetism, and so the importance of reviewing this topic. The history of this period, and of subatomic physics since, is fascinating and informative, but diverts time and attention from the study of our present state of knowledge, the focus of this course. Readings are provided for the curious, but even–or maybe especially–the non-curious are encouraged to peruse them.

When one considers the full history of our quest to understand what, fundamentally, everything is made of, our current notion of fundamental constituents as *both* chunks separated, relative to the size scale of these chunks, by enormous voids, *and* waves, which, in principle, spread out through all of space–such notions are quite astonishing individually, but even more so conjoined as they are. We shall call these conjoined objects subatomic entities.

What may not be so suprising, at least to some, is that each type of subatomic entity–and there aren't so many different *fundamental* types–is identically duplicated. The uncountable ^{12}C atoms are intrinsically indistinguishable, as are electrons, protons, neutrons, and so forth. Fortunately for us, such indistinguishability simplifies the development of the physics, as there is less to explain.

We are also helped by the fact that the number of ways these entities interact is small. On the other

hand, there are no direct means to observe these interactions. All we know about them derives from three indirect techniques:

1. measuring properties of joined or bound entities (spectroscopy)
2. observing what happens when one entity scatters off another
3. examining natural, spontaneous transformations of entities

1.1 Observables

Different techniques measure some of the same observables. Many of the oberservables regardless of technique are related. Both of these sets of redundancies are obviously good things.

1.1.1 Spectroscopy

1. energy spectrum
2. lifetime, τ
3. mass
4. width, Γ
5. transformation outcomes
6. magnetic moments

The natural width is inversely related to the lifetime, $\Gamma = \hbar/\tau$. The total width is the sum of all transformation widths (final states). The lifetime, mass, and width are related by the mass distribution of bound-state resonances through the (relativistic) Breit-Wigner probability distribution $c = \hbar = 1$:

$$P(E) = \frac{k}{(E^2 - M^2)^2 - M^2\Gamma^2} \tag{1.1}$$

where E is the center-of-mass energy of the constituents, and

$$k = \frac{2\sqrt{2}M\Gamma\gamma}{\pi\sqrt{M^2 + \gamma}} \tag{1.2}$$

and

$$\gamma = \sqrt{M^2(M^2 + \Gamma^2)} \tag{1.3}$$

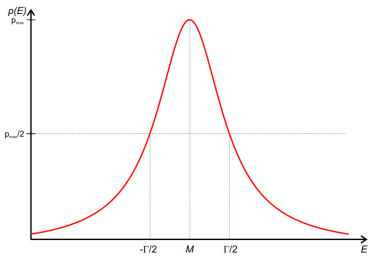

Figure 1.1: A Breit-Wigner distribution, here of the probability that the given center-of-mass energy produces the resonance. The full-width of the resonance distribution at half its maximum probability ($p/2$) is directly related to the width, and therefore the lifetime, of the resonance: $FWHM = \Gamma/2 - (-\Gamma/2) = \Gamma$

1.1.2 Scattering

1. Total cross section
2. Partial cross section

A cross section is the effective area (for interaction) presented by a target entity.

In subatomic physics, scattering events involve projectiles whose relative velocities, $\frac{v}{c} \gg 0$, and the sizes of the objects involved, ~ 1 fm, 10^{-15} m, means a typical reaction time interval $\Delta t \lesssim 10^{-23}$ s. This also implies a 2-body scatter process in which the scattered object is free before and after the interaction.

Assuming only a small number of interactions will occur in one pass (thin target), then the number of interactions, N_i is proportional to

1. the number of incident (beam) entities, N_b
2. the numerical density (number/unit volume) of target entities, n_t
3. the "sheet" thickness, z

$$N_i = \sigma N_b n_t z \tag{1.4}$$

The product $N_b n_t z$ is sometimes referred to as the luminosity, $\mathcal{L}$. The proportionality constant, σ, gives the probability of an interaction given the beam and target characteristics. Its units are area.

$$\sigma = \frac{\text{Number of interactions}}{\text{Number of incident entities} \times \text{Number of target entities per unit volume} \times \text{thickness}} \tag{1.5}$$

This is known as the total cross section, a somewhat ambiguous term. It can be comprised of the sums of cross-sections for different types of interactions between the same species of incident and target entities, for example σ_{elastic}, $\sigma_{\text{inelastic}}$, and $\sigma_{\text{electron production}}$, etc. It can also refer to the integral over all scattering angles, which leads to the concept of differential cross-section, $\frac{d\sigma}{d\Omega}$, where $d\Omega = \sin\theta d\theta d\phi$, the infinitesimal element of the solid angle, which, when measured, is equal to $\frac{dA}{r^2}$, a differential area at some distance r from the target. Then

$$\sigma = \int \frac{d\sigma}{d\Omega} d\Omega \tag{1.6}$$

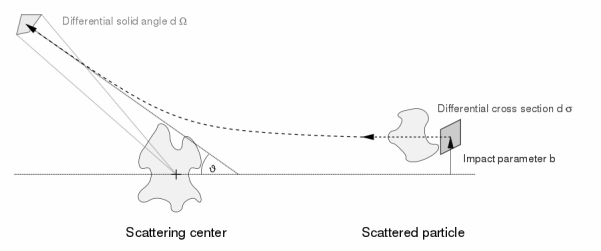

Figure 1.2: Differential cross section, $d\sigma$ and solid angle, $d\Omega$.

Let's get an intuitive sense of this latter meaning by considering, classically, the scattering of a point particle by a hard sphere.

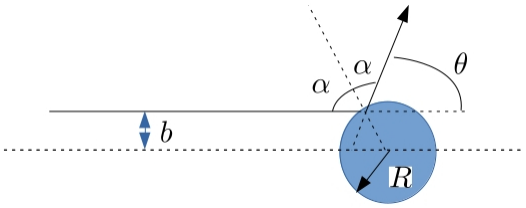

Figure 1.3: A point particle scattering at angle θ off a hard sphere of radius R.

Scattering angle: $\theta = \pi - 2\alpha$

Impact parameter: $b = R \sin \alpha$

Therefore:

$$b = R \sin\left[\tfrac{1}{2}(\pi - \theta)\right] = R \cos\left(\tfrac{\theta}{2}\right)$$

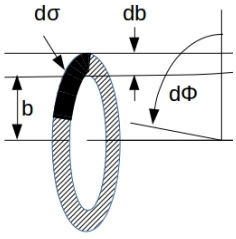

Figure 1.4: Impact parameter, b, and azimuthal angle, ϕ, contributions to the differential cross section, $d\sigma$.

The contributions to the total cross section from different impact parameters and azimuthal angles [see Figure 1.4]:

$$\begin{aligned} d\sigma &= -bdbd\phi \\ &= -b\frac{db}{d\theta}d\theta d\phi \\ &= \frac{1}{2}R^2\cos\left(\frac{\theta}{2}\right)\sin\left(\frac{\theta}{2}\right)d\theta d\phi \\ &= \frac{1}{4}R^2\sin\theta d\theta d\phi \\ &= \frac{1}{4}R^2 d\Omega \end{aligned}$$

$$\Rightarrow \frac{d\sigma}{d\Omega} = \frac{R^2}{4}$$

which, integrated over all angles gives the total cross section:

$$\sigma = \pi R^2$$

the cross-sectional area of the hard sphere.

1.1.3 Transformations (decays)

1. Lifetime
2. Transformation rates
3. Branching ratios

If the decay rate, or probability per unit time of a transformation is Γ. If there are $N(t_i)$ entities at time t_i, then $N(t_i)\Gamma dt$ is the number that transform in interval dt, reducing the number of original entities by dN. Thus, in general:

$$dN = -N(t)\Gamma dt \tag{1.7}$$

where the negative sign indicates that the number is decreasing.

Integrating

$$N(t) = N(t_0)e^{-\Gamma t} \tag{1.8}$$

for some arbitrary initial time, t_0.

The mean lifetime is the inverse of the decay rate:

$$\tau = \frac{1}{\Gamma} \tag{1.9}$$

Most entities transform in a number of different ways, referred to as channels or modes, and each channel is characterized by a different rate, Γ_i, say. Then the total decay rate is the sum of all partial decay rates:

$$\Gamma_{\text{total}} = \sum_i \Gamma_i \tag{1.10}$$

The mean lifetime of the entity, accounting for all channels, is, then:

$$\tau = \frac{1}{\Gamma_{\text{total}}} \tag{1.11}$$

What is typically measured are branching ratios or branching fractions, BR, the fraction of transformations into each mode. If the fraction to all modes can be measured, they will sum to 1.

Branching fractions can be related to decay rates, which are what is calculated from theory.

$$BR_i = \frac{\Gamma_i}{\Gamma_{\text{total}}} \tag{1.12}$$

1.2 Modeling Interactions

Scientific understanding evolves as results of investigations are compared to predictions of a pre-conceived model or from constructing a model that accounts for the results of investigations while, in turn, predicting the outcome(s) of further investigations.

In physics, mathematical models of mechanical and electromagnetic interactions are second-order differential equations. Presumably, interactions between subatomic entities will include mechanical and electromagnetic processes, and so we should look for one or more differential equations.

Chunks (objects composed of "matter") have well-defined energy E and momentum p, which are related by

$$E = \frac{p^2}{2m} + V \tag{1.13}$$

where V is a potential, which can depend on position and time, representing the interaction. In the case of a constant potential, which can be defined as zero, energy and momentum will be conserved. The chunk is what is called a free particle. The wave associated with a free particle can be represented by a sinusoidal function that also depends on time and position in, say, one dimension,

$$\Psi(x,t) = \cos 2\pi \left(\frac{x}{\lambda} - \nu t\right) + \gamma \sin 2\pi \left(\frac{x}{\lambda} - \nu t\right) \tag{1.14}$$

where λ is the wavelength, ν is the frequency of the wave, and γ is a constant to be determined. The final equation of motion has to be linear in this function to ensure that when different such functions add together they produce constructive and destructive interferences. In short, there can be no constant terms or quadratic or higher powers of Ψ.

Chunk parameters (energy and momentum) must somehow relate to to the wave parameters (wavelength and frequency). The de Broglie and Einstein postulates do this:

$$p = \frac{h}{\lambda} \tag{1.15}$$

$$E = h\nu \tag{1.16}$$

Combining these with Equation 1.13,

$$\frac{h^2}{2m\lambda^2} + V(x,t) = h\nu \tag{1.17}$$

The wavenumber $k = 2\pi/\lambda$, the angular velocity $\omega = 2\pi\nu$, and the reduced Planck's constant $\hbar = \frac{h}{2\pi}$.

$$\frac{\hbar^2 k^2}{2m} + V(x,t) = \hbar\omega \tag{1.18}$$

and, from Equation 1.14

$$\Psi(x,t) = \cos(kx - \omega t) + \gamma \sin(kx - \omega t) \tag{1.19}$$

The factors of k^2 and ω in Equation 1.18 suggest Equation 1.19 could be related to it by taking a second derivative with respect to position and a first derivative with respect to time:

$$\alpha \frac{\partial^2 \Psi(x,t)}{\partial x^2} + V(x,t)\Psi(x,t) = \beta \frac{\partial \Psi(x,t)}{\partial t} \tag{1.20}$$

where α and β are constants, like γ, to be determined. This equation yields, gathering terms

$$[-\alpha k^2 + V(x,t) + \beta\omega\gamma]\cos(kx - \omega t) + [-\alpha\gamma k^2 + \gamma V(x,t) - \beta\omega]\sin(kx - \omega t) = 0 \tag{1.21}$$

There are now three equations for the three unknown constants, α, β, and γ.

$$\frac{\hbar^2 k^2}{2m} + V(x,t) = \hbar\omega \tag{1.22a}$$

$$-\alpha k^2 + V(x,t) = -\beta\omega\gamma \tag{1.22b}$$

$$-\alpha\gamma k^2 + \gamma V(x,t) = \beta\omega \tag{1.22c}$$

Dividing Equation 1.22c by Equation 1.22b gives $\gamma = -\frac{1}{\gamma} \Rightarrow \gamma^2 = -1$ or $\gamma = \pm i$. Plugging this into Equation 1.22b gives $-\alpha k^2 + V(x,t) = \mp i\beta\omega$ and comparing to Equation 1.22a allows us to conclude that $\alpha = -\frac{\hbar^2}{2m}$ and $\beta = \pm i\hbar$. Choosing the plus sign by convention (it makes no physical difference), we get for our differential equation

$$-\frac{\hbar^2}{2m}\frac{\partial^2 \Psi(x,t)}{\partial x^2} + V(x,t)\Psi(x,t) = i\hbar \frac{\partial \Psi(x,t)}{\partial t} \tag{1.23}$$

This, of course, is Schrödinger's equation, which implies that the model building and testing of interactions among subatomic entities has to be guided by general principles in quantum mechanics. This is a direct consequence of the manifestly dual wave and particle natures of these entities.

Equation 1.13 is the low-velocity, non-relativistic form of the total energy. That it served as a premise for our plausibility argument means that Equation 1.23 is a low-velocity, non-relativisitic form for describing the behavior from an interaction defined by the potenial V. While atomic physics and (some) nuclear physics, both amalgamations of subatomic entities, can be described quantum mechanically without special relativity, particle physics, the physics of the interactions of the entities themselves, usually requires creating models of these interactions within the context of quantum field theory (QFT, a topic primarily for another course, but whose essential ideas are necessary in this course), a merging of special relativity and quantum mechanics. This merger requires replacing the non-relativistic total energy, Equation 1.13, with the relativistic form:

$$E = \sqrt{c^2 p^s + m^2 c^4} + V \tag{1.24}$$

This would give a relativistic formalism for a single subatomic (quantum mechanical) entity, an approach known as relativistic quantum mechanics. It explains, for example, the Pauli exclusion principle that, among othe things, accounts for the electronic structure of atoms.

Quantum field theory is a broader conception of interactions, in that it includes any number of entities and (quantized) fields. In its present state of development, QFT is not well-equipped to deal with bound states. Its formalism is primarily designed to analyze interactions of infinitesimally small duration between initally and finally free objects.

Non-relativistic quantum mechanics (Schröder's equation) was designed to analyze subatomic bound states, and is very good at it. It provides a formalism for addressing the indeterminacy of scattering behavior, lifetimes, and transformation products, while quantum field theory provides one for addressing the existence of "anti-chunks" and their similarities to and differences from chunks.

One consequence of special relativity is that so-called rest mass may not be conserved in an interaction, even though energy and momentum are, and such is seen in the spontaneous transformations of some subatomic entities. Furthermore, special relativity allows for massless chunks, which some subatomic entities are.

1.2.1 Fields and Mediators

Classically, action-at-a-distance is conceptualized as objects interacting with one another due to the effect of a potential or a field. In quantum field theory, interactions are viewed as exchanges of quanta (known as mediating bosons) characteristic of the type of interaction. Macroscopically, such details are irrelevant.

Classical: $F = Q_2 E(r) \sim Q_1 Q_2 / r^2$

QFT: Exchange of virtual photon with momentum q
But $qr \sim \hbar$ (Heisenberg's uncertainty principle), and $t = r/c$, so $dq/dt \sim 1/r^2$. Assuming the number of photons absorbed and emitted is directly related to charge gives the classical result.

Neither of these conceptualizations is directly observable. However, the quantization of propagating electromagnetic fields as free photons justifies the notion of virtual photon exchange on the microscopic scale. And, it works, as we'll see.

Visualizations of Interactions

Classical field lines:

(a) Radial field (b) Feld of two charges

Figure 1.5: Electric fields associated with point charges

(a) Uniform field (b) Magnetic quadrupole field

Figure 1.6: Representative electromagnetic field lines

QFT Feynman diagrams: In the convention used here, the only physical aspect of the diagram is time flowing from left to right. No spatial information can be inferred from them.

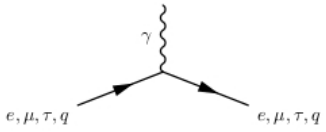

Figure 1.7: QED primative or photoelectric effect

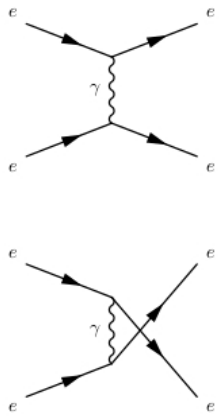

Figure 1.8: Two-electron processes

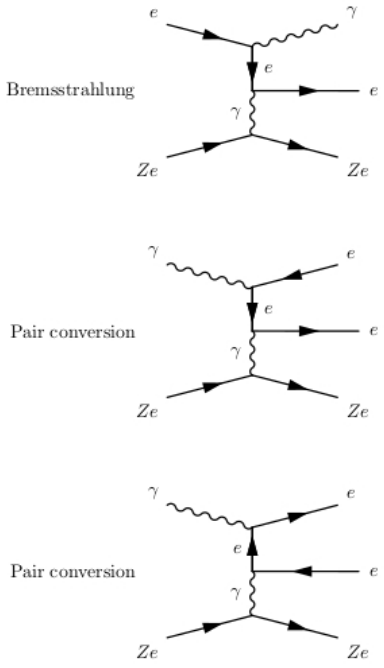

Figure 1.9: Electromagnetic interactions with a nucleus

1.3 Natural Dimensions and Units

As the typical nuclear radius is order 10^{-15} m, and the typical nuclear energy is in the 10^{-10} J range, SI units are not convenient for subatomic physics, whose constituents are smaller with rest energies of roughly the same magnitude . Instead, lengths are usually quoted in terms of femtometers or, equivalently, fermi, 1 fm $= 10^{-15}$ m. Areas, or, more precisely, cross-sections are reported in terms of barns, 1 b $= 10^{-28}$ m^2. Energies are referred to in terms of electron volts, 1 eV $= 1.6 \times 10^{-19}$ J.

Mathematical expressions in subatomic physics, which exists in relativistic and quantum realms, are repleat with the physical constants c and $\hbar$. It's convenient to define them away by setting them both to unity: $c = \hbar \equiv 1$. Now, kinematics depends on three independent parameters, which are typically identified as length, time, and mass. Constraining c and $\hbar$, which are combinations of these, $[c] = \frac{L}{T}$, $[\hbar] = \frac{ML^2}{T}$, leaves just one kinematical degree of freedom.

The experimental techniques of subatomic physics–measuring bound states, scattering, and transformations–all involve projectiles, whose primary characterization is their energy. It's therefore become natural in subatomic physics to refer to everything in terms of units of energy. Setting $c = \hbar \equiv 1$ and choosing the remaining kinematic parameter to be energy is therefore referred to by physicists engaged in subatomic physics as working in natural dimensions. Since, in subatomic physics $E = \sqrt{p^2c^2 + m^2c^4}$, the dimensions of momentum and mass are also energy. A plane wave solution to Schrödinger's equation is $\Psi(x,t) = Ce^{i(x/\lambda - \nu t)} = Ce^{i(px - Et)/\hbar}$, so the dimensions of length and time are 1/energy. Heisenberg's Uncertainty principles, $\Delta x \Delta p \gtrsim \hbar$ and $\Delta E \Delta t \gtrsim \hbar$, lead to the same conclusions. In quantum mechanics, the magnitude of the orbital angular momentum is $L^2 = l(l+1)\hbar$, which means that angular momentum, like velocity, is dimensionless. Of course, this could also be seen by the classical relationship, $\mathbf{L} = \mathbf{r} \times \mathbf{p}$.

In SI units, Coulomb's Law is

$$F = \frac{1}{4\pi\varepsilon_0}\frac{Q_1 Q_2}{r^2} \tag{1.25}$$

Since $F = \frac{dp}{dt}$ and the dimension of momentum is energy and the dimension of time is 1/energy, the dimension of force is energy^2. Because the dimension of length is 1/energy, $\frac{1}{r^2}$ has the same dimension as force. This implies that the ratio $Q_1 Q_2/\varepsilon_0$ is dimensionless. As $c^2 = \frac{1}{\varepsilon_0 \mu_0} = 1$, it is convenient to set $\varepsilon_0 = \mu_0 = 1$ in natural units. Once that is done, electric charge is fixed to be dimensionless.

The fine structure constant,

$$\alpha = \frac{e^2}{4\pi\varepsilon_0\hbar c} = \frac{1}{137} \tag{1.26}$$

in all systems of units. This leads to $e = \sqrt{\frac{4\pi}{137}} = 0.303$. That is, the charge of the proton is 0.303 in natural units.

To summarize,

Quantity	Natural Dimension
mass	Energy
length	1/Energy
time	1/Energy
energy	Energy
momentum	Energy
velocity	none
angular momentum	none
cross-section	$1/\text{Energy}^2$
force	Energy^2
charge	none

The natural unit of measurement is, again, the electronvolt 1 eV $= 1.6 \times 10^{-19}$ J. Notice, $[\hbar]$ = Energy $\times$ Time and $[c]$ = Length/Time. Thus to convert a quantity in Natural Units into, say, SI units, insert the appropriate $\hbar$ or c or $\hbar c$. So, $m_{SI} = m_{NU}/c^2$, $p_{SI} = p_{NU}/c$, $\sigma_{SI} = \sigma_{NU} \times (\hbar c)^2$, $t_{SI} = t_{NU} \times \hbar$, and $\Gamma_{SI} = \Gamma_{NU}/\hbar$.

Here's a list of some conversion factors in ranges appropriate for subatomic physics (1 GeV $= 1.6 \times 10^{-10}$ J):

Quantity	Typical Natural Unit	Conversion
$\hbar$	1	6.6×10^{-25} GeV-s
c	1	3×10^8 m/s
$\hbar c$	1	2×10^{-16} Gev-m
Energy	1 GeV	10^9 eV $= 1.6 \times 10^{-10}$ J
Mass	1 GeV	1.8×10^{-27} kg
Momentum	1 GeV	5.3×10^{-19} kg-m/s
Length	1 GeV^{-1}	2×10^{-16} m
Cross Section	1 GeV^{-2}	4×10^{-32} $\text{m}^2 = 0.4$ mb
Time	1 GeV^{-1}	6.6×10^{-25} s
Decay Rate	1 GeV	1.5×10^{24} s^{-1}

Chapter 2

Interactions with Matter

2.1 Introduction

All methods of detection in nuclear and particle physics depend on the interactions of charged particles and electromagnetic radiation with bulk matter. Directly or indirectly, the particles or radiation transfer energy to this matter as they traverse it, exciting or ionizing the constituent atoms.

2.2 Charged Particle Ionization Loss

The average energy per unit density and unit distance transferred to the bulk as a result of ionization by the traversal of a fast moving charged particle of mass $M \gg m$, the mass of an electron, is given by the (Hans) Bethe formula,

$$-\left\langle \frac{dE}{dx} \right\rangle_{\text{ion}} = \frac{4\pi z^2 \alpha^2 N_A}{m\beta^2} \frac{Z}{A} \left[\ln\left(\frac{2\beta^2\gamma^2 m}{I} \right) - \beta^2 \right] \tag{2.1}$$

where β and z are the velocity and charge per proton charge of the incident particle (assumed to be spinless in this approximation), N_A is the Avogadro constant, Z, A, and I are the atomic number, mass number, and mean excitation potential, respectivley, of the bulk, and m is the electron's mass. The magnitude of $I \approx 10Z$ eV.

Note that

1. $\frac{dE}{dx} = z^2 f(\beta)$, independent of M
2. For a given z: $\frac{dE}{dx} \propto \frac{1}{v^2}$ for $\beta \ll 1$; $\left(\frac{dE}{dx}\right)_{\text{min}}$ at $\beta\gamma \approx 3$; $\frac{dE}{dx} \propto \ln \gamma^2$ for $\beta \to 1$.
3. Since the dependence on I is logarithmic and $\frac{Z}{A} \approx 0.5$ for all but hydrogen and large A matter, $\frac{dE}{dx}$ depends only weakly on the bulk.

Note also that in principle the interaction could be with protons rather than electrons, but then $dE/dx \propto 1/m_p$ instead of $1/m_e$, and the energy loss would be 2000 times smaller.

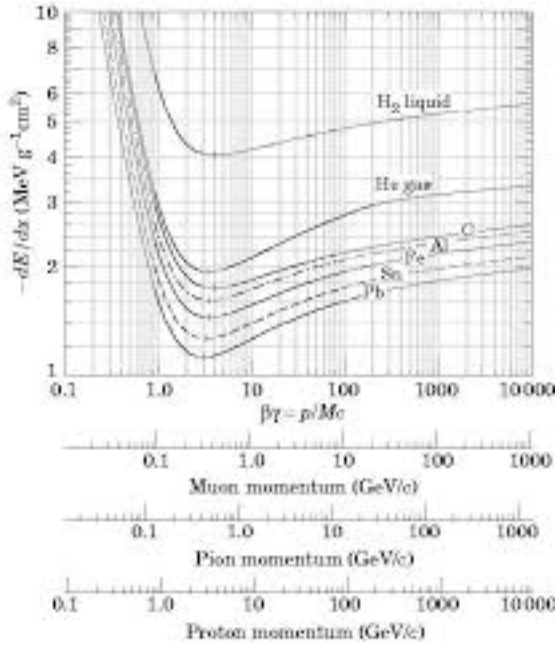

Figure 2.1: Bethe curve for several different elements as a function of $\beta\gamma = p/Mc$ and incident particle (muon, pion, proton) momentum, p

The effect of the traversing particle's spin is negligible. The dE/dx losses of a traversing electron are smaller by a few percent than Equation 2.1 would indicate, but additional radiation losses are a much more important effect.

The so-called relativistic rise of Equation 2.1 is due in part to knock-on effects of so-called δ-rays–highly energetic ionized electrons–causing additional ionization, and in part to relativistic effects on the electric field when transforming into the lab frame: the transverse component is proportional to γ, so it grows as γ grows, increasing the number and magnitude of more distant (transverse) collisions, until, at around $\gamma = 10$ where the effect reaches interatomic distances, polarization in the dielectric begins to shield against the field, and the curve flattens out.

Equation 2.1 is the average energy loss dE in a layer dx of matter, but this average will be subject to large fluctuations to the high loss side. The asymmetric distribution about the mean is described by a Landau distribution.

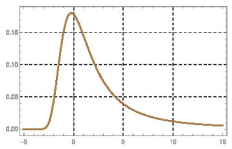

Figure 2.2: Landau distribution (shape)

Disgarding outliers, then, energy loss measurements of many layers can lead to a few percent deter-

mination of the mean energy loss, from which γ, and therefore β, can be estimated. With these and an independent measurement of the momentum, the particle mass, and therefore its species, can be determined.

2.3 Ionization Loss and Range

(Kinetic) energy loss implies that a traversing particle can range out in the bulk:

$$R = \int_0^K \frac{dE}{dE/dx} \tag{2.2}$$

While the non-relativistic, $\frac{1}{v^2} \propto E^{-1}$ dependence of dE/dx_{ion} might suggest $R \propto K^2$, empirically, for mid-A matter and $0.1 < \beta < 0.7$,

$$R \propto K^{1.75} \tag{2.3}$$

This relationship is subject to the same fluctuations as the average $(dE/dx)_{\text{ion}}$, which, in this case is known as straggling. With an independent momentum measurement and the range-determined energy, the mass, and therefore the species, of a particle can be identified.

2.4 Cerenkov Radiation

Cerenkov radiation is related to the polarization limitation on the relativistic increase of dE/dx: part of this limitation is due to Cerenkov radiation, which occurs whenever a particle's $\beta > \frac{1}{n}$, where n is the index of refraction of the matter.

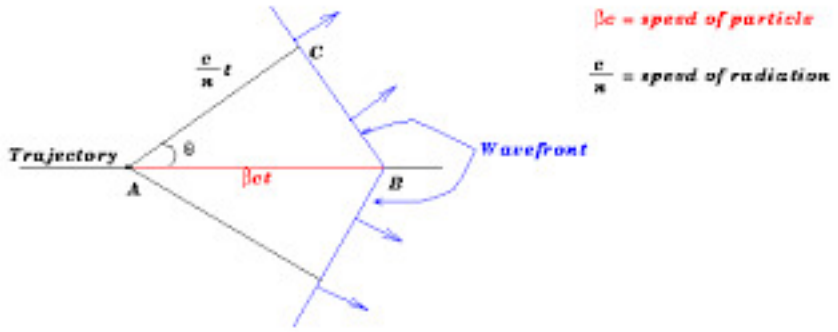

Figure 2.3: Cerenkov radiation

The radiation from atoms excited along the path of a trajectory form a coherent wavefront at a certain angle relative to that trajectory,

$$\cos\theta = \frac{t/n}{\beta t} = \frac{1}{\beta n} \tag{2.4}$$

in time t. The radiation will of course form a continuous spectrum. As the index of refraction is wavelength-dependent in a dispersive medium, θ, too, will vary with wavelength.

By the appropriate choice of photon detector, this effect can be exploited to measure velocities for $\beta \to 1$ and thereby differentiate among highly energetic particles with different velocities, given an independent momentum measurement.

2.5 Scattering

Recall that the likelihood of a projectile scattering off a second object is related to the effective collision area, called a *cross section*, σ, which in nuclear and particle physics is measured in units called barns, 1 b $= 10^{-28}$ m^2. For a circular target,

$$\sigma = \pi r^2 \tag{2.5}$$

or the area of a circle with radius r.

The cross section for scattering (that is, the effective collision area) of a beam of particles off a tiny target, in which the cross-sectional area of the beam is much larger than the cross-sectional area of the target, may have a statistical interpretation. If the scattering is due, for example, to a central, inverse-square interaction, such as the gravitational or Coulomb interaction, that is, of the form $-\frac{k}{r^2}$, where k is a parameter characterizing the interaction,[1] there is an inverse relation between the magnitudes of the scattering angle and the *impact parameter*, b, the perpendicular distance from the target to the trajectory of a beam particle if it weren't scattered, and, hence, the radius of the effective collision area.

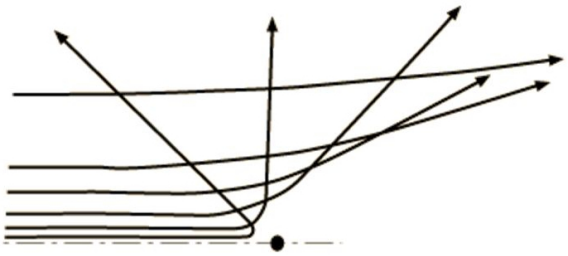

Figure 2.4: Coulomb scattering

The trajectory of a projectile repelled by a conservative central force is hypberbolic. The incoming momentum is $\vec{p}_i$, and the outgoing momentum is $\vec{p}_f$; $\Delta\vec{p} = \vec{p}_f - \vec{p}_i$. b is the impact parameter; $\vec{r}$ is the position vector of the projectile relative to the center of the much more massive target; $r_{\min}$ is the position of closest approach; and θ is the scattering angle. $\vec{r}$ sweeps out an angle, ϕ relative to $r_{\min}$: $-\frac{1}{2}(\pi - \theta) \leq \phi_i \leq 0 \leq \phi_f \leq \frac{1}{2}(\pi - \theta)$.

[1] With this notation, the interaction is assumed to be attractive, as, for example, the gravitational interaction, where $k = GMm$, while for an Coulomb interaction $k = -kq_1q_2$.

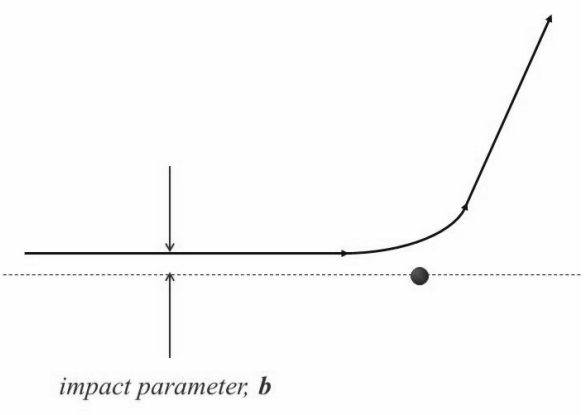

Figure 2.5: Definition of impact parameter

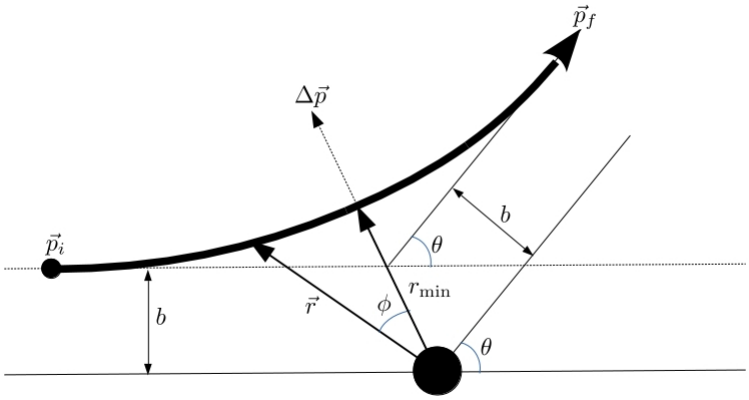

Figure 2.6: Parameters of collisions

2.5.1 Elastic Collisions without Contact

A central, inverse-square interaction (that is, a potential of the form k/r) is conservative (energy transformations do not depend on trajectory). It is elastic if the particle's mechanical energy and angular momentum are unchanged:

$$E = K - \frac{k}{r} = \text{constant} \tag{2.6}$$

$$L = I\dot{\phi} = \text{constant} \tag{2.7}$$

where, here, r is the distance of the particle from a fixed reference point, and for a single particle of mass m, $K = \frac{1}{2}mv_r^2$ is the particle's kinetic energy at radial distance r from the fixed point, and $I = mr^2$ is its moment of inertia relative to the fixed point. We consider for the moment only non-relativistic motion.

Consider the case where the projectile mass $m \ll M$, the target mass (otherwise, use reduced mass). Let $\vec{r}$ be the position vector of m relative to M, so m's radial velocity at any instant is $\dot{\vec{r}}$.

The (radial) equation of motion of m is, then,

$$-\frac{k}{r^2} = m\ddot{r} - mr\dot{\phi}^2 \tag{2.8}$$

Since, from Equation 2.7, $\dot{r} = \frac{dr}{dt} = \frac{dr}{d\phi}\frac{d\phi}{dt} = \frac{dr}{d\phi}\frac{L}{I}$,

$$\ddot{r} = \frac{d\dot{r}}{dt} = \frac{d(dr/d\phi)}{d\phi}\left(\frac{d\phi}{dt}\right)^2 - \frac{dr}{d\phi}\frac{2L}{Ir}\frac{dr}{dt} = \frac{d^2r}{d\phi^2}\left(\frac{L}{I}\right)^2 - \frac{2}{r}\left(\frac{dr}{d\phi}\right)^2\left(\frac{L}{I}\right)^2$$

so, substituting the expression for the moment of inertia of a single particle, $I = mr^2$,

$$\ddot{r} = \frac{L}{m^2r^4}\left[\frac{d^2r}{d\phi^2} - \frac{2}{r}\left(\frac{dr}{d\phi}\right)^2\right] \tag{2.9}$$

Plugging Equation 2.9 into Equation 2.8 and rearranging,

$$-\frac{mk}{L^2} = -\frac{1}{r} + \frac{1}{r^2}\frac{d^2r}{d\phi^2} - \frac{2}{r^3}\left(\frac{dr}{d\phi}\right)^2 \tag{2.10}$$

On substituting $u \equiv \frac{1}{r}$,which implies that $\frac{dr}{d\theta} = -\frac{1}{u^2}\frac{du}{d\theta}$ and $\frac{d^2r}{d\theta^2} = \left(\frac{2}{u^3}\right)\left(\frac{du}{d\theta}\right)^2 - \left(\frac{1}{u^2}\right)\frac{d^2u}{d\theta^2}$, Equation 2.10 simplifies to

$$\frac{d^2u}{d\theta^2} + u = \frac{mk}{L^2} \tag{2.11}$$

The general solution to Equation 2.11 is

$$u = \frac{1}{r} = A\sin\phi + B\cos\phi + \frac{mk}{L^2} \tag{2.12}$$

Initial and boundary conditions determine the coefficients of the trigonometric terms. Energy and momentum conservation require that the line through the distance of closest approach $r_{\min}$ be an axis of symmetry of the motion. This line is at $\phi = 0$, at which $|\vec{r}| = r_{\min}$ and $\dot{\vec{r}} = 0$. The first condition implies that $B = \frac{1}{r_{\min}} - \frac{mk}{L^2}$. Since, taking the time derivative of Equation 2.12 and inserting $\phi = 0$, $-\frac{1}{r_{\min}}\dot{r} = A\dot{\phi}$, the second condition implies $A = 0$. Thus,

$$\frac{1}{r} = \left(\frac{1}{r_{\min}} - \frac{mk}{L^2}\right)\cos\phi + \frac{mk}{L^2}$$

or, finally,

$$r = \frac{L^2/mk}{1 + (L^2/mkr_{\min} - 1)\cos\phi} \tag{2.13}$$

or, since $E = \frac{L^2}{2mr_{\min}^2} - \frac{k}{r_{\min}}$,

$$r = \frac{2r_{\min}(1 + Er_{\min}/k)}{1 + (2Er_{\min}/k + 1)\cos\phi} \tag{2.14}$$

Each is an equation in polar coordinates of a conic section with eccentricity $e = L^2/mkr_{\min} - 1 = 2Er_{\min}/k + 1$. If $e = 0$, m circles about M with a constant radius of $\left|\frac{L^2}{mk}\right| = \left|\frac{k}{2E}\right|$. If $0 < e < 1$, m revolves around M in an ellipse with semi-major axis

$$a = \left|\frac{mkr_{\min}^2}{2kmr_{\min} - L^2}\right| = \left|\frac{k}{2E}\right| \tag{2.15}$$

and semi-minor axis (not to be confused with the impact parameter)

$$b = \frac{Lr_{\min}}{\sqrt{|2mkr_{\min} - L^2|}} = r_{\min}\sqrt{|1 + k/(Er_{\min})|} \tag{2.16}$$

2.5.2 Scattering in Two- and Three-Dimensions

If $e > 1$, m's trajectory is hyperbolic, with M at the focus. This is the motion of scattering. If the scattering is repulsive, then $k < 0$. if attractive, $k > 0$, and the bend is in the opposite direction.

The parameters of interest in the physical condition of scattering are typically the incident (and outgoing) kinetic energy, $K_i = K_f \equiv K$, the impact parameter, b, and the scattering angle, θ rather than L (or E), $r_{\min}$, and ϕ.

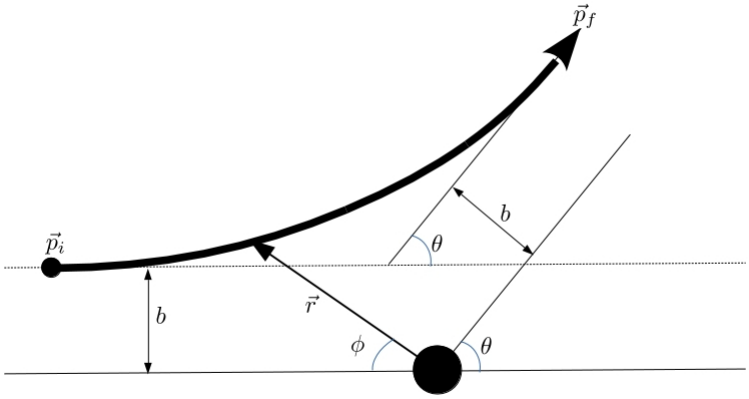

Figure 2.7: Scattering parameters

In terms of these parameters, Equation 2.12 is reevaluated with the initial condition at $\vec{r} = -\infty$,[2]: $u = 0$ and $\phi = 0$, increasing to $\pi - \theta$ when $r = \infty$. Also, $\dot{r}_{\pm\infty} = v_{\pm\infty} = \sqrt{2K/m}$.

Note also that the momentum $|\vec{p}_i| = |\vec{p}_f| \equiv p = \sqrt{2mK}$, and $L = I\dot{\phi} = \vec{r} \times \vec{p} = r_\perp p = b\sqrt{2mK}$, so $\dot{\phi} = \frac{b\sqrt{2mK}}{I}$.

Then, from Equation 2.12,

$$B = -\frac{mk}{L^2} = -\frac{mk}{2mKb^2} = -\frac{k}{2Kb^2} \tag{2.17}$$

[2]With respect to the size of M, a beam particle approaches from, and receeds, very far away.

and, because $\dot{u} = -\frac{1}{r^2}\dot{r} = (A\cos\phi - B\sin\phi)\dot{\phi}$

$$\begin{aligned} -\frac{1}{r^2}\sqrt{\frac{2K}{m}} &= A\dot{\phi} = A\frac{b\sqrt{2mK}}{I} \\ A &= -\frac{1}{b}\frac{I}{mr^2} = -\frac{1}{b} \end{aligned}$$

so that

$$\frac{1}{r} = -\frac{1}{b}\sin\phi + \frac{k}{2Kb^2}(1-\cos\phi) \tag{2.18}$$

At $|\vec{r}| = +\infty|$, $\frac{1}{r} = 0$ and $\phi = \pi - \theta$, so Equation 2.18 becomes

$$0 = -\frac{1}{b}\sin\theta - \frac{k}{2Kb^2}(1+\cos\theta) \tag{2.19}$$

and, therefore, because $\sin\theta = \sqrt{1-\cos^2\theta} = \sqrt{(1+\cos\theta)(1-\cos\theta)}$,

$$b = \left|\frac{k}{2K}\right|\sqrt{\frac{1+\cos\theta}{1-\cos\theta}} = \left|\frac{k}{2K}\right|\cot\frac{\theta}{2} \tag{2.20}$$

where the last result uses half-angle formulae.

Recalling the distribution of the cotangent function, we see the inverse relationship between impact parameter and scattering angle: larger scattering angles occur at smaller impact parameters.

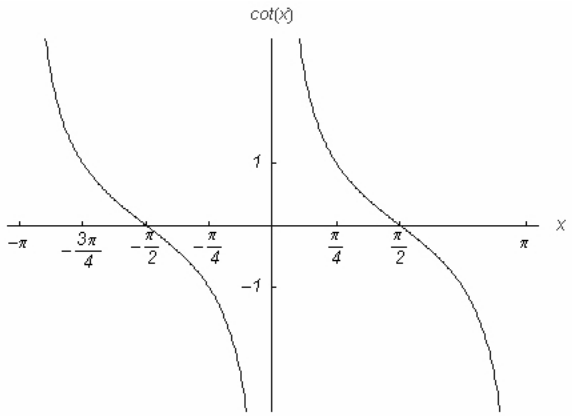

Figure 2.8: The cotangent function

Because any beam particle arriving closer than b will scatter with an angle larger than a particle arriving with impact parameter b, the circle with radius b gives the total cross section for particles with kinetic energy K to scatter at angles larger than the angle associated with b given by Equation 2.20 [see Equation 2.5]:

$$\sigma = \pi b^2 = \pi\left(\frac{k}{2K}\right)^2\frac{1+\cos\theta}{1-\cos\theta} \tag{2.21}$$

The expected number of particles scattering at angles larger than that associated with a certain impact parameter depends on the number of beam particles and the number of targets.

Assume the targets are situated in a crystal lattice of a pure substance, an element with atomic mass number A, the number of nucleons in an atom of the element, but also the mass in grams of one mole of these atoms. Then, the ratio of Avogadro's constant, $N_A = 6.022 \times 10^{23}$ mol^{-1}, to A, yields the number of such atoms per gram. Multiplying by the density of targets, ρ, gives the number per unit volume, n, of these atoms:

$$n = \frac{\rho N_A}{A} \tag{2.22}$$

Multipling n by the product of the thickness of the target crystal lattice, t, with the cross section, σ, yields the number of targets within a radius of the respective impact parameter, that is, the fraction of beam particles that would scatter. Multiplying this by the rate of incident beam particles, R_i, gives the scattering rate R_s:

$$R_s = \frac{\rho N_A t \sigma}{A} R_i = \frac{\pi \rho N_A t}{A} \left(\frac{k}{2K} \right)^2 \frac{1 + \cos\theta}{1 - \cos\theta} R_i \tag{2.23}$$

Because detectors have finite coverage, the rate of scatters into a finite angular band is usually the measured quantity in an experiment. The expected rate is calculated not with the total cross section σ, but with the so-called *differential (scattering) cross section*, $\frac{d\sigma}{d\Omega}$, where Ω is the solid angle. The differential cross section is the fraction of beam particles scattered into the solid angle band of size $d\Omega$.

For a sphere of radius r,

$$\Omega = \frac{A}{r^2} \tag{2.24}$$

where A now is the area of the sphere's surface. The differential area, $dA = r^2 \sin\theta d\theta d\phi$, is that portion of the sphere's surface subtended by a differential polar (here, scattering) angle, $d\theta$, and a differential azimuthal angle $d\phi$. Then, the (always positive) differential solid angle is

$$d\Omega = |\sin\theta \; d\theta \; d\phi| \tag{2.25}$$

For a beam particle with kinetic energy K to scatter at an angle between θ and $\theta - d\theta$, it must have an impact parameter between b and $b + db$ (recall the inverse relationship between the magnitudes of the impact parameter and respective scattering angle).

$$d\sigma = |b \; db \; d\phi| \tag{2.26}$$

But it is also true that

$$d\sigma = \frac{d\sigma}{d\Omega} d\Omega = \frac{d\sigma}{d\Omega} |\sin\theta \; d\theta \; d\phi| \tag{2.27}$$

so the differential cross section is

$$\frac{d\sigma}{d\Omega} = \frac{b}{\sin\theta} \left| \frac{db}{d\theta} \right| \tag{2.28}$$

From Equation 2.20,

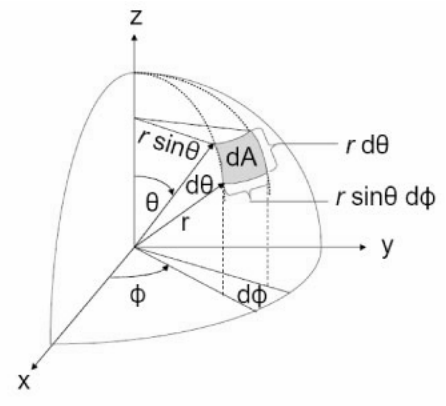

Figure 2.9: Definition of solid angle

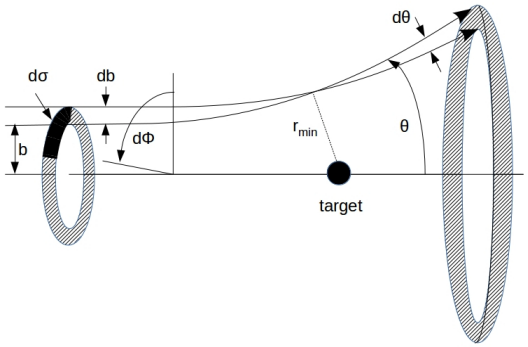

Figure 2.10: 3-D Differential Cross Section

$$\left|\frac{db}{d\theta}\right| = \left|\frac{k}{4K}\right| \csc^2\frac{\theta}{2} \tag{2.29}$$

so, because $\sin\theta = 2\sin\frac{\theta}{2}\cos\frac{\theta}{2}$, Equation 2.28 becomes

$$\frac{d\sigma}{d\Omega} = \left(\frac{k}{4K}\right)^2 \frac{1}{\sin^4\frac{\theta}{2}} = \left(\frac{k}{8K}\right)^2 \frac{1}{(1-\cos\theta)^2} \tag{2.30}$$

This is the fraction of incident beam particles scattered in the direction between θ and $\theta - d\theta$ and ϕ and $\phi + d\phi$ per unit solid angle per unit time.

The estimated rate of scattered particles into a detector depends on the rate of incident beam particles [see Equation 2.23], the nature (composition and thickness) of the target, and the dimensions (cross-sectional area) of the detector and its distance from the target.

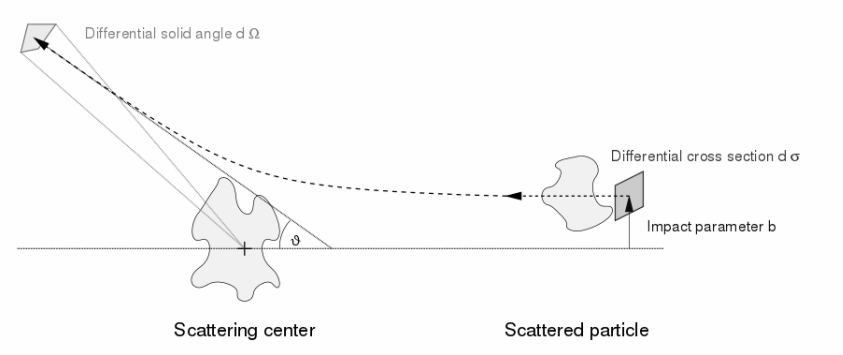

Figure 2.11: Differential cross section

2.6 Multiple Coulomb Scattering

As we've seen, the energy a charged particle traversing a medium loses due to electromagnetic interactions is inversely proportional to the mass of the electrons and protons with which it interacts. While the loss is therefore much larger to electrons than protons, the greater mass of the protons results in significantly greater scattering, as described by Equation 2.30.

As that equation shows, the cross section is large for small scatters, the result being that in traversing a layer of matter of thickness t, a particle is likely to undergo numerous small deviations, each one independent of its predecesors. The scattering angle distribution of these multiple scatters is approximately Gaussian

$$P(\phi)d\phi = \frac{2\phi}{\langle\phi^2\rangle}\exp\left(\frac{-\phi^2}{\langle\phi^2\rangle}\right)d\phi \tag{2.31}$$

where ϕ is the scatter angle in 3-space ($\phi/\sqrt{2}$ is the projection onto a plane normal to the trajectory), and $\langle\phi^2\rangle$ is the mean square of that angle, which can be calculated approximately

$$\langle\phi^2\rangle \approx z^2\left(\frac{E_s}{\beta p}\right)^2\frac{t}{X_0} \tag{2.32}$$

where

$$E_s = \sqrt{\frac{4\pi}{\alpha}}m_e \approx 21 \text{ MeV} \tag{2.33}$$

and X_0 is the radiation length, found in tables, but

$$\frac{1}{X_0} = \frac{4Z(Z+1)\alpha}{m^2}\ln\left(\frac{183}{Z^{1/3}}\right) \tag{2.34}$$

Thus, a singly-charged particle, $z = 1$, undergoes an rms deflection of $\langle\phi^2\rangle^{1/2}\frac{21}{\beta p}$ radians traversing one radiation length (p in MeV).

Note that scattering is not really normally distributed, because of the non-zero cross-section for large-angle deflections, which obey Equation 2.30 and add long tails to the distribution.

2.7 Bremsstrahlung

Electrons traversing matter lose energy not just from ionization, but also from radiation. In fact, for energies above a few MeV, radiation loss, known as bremsstrahlung (braking radiation), becomes the dominant mode. It is principally due to interactions with nuclei, rather than with other electrons.

The nuclear electric field transfers energy to or from (accelerates) the traversing electron, and, while some of that energy manifests in the changes to the electron's (and, in fact, though often barely manifest, to the nucleus') kinetic energy, much of it is radiated as a continuous spectrum cut off by the electron's energy.

The spectrum is roughly inversely related to the energy, and the loss per unit thickness dx is given by

$$\left(\frac{dE}{dx}\right)_{\text{rad}} = -\frac{E}{X_0} \tag{2.35}$$

where, again X_0 is the radiation length. Note that this says that radiation loss is proportional to E, while Equation 2.1 says that ionization energy loss is independent of energy. Comparing the two equations gives the cross-over energy:

$$E_c \approx \frac{600}{Z} \text{ MeV} \tag{2.36}$$

Integrating over the thickness gives the average energy lost

$$\langle E \rangle = E_0 \exp\left(-\frac{t}{X_0}\right) \tag{2.37}$$

where E_0 is the electron's initial energy. This is actually the standard way of determining radiation lengths: measuring the thickness at which the energy is reduces by a factor e.

The effect can also be pictured as a sort of quantum field theory process.

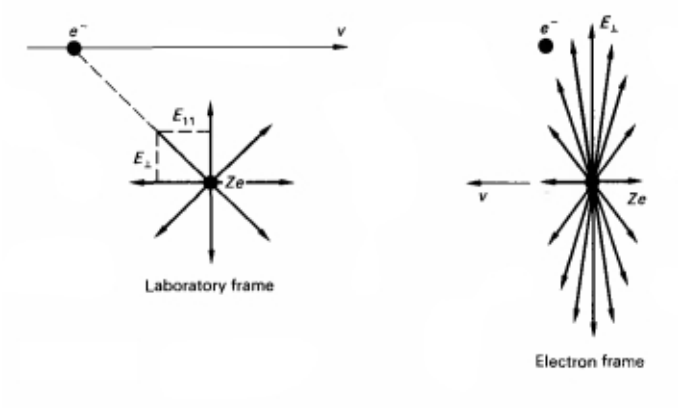

Figure 2.12: "Field-theory" representation of bremsstrahlung

Viewed from the traversing electron's rest frame, the charged nucleus approaches the stationary electron. The transverse component of the nuclear electric field, $E_\perp$, increases as γ, and it will be accompanied by a transverse magnetic field $B_\perp = \beta E_\perp \approx E_\perp$. From the viewpoint of the electron, an electromagnetic pulse–that is, a stream of virtual photons–from the nucleus approaches at velocity β. It may then scatter one of the photons, via the Compton effect, into a real state, losing energy in the process.

2.8 Photon Absorption

Three physical phenomena are primarily responsible for matter's absorption of γ-rays:

1. photoelectric effect
2. Compton scattering
3. pair production

Both the photoelectric effect and pair production result in total absorption; Compton scattering results in energy loss.

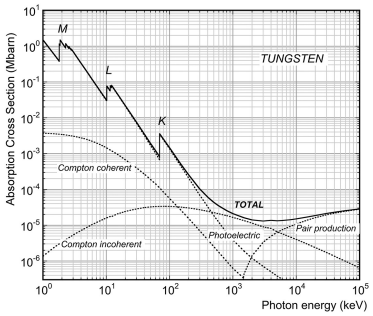

Figure 2.13: Competing processes of photon absorption as a function of photon energy

For photons of energy E traversing matter with atomic number Z, the photoelectric cross section varies as Z^4/E^3; the Compton scattering cross section varies as Z/E; and the pair-production cross section, just above the $2m_e = 1$ MeV threshold, varies as Z^2E, but flattens out to become approximately independent of energy at $E > 1$ GeV. Note that the photoelectric cross section exhibits discontinuities at the binding energies of each element's electron shell.

So different absorption processes dominate at different energies in different materials.

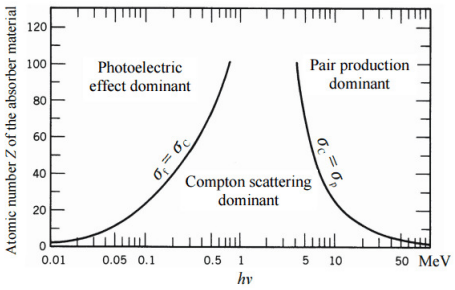

Figure 2.14: Energy and atomic number dependence of photon absorption process dominance

Like other absorption effects, pair production attenuates exponentially with depth. If I_0 is the intensity of a beam of high-energy photons,

$$I = I_0 \exp\left(-\frac{7t}{9X_0}\right) \tag{2.38}$$

The distance $\frac{9}{7}X_0$ is referred to as the conversion length.

2.9 Electromagnetic Showers

The combination of bremsstrahlung of high energy electrons and pair production of high energy photons results in cascade showers, in which an electron radiates photons which pair produce leading to annihilation or bremsstrahlung resulting in additional photons. And so on. The number of particles increases exponentially in the material.

Ignoring other effects, including those we've already discussed, we can imagine in a simplified way that the number of particles doubles, and the energy per particle halves, each radiation length, so that after n radiation lengths, there will be $N = 2^n$ particles each with energy $E(n) = E(0)/2^n$. We assume further that at E_c, radiation loss ceases and ionization loss completely takes over. In other words, the shower will cease developing at depth

$$n_{\max} = \frac{\ln\left(E(0)/E_c\right)}{\ln 2} \tag{2.39}$$

where the shower size (in terms of numbers) will be

$$N_{\max} = e^{n_{\max}\ln 2} = \frac{E_0}{E_c} \tag{2.40}$$

This will also approximately be the length of the shower in units of radiation lengths:

$$\ell \approx \int_0^{n_{\max}} N dn = \int_0^{n_{\max}} 2^n dn = \frac{2^{n_{\max}} - 1}{\ln 2} \approx \frac{E_0}{E_c} \tag{2.41}$$

The number of particles with energies greater than E:

$$N(>E) = \int_0^{n(E)} N dn = \int_0^{n(E)} e^{n\ln 2} dn \approx \frac{e^{n(E)\ln 2}}{\ln 2} = \frac{E(0)/E}{\ln 2} \tag{2.42}$$

Thus, the differential energy spectrum of particles is

$$\frac{dN}{dE} \propto \frac{1}{E^2} \tag{2.43}$$

In sum, the maximum track depth increase logarithmically with initial energy, the number of shower particles at the maximum is proportional to the initial energy, as is the total track length integral. Thus, it is possible to determine the energy of high energy photons and electrons by measuring any or all of these quantities.

Chapter 3

Accelerators

3.1 Introduction

Creating bound states and unstable particles and studying the structure of objects through scattering requires projectiles, which are characterized by energy

$$E = \begin{cases} K + m \\ \frac{2\pi}{\lambda} \end{cases} \tag{3.1}$$

in terms of "matter" or wave.

Naturally occurring projectiles are produced in radioactive decays and by cosmic sources, but these have limited intensity, lack energy tunability, and are, by nature, stochastic. Investigation requires control. "Artificial" sources–accelerators and beam transport systems–provide this.

Providing projectiles for an experiment involves

1. Isolating a species of projectile
2. Accelerating ensembles of these projectiles
3. Steering and delivering the projectiles to the experiment

3.1.1 Beam or Accelerator Physics

The study of, and the development of technology associated with, isolating desired projectiles (usually some species of charged particle), collecting them into ensembles occupying similar phase-space (position and momentum) coordinates, and interacting them with electromagnetic fields, is the domain of beam or accelerator physics. On occasion, additional parameters, such as mass, charge, or spin, may be included.

Ensembles whose constituents share these mechanical parameters are referred to as beams. Controlling such a beam typically implies conserving this constrained volume in phase space, referred to as the emittance.

A standard approach to studing and designing for beam ensembles is to identify a reference particle against which to consider all other particles' motion. Frequently, beam density is low enough to neglect interactions between consituents, allowing for a simpler collective model. Violations of this assumption are important concerns.

The fields interacting with the ensemble are electromagnetic, so the motion is governed by the Lorentz force

$$\mathbf{F} = q(\mathbf{E} + \mathbf{v} \times \mathbf{B}) = \mathbf{F}_E + \mathbf{F}_B \tag{3.2}$$

Since $\mathbf{v} \times \mathbf{B} \perp \mathbf{v}$, $\mathbf{F}_B$ does no work on the particle, and so increasing particle energies is done by $\mathbf{F}_E$.

On the other hand, since, as $v \Rightarrow c$, an electric field gradient of about 300 MV/m would be required to bend the particle trajectories as much as would a 1-tesla magnetic field, and since a 1-tesla magnetic field is commonplace, while 300 MV/m electric field gradients are not (yet) feasible,[1] $\mathbf{F}_B$ is more effective than $\mathbf{F}_E$ at steering trajectories.

3.2 Sources

3.2.1 Electrons

Quasi-free electrons are in abundance in metals, from which they can be extracted by various means and formed into beams.

Electrons, normally emitted at low energy, are accelerated away from the cathode by an electric field, but the resulting space charge reduces the field at the surface of the cathode. If the field falls to zero, no further current can be can be drawn from the cathode. The current density at which the electric field goes to zero is called the Child-Langmuir current limit, which, for a parallel-plate arrangement is,

$$J_{\mathrm{CL}} = \frac{1}{9\pi}\sqrt{\frac{2e}{m}}\left(\frac{V^{3/2}}{d^2}\right) \tag{3.3}$$

where V is the voltage difference between anode and cathode, d is the distance between plates, and e and m are the charge and mass of the electron.

Heating

The Fermi-Dirac distribution describes how electrons inside a (solid) metal are arranged in terms of energy levels

$$n(E)dE \propto \frac{\sqrt{E}\ dE}{1 + e^{(E-E_F)/T}} \tag{3.4}$$

where E_F the highest energy level filled at $T = 0$ K, and $k_B = 1$ in natural units. Increasing the metal's temperature moves electrons to higher energy states, which may eventually exceed the metal's work-function, ϕ_w. The resulting current density of such extractable elections is given by the so-called Richardson-Dushman equation,

$$J = AT^2 e^{-e\phi_w/T} \tag{3.5}$$

The factor A is independent of the temperature, but is characteristic of the metal.

Thus, one chooses the working metal by optimizing A and work function such that the electron intensity requirement is satisfied at a temperature below the metal's melting point. Often, this involves coating a metal with another metal or developing compounds.

High currents are possible, but the emission surface is large and the momenta are varied, leading to a large emittance.

[1] The RF cavities of the LHC have electric field gradients of about 100 MV/m; plasma wakefield acceleration has achieved gradients of about 200 MV/m, but hopes to reach 1 GV/m.

Photoelectic effect

Electrons will be emitted from the surface of a metal or semi-conductor when it is impinged by a photon whose energy exceeds the material's workfunction.

$$K_{\max} = h\nu - \phi_w \tag{3.6}$$

Considering wavelengths to be measured in nanometers, the maximum photon wavelength leading to emission is given by

$$\lambda_{\max} = \frac{1240}{\phi_w} \tag{3.7}$$

Actually, taking into account thermal effects, leading to electrons occupying levels above the Fermi energy, low currents can be extracted with photons abovw this threshold.

Because metals tend to reflect as well as absorb photons, leading to low photoelectron production efficiency, measured by what is known as the quantum efficiency Q_e, the ratio of emitted electrons to incident photons. Semiconductors are not as conductive or reflective, so, not only do few photons reflect off the surface, but more penetrate well below the surface leading to much larger quantum efficiencies.

Again, the emittance of electrons from the photoelectric effect is large, due to large surfaces and wide range of momenta.

Field Emission

A sharp metal needle in an electric field becomes an equipotential surface, and a very strong field is induced at the tip (think of a lightening rod). With a strong enough potential difference between cathode and anode, electrons can be pulled from the tip, emerging thus from a point with ratherly uniformly low momenta. This can provide a low emittance beam, but tends to break down, limting current.

3.2.2 Ions

The great variety of ions that are accelerated demand many different approaches to their production, but essentially all ion sources consist of two parts, a plasma generator and an extraction system. A plasma generator provides ions to the extraction system, which selects the correct ions, rejects the wrong ones (as well as electrons and neutral particles), shapes an ensemble of ions in terms of position and divergence angles, and finally delivers it to the next stage of the accelerator.

Among the methods for producing plasmas include electrical discharges, heat, lasers, and even beams of other particles. The key factor is that the plasma must be stable for long enough to extract the sort of beam the application requires.

Bombarding surfaces with electrons, protons, or photons can extract ionized atoms from non-gaseous materials. The ions can be drawn away with an electric field. The resulting current from this method is usually small.

A common method for extracting ions from a gas is to pass an intense electron beam through it. The electrons are accelerated to a kinetic energy in excess of the ionization energy of the gas atoms. A magnetic field locks the electrons in an helical orbit from gun to trap, increasing the pathlength through the gas. Collisions form ions extracted with an electric field.

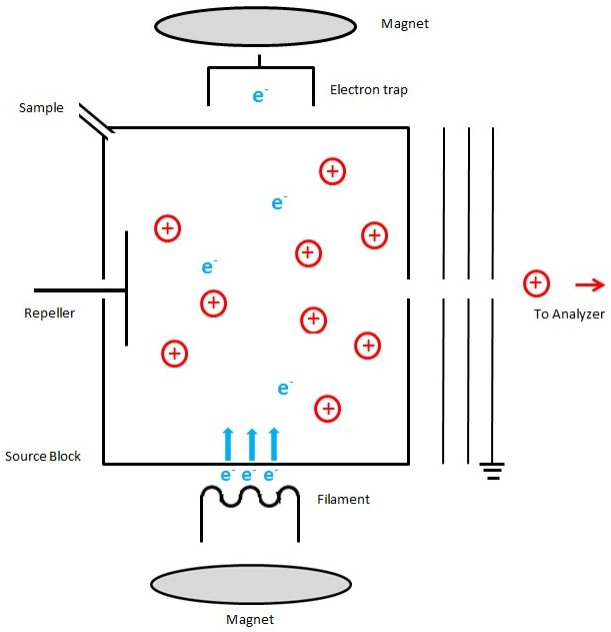

Figure 3.1: Creating and extracting ions from a gas

3.3 Acceleration

Accelerating charged particles can be accomplished with DC voltages or time-varying fields.

DC Acceleration

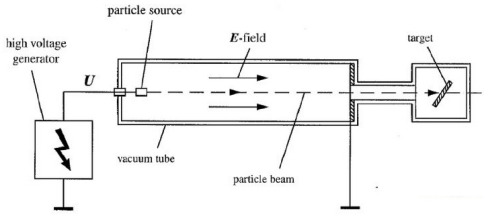

Figure 3.2: Simple DC acceleration by electric field: $\Delta E = qV$

The simplest mode of DC acceleration involves a constant electric field, **E**, between two electodes, one of which contains particle source. The voltage is limited to the energy at which the beam ions or electrons begin creating additional ions and electrons in collisions, which leads to a breakdown of the field.

A somewhat more sophisticated approach to DC acceleration is to stage voltage drops with resister chain, so that the beam particles accelerate over multiple gaps.

This approach is also subject to voltage breakdown, with a limit of about 10 MV.

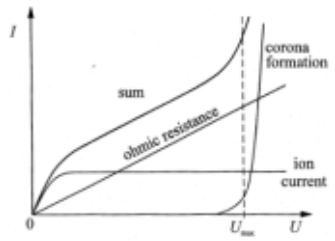

Figure 3.3: Current versus DC voltage, showing field breakdown

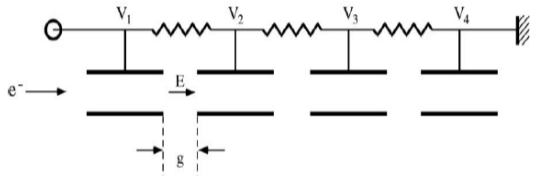

Figure 3.4: DC acceleration with a resistor chain; each stage at a different voltage, so there's a field across the gap

Cockcroft & Walton rectifier: Another way to create a DC voltage is to rectify (with a diode-capacitor circuit) an AC voltage. A high DC voltage can be created from a low AC voltage by cascading rectifier circuits. Each rectifier-capacitor group doubles voltage difference, so, given n rectifers, $V_{\max} = 2nV$ is the theoretical maximum. In practice, current losses limit the maximum voltage to $V_{\max} \approx 4$ MV.

$$V_{\max} = 2nV - \frac{2\pi I}{\omega C}\left(\frac{2}{3}n^3 + \frac{1}{4}n^2 + \frac{1}{12}n\right) \tag{3.8}$$

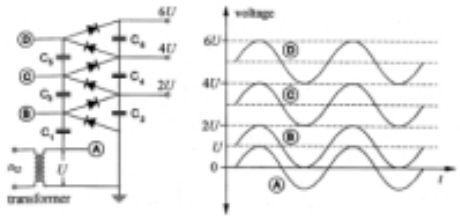

Figure 3.5: A Cockcroft-Walton rectifier ladder, to which the input is $V(t) = V \sin \omega t$ and the output is $V_{out} < 2nV$

Van de Graaf generator: Yet another method for generating strong DC voltages is to collect charge mechanically on one side of a capacitor. A Van de Graaff generator accumulates charge on a hollow metal sphere atop an insulated column. The charge is transferred to a belt by rubbing it against a dissimilar material. It carries these charges to the sphere where they are transferred from the belt.

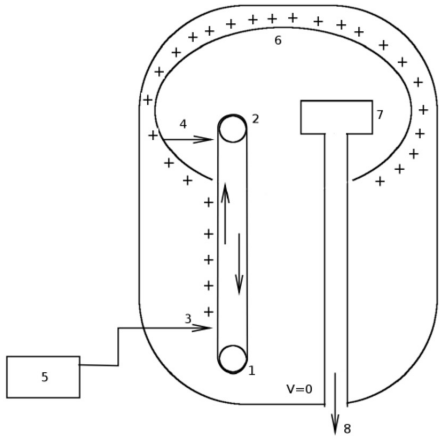

Figure 3.6: Van de Graaff generator: (1) lower roller, (2) upper roller, (3) charging electrode, (4) electrode collecting positive charge, (5) voltage generator, (6) spherical electrode (high voltage terminal), (7) ion source, (8) extracted ion beam; a resistor-electrode train accelerates beam down extraction tube to target, greatly reducing possibility of spark discharge

A Van de Graaff generator can produce voltage differences of $V_{\max} \approx 2 - 10$ MV. It is used for low-energy nuclear physics experiments, to produce X-ray beams for nuclear medicine, to sterilize food, and to process materials.

Tandem accelerator: The DC acceleration of a Van de Graaff generator may be approximately doubled by employing it in tandem mode first accelerating negatively-charged beam particles and then accelerating the same particles again, but now positively-charged. The ion source produces negative ions which are accelerated and sent through a stripping foil, which strips at least two electrons from the negative ions, leaving them positively charged. These are accelerated through same potential difference but opposite polarity to extraction. The energy is thus approximately doubled: $V_{\max} \approx 4 - 20$ MV.

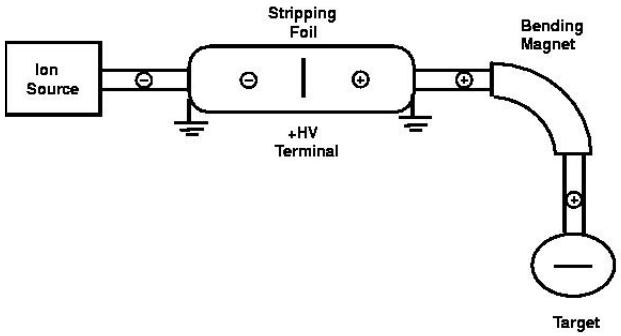

Figure 3.7: Tandem accelerator

Time-Varying Fields

In general, acceleration by time-vaying fields is accomplished with oscillating EM fields at radio-wave frequencies (RF).

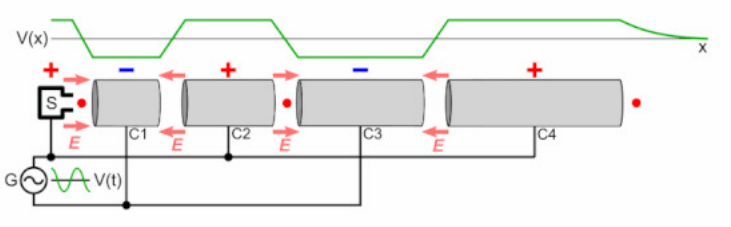

Figure 3.8: Linear accelerator employing time-varying fields

Beam particles interact with the field only half the time, when its direction is that of the boost direction. This is referred to as the synchronism condition:

$$T_{\text{particle}} = \frac{1}{2} T_{\text{RF}} \tag{3.9}$$

$$\ell = \frac{1}{2} v T_{\text{particle}} \tag{3.10}$$

where ℓ is the length of the drift or conducting tube. Acceleration thus occurs over only half the cycle. An important consequence of this is that the beam forms a microstruction, called bunching. This happens by applying the boosting field between edges of conducting tubes of increasing length, so particles are shielded from reverse fields during the other half of the cycle.

Charged particles lose energy by radiating when accelerated, but such losses have been limited by the development of cavities to store EM power in resonant volumes.

Non-resonant (unbunched)

Betatron: A circular apparatus is an alternative to a linear acceleration, and a monotonic interaction is an alternative to an alternating voltage. The betatron exploits Faraday's Law of Induction, in which an electromotive force (EMF)–the electromagnetic work done on a unit charge as it travels around a conductive loop–arises when the magnetic flux through the surface enclosed by the loop varies in time. If the magnetic field increases with the momentum of the particle, the particle's orbital radius will remain unchanged.

As the machine name implies, the betatron is an electron accelerator.

Figure 3.9: Betatron schematic (left) and operating principle (right)

$$
\begin{aligned}
\mathcal{E} &= \frac{d\phi_B}{dt} \\
e\mathcal{E} &= e\frac{d\phi_B}{dt} = dW \\
F &= \frac{dp}{dt} = \frac{dW}{ds} = \frac{e\mathcal{E}}{2\pi r} = \frac{e}{2\pi r}\frac{d\phi_B}{dt} \\
dp &= \frac{e}{2\pi r} d\phi_B \\
evB &= \frac{\gamma m v^2}{r} \\
\gamma m v &= p = eBr \\
dp &= er\ dB \\
\frac{e}{2\pi r} d\phi_B &= er\ dB \\
d\phi_B &= 2\pi r^2 dB \\
\phi_B(t) &= 2\pi r^2 B(t) \\
B(t) &= \frac{1}{2}\frac{\phi_B(t)}{\pi r^2}
\end{aligned}
\tag{3.11}
$$

The instantaneous magnet field at the orbit is half the average flux through the loop. The current loop is a donut-shaped vacuum tube that runs through a gradient field at the edge of a dipole.

The maximum energy, about 100 MeV, is limited by the magnetic field strength, which is itself limited by the size of the magnet and flux saturation in the iron.

Resonant (bunched)

Cyclotron: An electric field alternating at a fixed frequency and a constant, uniform magnetic field results in a spiraling particle beam with an increasing orbit.

In a cyclotron, "dees," D_1 and D_2 in the figure, are connected to opposite poles of a high-frequency (MHz) electromagnetic oscillator, with $V_{\max} = 10 - 200$ kV. A perpendicular magnetic field leads to circular orbits:

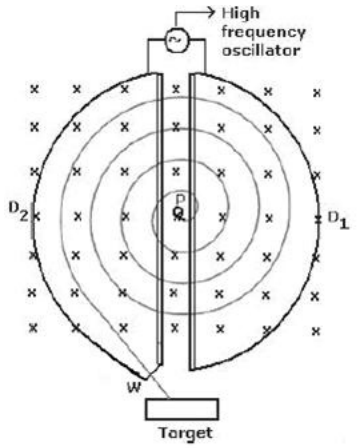

Figure 3.10: A schematic of a cyclotron; the ion source injects at the center (letter P)

$$qvB = m\frac{v^2}{r} \tag{3.12}$$

The field swaps polarity in the time it takes for particles to complete a half-circle, so, at each crossing, they are accelerated by the field:

$$\begin{aligned} v &= \frac{qBr}{m} \\ T &= \frac{\pi r}{v} = \frac{\pi m}{qB} \end{aligned} \tag{3.13}$$

Notice that the period is independent of trajectory radius. The radius of the beam's trajectory increases with momentum until extracted to bombard target.

The proper cyclotron frequency, ω_c, can be found by solving the magnetic term of the Lorentz force:

$$\mathbf{F} = q\mathbf{v} \times \mathbf{B} \tag{3.14}$$

$$F = \frac{dp}{dt} = m(\dot{v}_x, \dot{v}_y, 0) = q(v_y B_z, -v_x B_z, 0) \tag{3.15}$$

$$\ddot{v}_x = \frac{q}{m}\dot{v}_y B_z = -\frac{q^2}{m^2} v_x B_z^2 \tag{3.16}$$

$$\ddot{v}_y = -\frac{q}{m}\dot{v}_x B_z = -\frac{q^2}{m^2} v_y B_z^2 \tag{3.17}$$

$$v_x(t) = v_0 \cos(\omega_c t) \tag{3.18}$$

$$v_y(t) = v_0 \sin(\omega_c t) \tag{3.19}$$

$$\omega_c = \frac{q}{m} B_z \tag{3.20}$$

For different $\frac{m}{q}$ (that is, different ions), either the magnetic field or the oscillator/cyclotron frequency has to be adjusted.

Relativistic effects limit the acceleration of light particles to around 20 MeV, since, at relativistic velocities, increases in v diminish with energy. Higher masses can be accelerated to higher energies at non-relativistic speeds.

Cyclotrons are currently used to analyze materials, transmute elements, proton cancer therapy, and production of positron-emitting isotopes (PET imaging) and other radioisotopes for medical diagnostics.

Betatrons are used to accelerate electrons, while cyclotrons are used to accelerate protons and ions–all at relatively low energies.

Linac: Again, a linac (linear accelerator) consists of metal drift tubes arranged along the beam axis and alternately connected to opposites sides of an alternating voltages source:

$$V(t) = V_{\max} \sin(\omega t) \tag{3.21}$$

where ω is in the radio frequency range, 20 kHz - 300 GHz. By the time particles of charge q reach the nth drift tube, they have energy

$$E_n = nqV_{\max} \sin \Phi_s \tag{3.22}$$

where Φ_s is the average phase at the gap. Note that $V < V_{\max}$, so that the linac can work at maximum potential without breakdown due to the presence of charged particles. Assuming $v \ll c$, $E_n = \frac{1}{2}mv_n^2$ at the nth drift tube. Alternating drift tubes are a half-period apart, so the distance from one gap to the next is

$$\ell_n = v_n \frac{T_{\mathrm{RF}}}{2} = \frac{v_n}{2\nu_{\mathrm{RF}}} = \frac{1}{\nu_{\mathrm{RF}}} \sqrt{\frac{nqV_{\max} \sin \Phi_s}{2m}} \tag{3.23}$$

Continuous acceleration requires synchronization with the RF wave: particles must be injected with–and maintain–a well-defined phase with respect to the oscillating field. In practice, ensemble particles are in-phase and all at energy. If injection occurs prior to or at peak phase, phase differences will be amplified and the ensemble will disperse.

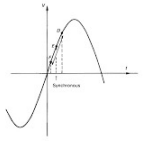

Figure 3.11: Linear accelerator beam synchronization

Phase focusing occurs, when $\beta \ll 1$, if

$$\Phi_s < \frac{\pi}{2} \tag{3.24}$$

$$V_{\mathrm{eff}} < V_{\max} \tag{3.25}$$

Synchrotron: The power capacity of a RF cavity is limited–when over-extended, the fields break down–limiting the energy increase per unit length. The only way to increase the beam energy is to add more cavities, but these, and real estate are expensive. Circular accelerators allow cavities to be reused continually. On the other hand, the particle trajectory must be closed, requiring magnets. Also, transverse acceleration results in higher radiation losses than longitudinal acceleration.

In a synchrotron, particles are constrained to a roughly circular, fixed-radius orbit by arrays of relatively small electromagnets. The particles traverse one or more RF cavities repeatedly and are thereby accelerated. To stay in orbit, both RF frequency and magnetic fields synchronously increase. The challenge: retain beam particles traveling thousands or millions of km at nearly light speed inside a small vacuum tube of constant (average) radius. The keys to this stability are phase stability and transverse focusing.

Phase Stability

The first step is to define a reference trajectory, s, referred to as a synchronous particle.

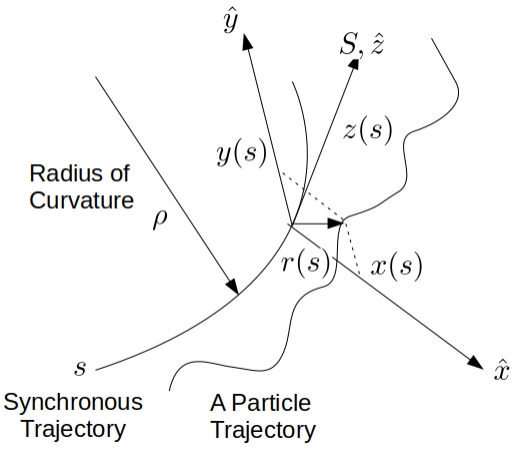

Figure 3.12: Coordinate system of a synchrotron accelerator

Being synchronous means that the RF frequency, ω_{RF}, and (a multiple of) the revolution frequency, ω_s, are locked.

$$\omega_{\mathrm{RF}} = h\omega_s \tag{3.26}$$

$$\begin{aligned} qv_sB &= \frac{Mv_s^2}{\rho} \\ \frac{v_s}{\rho} &= \omega_s = \frac{eB}{M} \end{aligned} \tag{3.27}$$

where h is the so-called harmonic number. As ω_s increases, both the RF frequency and must the magnetic field synchronously increase.

An oscillating RF-field can be represented as a sinusoidal function:

$$E_z = E_{\max} \sin\left(\omega_{\mathrm{RF}} t\right) \tag{3.28}$$

If the field is assumed constant during transit interval (no transit-factor), then the work done is:

$$\Delta E = W = \int F \; dz = q \sin(\omega_{\mathrm{RF}} t) \int E_{\max} \; dz = q V_{\max} \sin(\omega_{\mathrm{RF}} t) = q V_{\max} \sin \phi_s \tag{3.29}$$

where ϕ_s is an RF phase.

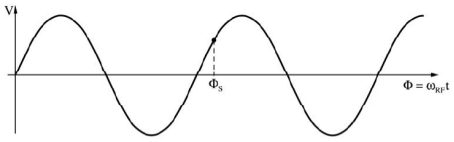

Figure 3.13: RF phase

A synchronous particle encounters the same RF phase, ϕ_s, each revolution. A bunch consists of $10^{11} - 10^{12}$ particles, few of which have the same momentum/energy. That is, there will be many non-synchronous particles, whose momenta will differ from that of the synchronous particles' momenta, p, by dp.

$$\begin{aligned} p &= \beta\gamma m = \beta\gamma E_0 \\ dp &= \gamma^3 E_0 d\beta \\ \frac{dp}{p} &= \gamma^2 \frac{d\beta}{\beta} \end{aligned} \tag{3.30}$$

Particles of different energies/momenta have different trajectories through the steering magnets, that is, they will see different magnetic fields and so be displaced differently. With reference to the position of the synchronous particle trajectory:

$$dx(s) = D(s) \frac{dp}{p} \tag{3.31}$$

where $D(s)$ is called the dispersion function, characteristic of the beam optics (arrays of magnets). Momentum spread thus results in beam radius spread

$$\frac{dr}{r} = \alpha \frac{dp}{p} \tag{3.32}$$

where α is called the compaction factor.

$$\alpha \equiv \frac{1}{C} \oint \frac{D(s)}{r(s)} ds \tag{3.33}$$

where C is the trajectory circumference.

With respect to orbital frequency, what happens to non-synchronous particles depends on the energy regime of the beam:

For $\beta \ll 1$, energy/momentum increases increase ω; as $\beta \to 1$, they do not. There's a maximum frequency at which a transition occurs.

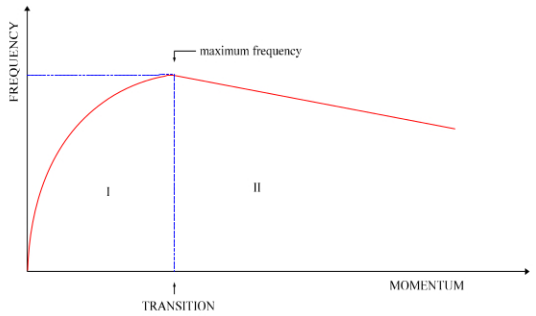

Figure 3.14: Revolution frequency as a function of momentum; note the transition in the function at a maximum frequency

$$\omega = \frac{\beta}{r}$$
$$\frac{d\omega}{\omega} = \frac{d\beta}{\beta} - \frac{dr}{r} = \left(\frac{1}{\gamma^2} - \alpha\right)\frac{dp}{p} \tag{3.34}$$

This leads to the so-called slip factor

$$\eta = \frac{d\omega/\omega}{dp/p} = \frac{1}{\gamma^2} - \alpha \tag{3.35}$$

which gives the relationship between revolution frequency and momentum for a given accelerator. Note that it depends on both optics and momentum. The slip factor $\eta > 0$ before the transition and negative after. This implies:

$$\alpha = \frac{1}{\gamma_{\mathrm{TR}}^2} \tag{3.36}$$

at the transition, and $d\omega/\omega = 0$, i.e., all particles have the same revolution frequency.

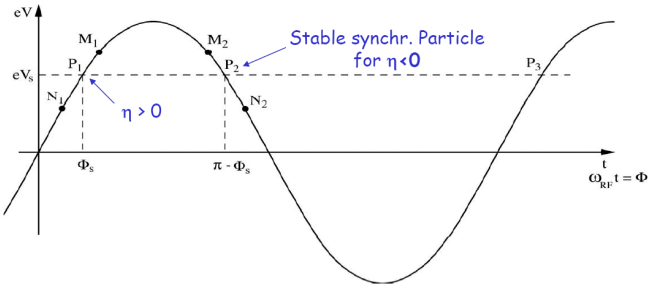

Figure 3.15: Phase stability on the RF phase diagram

When $\beta \ll 1$, momentum boosts increase particle velocity quickly, and the revolution frequency correspondingly increases quickly. Particles arriving ahead of synchronous particles receive a smaller boost than do the synchronous ones, and so don't gain as much momentum, their velocity and revolution frequency do not increase as much, and visa versa for those behind. At the transition energy/momentum, the revolution frequency is maximal and universal. As $\beta \to 1$, particle velocity is essentially constant, and momentum gain leads to smaller revolution frequencies. The RF phase for synchronous particles must be altered from $\phi_s \to \pi - \phi_s$. Particles arriving ahead of a synchronous particle receive a greater momentum boost, which, in the same field, means that their orbit radius will be larger and, therefore, their orbital velocity, $\omega < \omega_s$, and they tend toward the synchronous orbit. Particles arriving behind the synchronous ones receive a smaller momentum boost, which, in the same field, means their orbital radius will be smaller and, therefore, their orbital velocity $\omega > \omega_s$, and they tend toward the synchronous orbit. The result of all this is that the particles stay in the bunch by undergoing so-called synchrotron (longitudinal) oscillations about the synchronous orbit, maintining a condition referred to as phase stability.

The transition energy/momentum, again, depends on optics, so is characteristic of the accelerator, but is typically around 10 GeV for protons. For electrons, $\beta \to 1$ at relatively low momentum, nearly all electron synchrotons operate above transition.

3.4 Transport

To restate the situation: between 100 billion and 1 trillion particles, essentially all with different initial coordinates and velocities have to stay together within a few centimeters longitudinally and a few hundred microns perpendicularly for up to millions of kilometers traveling near the speed of light. We've already considered how ensembles of beam particles are created and how they are accelerated, and the way RF acceleration bunches the particles and maintains the longitudinal extent of those bunches. Here, we consider consider perpendicular motion, classified into radial (x) and transverse (y) directions, as opposed to the longitudinal or tangential (s) direction.

Focusing

Steering and transport of beams are accomplished through the use of arrays (often referred to as "strings") of magnetic, electrostatic, and/or electromagnetic devices interspersed with so-called drift (field-free) regions. The full collection of these devices is referred to as the lattice, now made up primarily of dipole and quadrupole magnets. Dipoles primarily determine the geometry of the transport system. Multipole magnets tend to be centered on the beam for the sake of focusing it. But recall the dispersion function, $D(s)$. The total effect of all of this is collectively called the accelerators optics.

As with longitudinal motion, particle motion is referenced to a certain class of particles, in this case, those that traverse precisely the center of the multipole magnets in a trajectory referred to as a central, equilibrium, or closed orbit.

Particles with the same momentum as the equilibrium ones, but slightly deviated spatially, undergo betatron (perpendicular) oscillations about the central orbit in both radial, $x(s)$, and transverse, $y(s)$, directions relative to the orbital plane. Particles whose momenta only differ from that of the equilibrium particles undergo off-momentum orbits, synchrotron oscillations, primarily a longitudinal issue. If these, however, are spatially deviated, as well, they (betatron) oscillate about the off-momentum orbit.

Dipole fields are perpendicular to the orbital plane, affecting the radial motion. With reference to the central orbit (curvature ρ),

$$F = qvB = \frac{mv^2}{\rho}$$
$$B\rho = \frac{p}{q} \tag{3.37}$$

Again, as p increases, B must increase.

The quantity $B\rho$ is referred to as the magnetic rigidity, and has units of tesla-meters when p is in GeV/c, and GeV in natural units (so magnetic field strength is in GeV^2). For a singly-charged particle, then, $B\rho \approx 3.33p$ GeV (recall that $e = 0.303$).

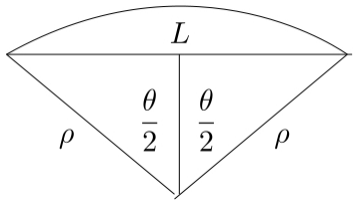

Figure 3.16: The trajectory geometry of in a dipole magnetic field

$$\sin\frac{\theta}{2} = \frac{L}{2\rho} = \frac{LB}{2B\rho}$$
$$\theta \approx \frac{LB}{B\rho} = \frac{qLB}{p} \tag{3.38}$$

That is, the bend for a given field strength is proportional to the length of the magnet traversed and inversely proportional to the beam particles' momentum.

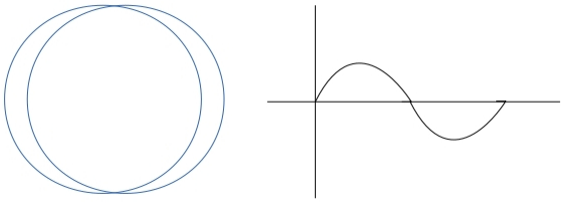

Figure 3.17: Off-axis trajectory

Particles displaced radially and/or transversely from the central orbit enter the dipole at a different initial angle and spiral around the central orbit, but never close, leading to instabilities. They need to be focused, to more closely approximate the central orbit. This is the job of quadrupole magnets, which has no field along the central axis, but otherwise $B_y \propto x$ and $B_x \propto y$.

Notice that a particle deviated from the central axis in the vertical plane, is deflected towards the center of the magnet, while a particle deviated in the horizontal plane is deflected further away from the center. That

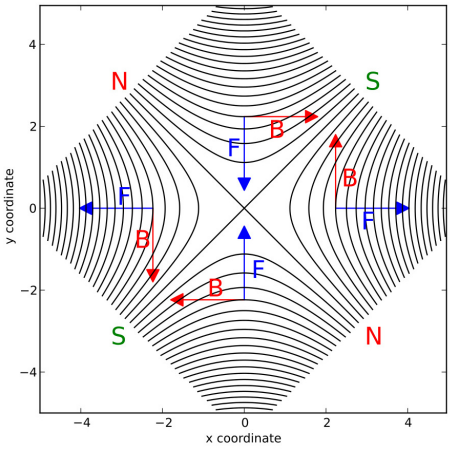

Figure 3.18: Quadrupole field; force vectors indicative of a beam of positively charged particles coming out of the page

is, this magnet, known as a defocusing quad (reference to the horizontal plane) focuses vertically deviated particles but defocuses horizontally deviated particles. The converse is true of a focusing quad. Overall focusing can be accomplished, in analogy with optical lense arrays, with series of alternating focusing and defocusing magnets separated by drift regions, often in sets referred to a a FODO lattice, to which one or more dipole magnets and a RF cavity may be integrated.

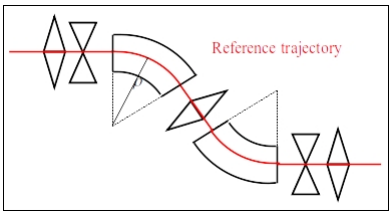

Figure 3.19: FODO lattice with dipole magnets

Perpendicular motion is characterized by its displacement from the central trajectory, $x(s)$ or $y(s)$, and its direction (small angle approximation) with respect to the central trajectory, $x'(s) = \frac{dx}{ds}$ or $y'(s) = \frac{dy}{ds}$. The resulting motion, called betatron oscillations, is oscillatory around the central trajectory.

The equation of perpendicular motion is given, then, by an equation like

$$\frac{d^2x(s)}{ds^2} + k(s)x(s) = 0 \tag{3.39}$$

and similarly for $y(s)$, where we now take the focusing plane to be horizontal and the defocusing plane to be vertical.

The restoring force is position-dependent, and therefore not constant, but it is periodic: $k(s+L) = k(s)$. Thus, the oscillation will be quasi-harmonic, such that the amplitude and phase will also depend on s.

Because $\mathbf{F}_B = q\mathbf{v} \times \mathbf{B}$, and quadrupole fields increase linearly with deviation along either axis

$$K = \frac{dB_y}{dx} = \frac{dB_x}{dy} \tag{3.40}$$

we can define

$$B_y = Kx \quad B_x = Ky \tag{3.41}$$

We note that in this situation (no E-field or currents), the Maxwell equation

$$\boldsymbol{\nabla} \times \mathbf{B} = 0 \tag{3.42}$$

so that

$$\mathbf{B} = -\boldsymbol{\nabla} V \tag{3.43}$$

so

$$V(x, y) = Kxy \tag{3.44}$$

Normalizing the gradient to the momentum, or, rather the magnetic rigidity

$$k = \frac{K}{B\rho} \tag{3.45}$$

gives us the ingredients of the differential equations (for the defocusing plane, $k \to -k$). The periodic nature of the restoring force makes Equation 3.39 a so-called Hill equation. It is an approximation ignoring accelerating fields and multipole magnets higher than quadrupoles. Assuming k is linear, B is constant, and we take only first-order terms, it has the general solution, for horizontal focusing,

$$x(s) = x(0)\cos(\sqrt{k}s) + \frac{x'(0)}{\sqrt{k}}\sin(\sqrt{k}s) \tag{3.46}$$

$$x'(s) = -x(0)\sqrt{k}\sin(\sqrt{k}s) + x'(0)\cos(\sqrt{k}s) \tag{3.47}$$

and vertically,

$$y(s) = y(0)\cosh(\sqrt{k}s) + \frac{y'(0)}{\sqrt{k}}\sinh(\sqrt{k}s) \tag{3.48}$$

$$y'(s) = y(0)\sqrt{k}\sinh(\sqrt{k}s) + y'(0)\cosh(\sqrt{k}s) \tag{3.49}$$

and vice versa for vertical focusing.

The trajectory in each quadrupole is a portion of an harmonic oscillation, but the idiosyncratic characteristics of different devices means that the solution will look different at each location, hence the s dependence. The number of oscillations per circumnavigation in each plane is called the tune, given by Q_x and Q_y, the horizontal and vertical beam tunes.

These transformations can be written in a matrix formalism:

$$\begin{pmatrix} x(s) \\ x'(s) \end{pmatrix} = M \begin{pmatrix} x(0) \\ x'(0) \end{pmatrix} \tag{3.50}$$

where

$$M_{\text{focus}} = \begin{pmatrix} \cos(\sqrt{k}s) & \frac{1}{\sqrt{k}}\sin(\sqrt{k}s) \\ -\sqrt{k}\sin(\sqrt{k}s) & \cos(\sqrt{k}s) \end{pmatrix} \tag{3.51}$$

and

$$M_{\text{defocus}} = \begin{pmatrix} \cosh(\sqrt{k}s) & \frac{1}{\sqrt{k}}\sinh(\sqrt{k}s) \\ -\sqrt{k}\sinh(\sqrt{k}s) & \cosh(\sqrt{k}s) \end{pmatrix} \tag{3.52}$$

Also, in drift and pure dipoles, $k = 0$

$$M_{\text{drift/dipole}} = \begin{pmatrix} 1 & s \\ 0 & 1 \end{pmatrix} \tag{3.53}$$

Notice that the determinants of each of the matrices equals 1, which, because they are square matrices, implies that they belong to the special linear group, in which geometric properties are preserved.

The properties of each accelerator element can be translated into one such matrix, and thus the amplitude and angle of each particle trajectory can be determined at that position in the lattice. Further, multiplying the different matrices provides the trajectory, given some intial position and angle.

$$M_{\text{total}} = M_{\text{focus}} M_{\text{drift}} M_{\text{dipole}} M_{\text{drift}} M_{\text{defocus}} \cdots \tag{3.54}$$

To turn the integration constants, $x(0)$ and $x'(0)$, from initial conditions into parameters characterizing the beam, identify the phase advance (with s),

$$\psi_{\text{x,y}}(s) = \sqrt{k}s = \int_0^s \frac{ds}{\beta_{x,y}(s)} \tag{3.55}$$

the beam emittance (the area covered in x - x' phase space) and beta function (the beam envelope, or modulation amplitude of the optics),

$$\varepsilon\beta_{x,y}(s) =^2 (0) + \frac{x'^2(0)}{k} \quad \text{or} \quad y^2(0) + \frac{y'^2(0)}{k} \tag{3.56}$$

and initial phase,

$$\phi_{\text{x,y}} = -\tan^{-1}\frac{x'(0)}{x(0)\sqrt{k}} \quad \text{or} \quad -\tan^{-1}\frac{y'(0)}{y(0)\sqrt{k}} \tag{3.57}$$

$$x(s) = \sqrt{\varepsilon}\sqrt{\beta_x(s)}\cos[\psi_x(s) + \phi_x] \tag{3.58}$$

$$x'(s) = -\frac{\sqrt{\varepsilon}}{\sqrt{\beta_x(s)}}\{\alpha_x(s)\cos[\psi_x(s) + \phi_x] + \sin[\psi_x(s) + \phi_x]\} \tag{3.59}$$

$$y(s) = \sqrt{\varepsilon}\sqrt{\beta_y(s)}\cosh[\psi_y(s) + \phi_y] \tag{3.60}$$

$$y'(s) = \frac{\sqrt{\varepsilon}}{\sqrt{\beta_y(s)}}\{\alpha_y(s)\cosh[\psi_y(s) + \phi_y] + \sinh[\psi_y(s) + \phi_y]\} \tag{3.61}$$

where

$$\alpha_{x,y}(s) = -\frac{1}{2}\frac{d\beta_{x,y}(s)}{ds} \tag{3.62}$$

Since $\psi_{x,y}(s)$ is inversely related to $\beta_{x,y}(s)$, when the beam's transverse dimension(s) are large, the corresponding phase advance is small, and vice versa. The beam tunes are the net phase advances of the transverse oscillations per revolution in units of 2π,

$$Q_{x,y} = \frac{1}{2\pi}\oint \frac{ds}{\beta_{x,y}(s)} \tag{3.63}$$

A plot of $x'(s)$ versus $x(s)$ is an ellipse, with (dropping subscripts) $x_{\max} = \sqrt{\varepsilon\beta}$, at which $x' = -\alpha\sqrt{\frac{\varepsilon}{\beta}}$, and $x'_{\max} = \sqrt{\varepsilon\gamma}$, at which $x = -\alpha\sqrt{\varepsilon}\gamma$, where

$$\gamma = \frac{1+\alpha^2}{\beta} \tag{3.64}$$

The ellipse is also described by the implicit equation

$$\varepsilon = \gamma x^2 + 2\alpha x x' + \beta x'^2 \tag{3.65}$$

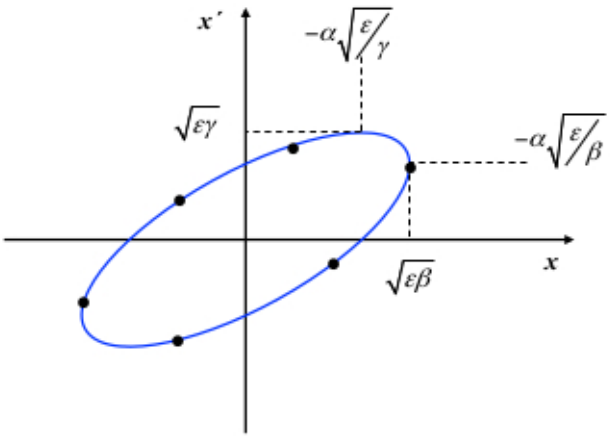

The area of this ellipse is $\pi\varepsilon$, which, according to Liouville's theorem, is constant under the influence of conservative forces. The beta-function (beam size) can be reduced with focusing, as it is near interaction regions, but then γ and therefore the trajectory angles increase. In any case, the beam size reduction is intrinsically limited by repulsion among the particles, known as the space-charge effect, and image charges along the vacuum tube.

Chapter 4

Detectors

4.1 Introduction

Reconstruction of a subatomic reaction implies satisfying the relativistic momentum-energy equation

$$m^2 = E^2 - |\mathbf{p}|^2 \tag{4.1}$$

not just for each constituent of the reaction individually, but for all of them simultaneously

$$\sum m = (\sum E)^2 - |\sum \mathbf{p}|^2 \tag{4.2}$$

Since each m and the sum of all m are invariants, and since each subatomic object is uniquely identified by its mass, satisfying these equations tells us what the parent and all daughters of the reaction were. In practice, the final state, which is comprised of especially long-lived particles–and not always all of these, is normally detectable.

Other methods for determining m include measuring the momentum and the velocity separately or determining the energy and the velocity separately:

$$p = \beta\gamma m \tag{4.3}$$
$$E = \gamma m \tag{4.4}$$

To reconstruct a subatomic reaction, then, it is necessary to determine some or all of the following: the identities of reaction constituents, where they were when, and such of their characteristics as momentum or velocity, energy, and spin and other angular momentum and associated values.

Rarely can a single instrument make all these measurements. Rather, combinations of detectors are integrated into an experiment. The core parts of experiments measuring subatom reactions include timing, tracking, and calorimetric (energy-measuring) instruments, as well as tools exploiting specific matter interactions to determine the velocities, momenta, energies, and/or identities of the constituents.

In general, tracking instruments, often embedded in a magnetic field, are closest to the reaction, followed in turn by those with precising timing and calorimeters. Interspersed and usually following are instruments for indentifying the various constituents.

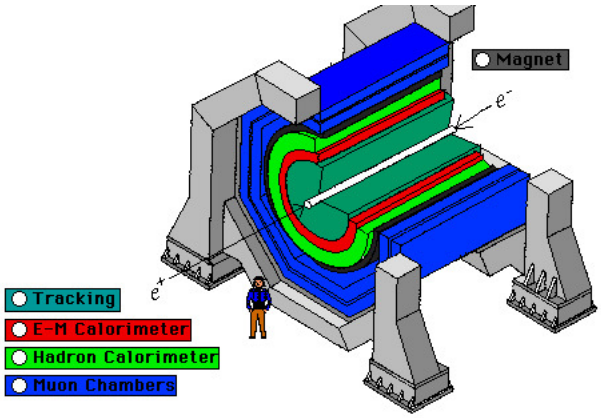

Figure 4.1: Typical, though basic, configuration of a modern sub-atomic particle experiment's detector

The quality of an experiment, quantified typically as a resolution or relative uncertainty, is limited by time, space, and energy resolution; detection efficiency; probability of misidentification; and two-particle time (rate) and space resolution. Momentum resolution is limited by space resolution and magnetic field strength. Velocity resolution is limited, depending on measurement method, by time resolution (time-of-flight), energy resolution (dE/dx), and space resolution (Cerenkov angle measurement).

4.2 Tracking

Due to ionization, charged particles traversing material can leave a record of their passage.

4.2.1 Emulsions

Cecil Frank Powell from Bristol University, the discoverer of the pion, is credited with developing emulsion exposures for detecting tracks of charged particles. His 1950 Nobel Prize was awarded for the development of the photographic method of studying nuclear processes and his discoveries regarding mesons made with this method. Emulsions have been used recently in neutrino experiments and are common in medicine.

Emulsion films are not really emulsions, but suspensions in a fluid. They contain AgBr and AgCl molecules suspended in geletin typically coated on a glass substrate. The geletin layer is about 50 times thicker, and silver the halide molecules are more than 50% denser, than the suspension of optical photographic film. The silver crystal grains are also 0.1 the size, and their sizes and distribution are more uniform.

Ionizing particles passing through the emulsion break up these molecules, leaving silver atoms. Individual silver atoms are unstable but are efficient electron traps. This leads to a clustering (nuclearization) of four or more silver atoms, known as a latent image center, whose typical diameters is around 0.5 μm.

The cluster is reduced to metallic silver when developed. Developing further fixes the metaliyc silver grains to the substrate, while the remaining gel and silver halide molecules are rinsed away. The grains may then be observed as black dots when viewed with a microscope.

The advantages of using emulsions include unsurpassed spatial resolution (0.2 μm) and the ability to measure both velocity (dE/dx) and momentum (amount of multiple scatter) in a single instrument. Disadvantages include limited volume, destructive processing required to visualize tracks, and no triggerability.

4.2.2 Gas-Filled Detectors

Whenever a charged particle passes through a gas, it collides with some of the molecules of the gas and disrupts these molecules. Often an electron may be driven away from the molecule, which is then said to be ionized. As a result of the presence of these ions and electrons the gas gains electrical conductivity. When exploiting these processes for particle detection, the equipment consists of a container to hold the gas and two electrodes across which there is a potential difference.

Proportional Counter

Proportional counters consist of metal or glass cylindrical tubes, which are filled with gas and kept at a negative potential (cathode). A fine wire is strung down the center of the tube and set to a positive potential (anode). If the potential difference is V_0, the tube radius is r_2 (typically around 1 cm), and the wire radius is r_1 (20 - 100 μm), the internal electric field is

$$E(r) = \frac{V_0}{r \ln(r_2/r_1)} \tag{4.5}$$

and an electron from an atom ionized by a charged particle passing through the gas at a perpendicular distance r_a from the center of the wire will gain kinetic energy

$$K = e \int_{r_a}^{r_b} E(r) dr \tag{4.6}$$

when it comes to a perpendicular distance r_b from the center of the wire. Once K exceeds the gas's ionization energy, additional electrons will be released, which in turn ionize atoms closer to the wire. This avalanche of electrons is quantified as the amplification factor or gain–the number of secondary electrons reaching the wire per initial ion pair–is characteristic of the gas and independent of the number of initial ion pairs. Thus, number of electrons reaching the wire is proportional the the intial ionization, hence the name proportional counter. A typical amplification factor/gain is around 10^5. Also typical is that approximately 100 electrons per cm are liberated by a traversing charged particle.

There's a limit to V_0. Set too high, it may lead to a breakdown (spark), which can damage the fine wire. But this can be controlled and exploited under certain conditions, in particular by the mixing in a quenching gas–usually a complex organic molecule–that readily captures electrons. With the right mixture and pressure, the discharge can propagate along the entire wire length. This is how a Geiger-Muller counter works. If the very high voltage is pulsed, one can localize the original avalanche, resulting in a so-called streamer chamber.

Multi-Wire Proportional Chamber

In the modern proportional counter, as developed by Georges Charpak (Nobel Prize 1992), spatial information is obtained by having many fine parallel wires in a plane as one set of electrodes, between planar steel meshes serving as the other. The applied voltage is typically 2000 V, with wires of diameter of order 50 μm separated by 0.1 to 1 cm. The gas filling is usually an argon-alcohol mixture at atmospheric pressure. Each wire has its individual transistor amplifier, and acts like a cylindrical proportional chamber. Amplification factors are of order 5000, sufficient for single minimum-ionizing particles to be detected with 100% efficiency. Two counters, with wires at right angles, one above the other, can be used to give the spatial position of a particle within about 5 mm.

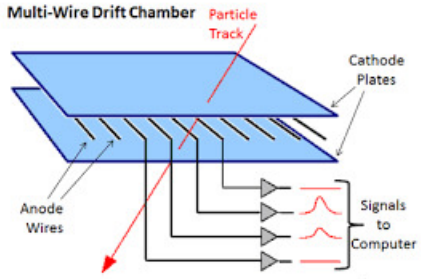

Figure 4.2: Schematic of a multi-wire proportional chamber

Drift Chamber

To achieve good spatial and time resolutions with a MWPC requires an enormous number of wires and amplifiers. Eqivalent resolutions at lower cost can be achieved by drifting the freed electrons from the primary ionization through a low-field region of roughly 10 cm to the high-field avalanche region near the anode wire. The time difference between a fast trigger and the time of the pulse on a wire on the wire gives the distance from the wire of the primary ionization, $r = vt$, where $v \approx 50$ μm/ns in a typical argon-alcohol (butane or ethane) mixture. The typical drift time of around 25 μs means that drift chambers are suitable only for relatively low incident particle rates.

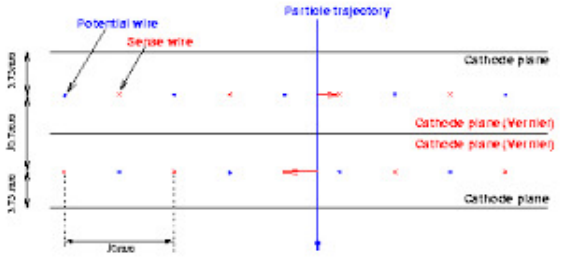

Figure 4.3: Schematic of a drift chamber

4.2.3 Silicon Detectors

Though solid, a silicon works roughly the same as gas, but with electron-hole pairs instead of ion pairs produced by ionization.

The electron density in silicon is a few thousand times larger than it is in gases, and the ionization energy is a factor of 10 smaller ($\sim$3 eV vs $\sim$30 eV), so large signals are available without the need for gas gains (avalanches) in high voltage. The detectors are thin and the drift velocities of both electrons and holes are high, so the detectors are fast, with, therefore, excellent time resolution. Narrow electrode strips and small detector pixels provide $\sim$5 μm position resolution. These detectors are very expensive, though, so are reasonable only for small instruments, usually around the interaction region, providing primary vertex information.

4.2.4 Measuring Charged Particle Momenta

Embedding tracking detectors in magnetic fields provides a means for measuring track momenta from the curvature of the trajectory:

$$p_\perp = rzeB \tag{4.7}$$

for p in GeV, B in tesla, and r in meters, so that $e = 0.3$.

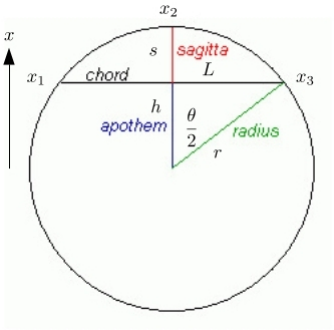

Assuming three positions have been measured along the trajectory, the sagitta

$$s = x_2 + \frac{x_1 + x_2}{2} \tag{4.8}$$

Assuming $L \ll r$. Since $r = s + h$, and $h = r\cos\frac{\theta}{2}$,

$$s = r(1 - \cos\frac{\theta}{2}) \approx \frac{1}{8}r\theta^2 = \frac{eBL^2}{8p_\perp} \tag{4.9}$$

Assuming that individual position measurements are known to the same resolution σ_x, then

$$\sigma_s = \sqrt{\frac{3}{2}}\sigma_x \tag{4.10}$$

so that

$$\left(\frac{\delta p_\perp}{p_\perp}\right)_{\text{spa}} = \frac{\sigma_s}{s} = \sqrt{\frac{3}{2}}\sigma_x \frac{8p_\perp}{eBL^2} = \frac{96}{\sigma_x}\frac{p_\perp}{eBL^2} \tag{4.11}$$

With more measurements, the contribution of one measurement to the overall uncertainty decreases. As the number N of measurements becomes large

$$\left(\frac{\delta p_\perp}{p_\perp}\right)_{\text{spa}} = \sqrt{\frac{720}{N+4}}\sigma_x \frac{p_\perp}{eBL^2} \tag{4.12}$$

So the position resolution contribution to the momentum resolutions becomes worse with momentum but improves with B and L as $1/BL^2$.

Multiple scattering also contributes to the momentum uncertainty independent of the position resolution. In fact, this dominates the uncertainty at low momentum, but becomes less important at higher momentum.

4.3 Timing

The multiple remnants of a reaction are associated with one another for analysis by comparing time stamps in the data. The greater the rate of reactions, the more precise the time needs to be.

4.3.1 Scintillator

Scintillation counters are among the most frequently used instruments in nuclear and particle physics. Modern scintillation materials include plastics such as polystyrene, organic liquids (for example, toluene); inorganic crystals (such as sodium or cesium iodide), and organic crystals (like anthracene). Ionization due to the traversal through such materials of an ionizing particle results in emission of fluorescent light over a broad range of wavelengths. In organic scintillators, for example, the emission is principally in the short (UV) wavelength region. A wavelength-shifting dye is usually mixed into the scintillator material. The UV emissions of the scintillator material excite the dye, which reemits in the visible region. The decay times of fast scintillator is typically of order 1 ns.

The light output of inorganic crystals, such as NaI(Tl), is essentially proportional to the ionization energy loss. These are therefore used for calorimetry. This is not the case with organic scintillators.

4.3.2 Photodetectors

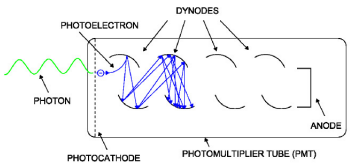

Figure 4.4: Photomultiplier tube

A scintillating material is usually enclosed on all but one face in a thin layer of reflecting material, such as aluminum foil, to optimize the chances that the light it emits falls onto the unshielded face. This ensures that as much of the light as possible is directed at the cathode of a photomultiplier, which is in direct contact with the unenclosed scintillator face or with the end of a light pipe which is optically attached (minimizing refractive-index-boundary-induced reflection at the interface).

The peak spectral response of the typical photomultiplier is around the shorter wavelength region of the visible spectrum, roughly the transition from violet to blue. The photocathode is coated with alkali metals, so that electrons are readily emitted as a result of the photoelectric effect. Maximum photocathode quantum efficiency

$$QE(\lambda) = \frac{N_e}{N_{\gamma(\lambda)}} \tag{4.13}$$

is typically around 25% for $\lambda = 400$ nm.

A minimum ionizing particle loses about 1.5 MeV of energy to ionization traversing 1 cm of plastic scintillator. Such a traversal liberates on average 10^4 photons, each with a mean energy $h\nu = 3$ eV, meaning that about 2% of the energy loss results in fluorescence. Assume 10% of the light makes it to the photocathode,

whose quantum efficiency over the full spectrum is 10%, then approximately 2000 photoelectrons will be emitted, sufficient to ensure nearly 100% efficiency.

For each photoelectron ejected from the cathode, the successive secondary-emission electrodes (dynodes), which emit on average 4 secondary electrons for each incident electron, ultimately generate some 10^8 electrons at the anode. The transit time from cathode to anode is about 50 ± 1 ns, where the uncertainty is known as the jitter. The output of the anode is a voltage pulse.

The width of the output pulse, referred to as the response time, depends on the time required for the light to make its way to the photocathode and the fluorescence decay time–between 3 and 30 ns for organic materials and around 250 ns for NaI–as well as the photomultiplier jitter. All of this limits this width to around 10 ns for plastic scintillatory.

The great advantages of the scintillation counter are that it is robust, simple, and efficient, giving large, sharp output pulses. Its spatial resolution is poor, since the pulse is not related in an obvious way to the location of the trajectory of the charged particle through the counter. Thus, if spatial information is required, it is necessary to use a large hodoscope array of very small counters with photomultipliers at each end. Coincident signals from each of them reduces random noise that characterizes all photomultiplier tubes, while the time difference between the two signals allows an estimation of the traversal point in a counter. The rate of accidental coincidences is small because of the good intrinsic time resolution time.

4.4 Calorimetry

Total absorption, in which a traversing particle's kinetic energy develps into a shower cascade due to multiple ionization or excitation processes, can in principle allow determination of both position and energy, the latter to a fractional energy resolution that varies as $1/\sqrt{E}$. At high energy (above 10 GeV), then, this resolution competes with that of a momentum determination by the bend in a magnetic field. In general, as well, the response time of total absorption instruments is an order of magnitude shorter than that of gas trackers (100 ns vs 1 μs), so that such signals can be used in event-selection decision making.

4.4.1 Electromagnetic Calorimeter

The electromagnetic cascading of photons and electrons through radiation energy loss (bremsstrahlung and pair production) in materials allows their total energy to be measured along the path of the shower. Coulomb scattering spreads the shower laterally, the extent of which depends on the radiation length, a characteristic of the material, and the angular deflection per radiation length at the critical energy, E_c, at which shower development ceases. This is expressed in terms of the Molière radius

$$R_m = 21 \left(\frac{X_0}{E_c} \right) \tag{4.14}$$

which is, by definition, the radius of a cylinder containing on average 90% of the radiated energy. Two Molière radii contain 95% of the energy. The smaller a material's Molière radius, the greater resolution of the shower position, and the less likely it is that showers will overlap (shower separation will be improved).

High Z materials with short radiation lengths are preferred for electromagnetic calorimeters. Typically, relative energy resolutions

$$\frac{\Delta E}{E} = \frac{0.05}{\sqrt{E}} \tag{4.15}$$

where E is measured in GeV, are achieved. This results from the facts that the number of particles at shower maximum $N \propto E$, while this number fluctuates as $\sqrt{N}$.

4.4.2 Hadron Calorimeter

Similarly, a hadron traversing matter can produce a shower if it collides inelastically with a nucleus. The longitudinal extent of such showers depend on the nuclear interaction length λ_I.

While the energy of electrons and photons ultimately leads to ionization, so that ionized electrons can be collected as a measure of energy, hadrons lose roughly 30% of their energy through nuclear fission, excitation, and evaporation, none of which will produce observable signals. This can be compensated somewhat through the use of materials that release nucleons with sufficient kinetic energy to ionize atoms in the material, but the typical energy resolution of a hadron calorimeter is an order of magnitude worse than the energy resolution of an EM calorimeter:

$$\frac{\Delta E}{E} = \frac{0.5}{\sqrt{E}} \tag{4.16}$$

The nuclear interaction length tends to increase with Z, while the radiation length tends to decrease, so hadronic showers tend to be much larger, both longitudinally and transversely. Hadron calorimeters thus tend to be much larger than electromagnetic calorimeters.

4.5 Particle Identification

Particle speed is sometimes measured directly by time of flight instruments, two fast, high-precision detectors, such as scintillator counters, separated by a known distance L. The difference between the traversal times at these detectors gives the speed, $\beta = L/\Delta t$. Then, a separate momentum measurement gives the particle identity:

$$m = \frac{p}{\beta\gamma} = p\sqrt{\frac{1}{\beta^2} - 1} = p\sqrt{\frac{(\Delta t)^2}{L^2} - 1} \tag{4.17}$$

Cerenkov detectors ($\beta = \frac{1}{n\cos\theta}$) and instruments that can measure ionization density ($\frac{dE}{dx} \propto \frac{1}{\beta^2}\ln\left(\beta^2\gamma^2\right)$) are other tools to determine speed.

Particle identification is also made possible by the fact that the different final state particles interact in different ways in different materials.

Traversing electrons leave ionization trails in low-density matter and shower electromagnetically while their energy is absorbed in dense matter. The showers begin forming rather deeply into the material and are relatively short and well-collimated.

Traversing photons do not leave an ionization trail in low-density matter, but do shower electromagnetically while their energy is absorbed in dense matter. The showers begin forming at the front surface of the material and are relatively short and well-collimated.

Sufficiently long-lived charged hadrons, principally protons, pions, and kaons, leave ionization trails in low-density matter and shower hadronically while their energy is absorbed in dense matter. The showers begin forming anywhere in the material and are long and diffuse.

Sufficiently long-lived neutral hadrons, principally neutrons and kaons, do not leave an ionization trail in low-density matter, but do shower hadronically while their energy is absorbed in dense matter. The showers begin forming anywhere in the material and are long and diffuse.

Muons, which are charged, leave ionization trails in both low- and high- density matter, but very rarely shower, so their energy is rarely absorbed.

Neutrinos, which are neutral, do not ionize material, leaving no trail of there passage through it. Their presence must be inferred by missing energy or momentum imbalance.

The identity of all other particles is inferred by reconstructing the energy and momentum of the particles just listed. Such reconstruction can result in invariant masses and displaced vertices.

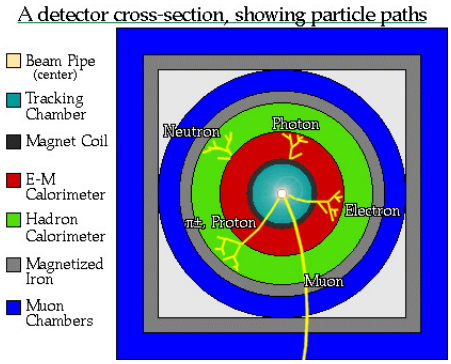

Figure 4.5: End view of typical detector showing various particle interactions in the different components

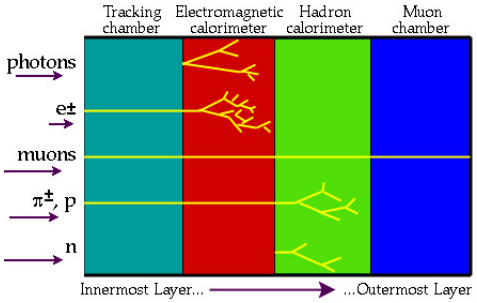

Figure 4.6: Signatures of various particles traversing detector layers

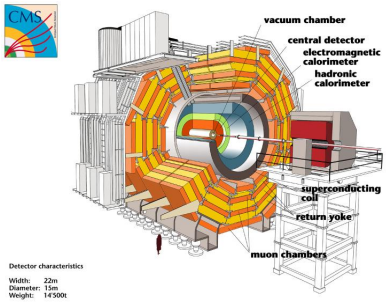

Figure 4.7: Schematic of the CMS detector at the LHC

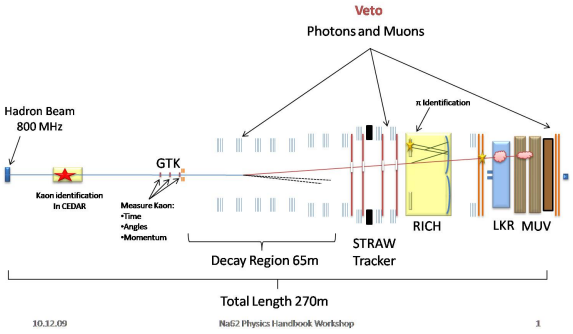

Figure 4.8: Layout of a fixed target experiment's detector array

Chapter 5

Non-Relativistic Bound States

5.1 Introduction

Schrödinger's equation and the apparatus of non-relativistic quantum mechanics were developed specifically for bound states, while relativistic quantum mechanics and quantum field theory were not. Therefore bound systems whose constituents' velocities remain substantially below c are more readily analyzed than systems with relativistic constituents. Although this is a course on subatomic physics, we will study a bit of atomic physics as a prototype for (non-relativistic) bound states.

A simple criteria for identifying a system as non-relativistic is that the binding energy is substantially smaller than the rest energies of the constituents. That is, if the composite mass is nearly the same as the sum of constituent masses, then the system is non-relativistic. If the composite mass is much smaller than the sum of constituent masses then the binding energy is large, and the constituents are probably moving relativistically. The total energy of a composite system consists primarily of constituent rest energies, constituent kinetic energies, and configuration potential energy. By the virial theorem (twice the time-averaged kinetic energy $2 < T >= n < V >$ the time averaged potential energy of the form $V(r) = Cr^n$), constituent kinetic energies and configuration potential energy have comparable magnitudes, implying that when the configuration potential energy (binding energy) is small relative to the sum of constituent rest energies, then so too is the sum of constituent kinetic energies.

5.1.1 Schrödinger's Equation

If the behavior of a non-relativistic object with mass m is represented by a function $\Psi(\mathbf{r}, t)$, then the time evolution of this function under the impact of a (in general, space- and time-dependent) potential, $V(\mathbf{r}, t)$ is given by Schrödinger's equation,

$$\left(-\frac{\hbar^2}{2m}\nabla^2 + V\right)\Psi = i\hbar\frac{\partial}{\partial t}\Psi \tag{5.1}$$

$$|\Psi(\mathbf{r}, t)|^2 d^3\mathbf{r} \tag{5.2}$$

is the probability of the object being in the infinitesimal volume $d^3\mathbf{r}$. Because it is somewhere,

$$\oint |\Psi(\mathbf{r},t)|^2 d^3\mathbf{r} = 1 \tag{5.3}$$

If V has no t-dependence, then the energy sytsem E can serve as a separation constant to solve the equation via separation of variables

$$\Psi(\mathbf{r},t) = \psi(r)e^{-iEt/\hbar} \tag{5.4}$$

$\psi(r)$, is the eigenstate of the Hamiltonian operator,

$$\hat{H} \equiv -\frac{\hbar^2}{2m}\nabla^2 + V \tag{5.5}$$

with eigenvalue E, and

$$\hat{H}\psi(r) = E\psi(r) \tag{5.6}$$

is called the time-independent Schrödinger equation.

If V is a central, spherically-symmetric potential, so that it depends only on r, then ψ itself is factorable in spherical coordinates

$$\psi(r,\theta,\phi) = \frac{u(r)}{r}Y_l^{m_l}(\theta,\phi) \tag{5.7}$$

$Y_l^{m_l}(\theta,\phi)$ are spherical harmonics whose labels l and m_l represent the quantum numbers of total orbital angular momentum and the z-projection of the total orbital angular momentum, respectively.

$u(r)$ satisfies the radial Schrödinger equation,

$$-\frac{\hbar^2}{2m}\frac{d^2u}{dr^2} + \left[V(r) + \frac{\hbar^2}{2m}\frac{l(l+1)}{r^2}\right] = Eu \tag{5.8}$$

which must be solved for a given potential, $V(r)$, to which is combined the relevant $Y_l^{m_l}(\theta,\phi)$ and $e^{-iEt/\hbar}$ to yield the full wave function. The bracketed terms are collectively referred to as an effective potential, with the second term, called the centrifugal barrier, modifying the interaction potential. The magnitude of this modification clearly depends on the magnitude of the orbital angular momentum. It is repulsive and acts to keep entities apart, since angular momentum is conserved; entities can merge only for $L = 0$.

Normalizable solutions to Equation 5.8 are found with only certain values of the energy E, so-called allowed energies, the primary objectives of investigations of the system.

5.2 Hydrogen-like Atoms

Atoms with a single electron are non-relativistic bound systems, in which even those with very large Z (many protons) have total ionization energies < 12 keV, while an electron's rest energy is 511 keV. Further, the binding potential, the Coulomb potential,

$$V(r) = -\frac{Ze^2}{r} \tag{5.9}$$

is due to the protons in the nucleus, which is thousands of times more massive than an electron, so, to excellent approximation, can be considered stationary. The atomic wave function of these entities is essentially that of the electron.

5.2.1 Hydrogen

For Hydrogen, $Z = 1$. The energies giving normalizable solutions are:

$$E_n = -\frac{me^4}{32\pi^2 n^2} = -\alpha^2 m\left(\frac{1}{2n^2}\right) = -\frac{13.6}{n^2}\ \text{eV} \tag{5.10}$$

where $n = 1,\ 2,\ \ldots$ is the principle quantum number, and

$$\alpha = \frac{e^2}{4\pi} = \frac{1}{137} \tag{5.11}$$

is the fine structure constant.

The corresponding normalized wave functions, which depend on the so-called Bohr radius

$$a = \frac{4\pi}{me^2} = 2.7 \times 10^{-4}\ \text{eV}^{-1} = 0.5 \times 10^{-8}\ \text{cm} = 0.5\ \text{Å} \tag{5.12}$$

the scale of an atomic radius, and associated Laguerre polynomials, $L_n^k(x)$, are, for completeness,

$$\Psi_{n,l,m_l}(r,\theta,\phi,l) = \left\{\left(\frac{2}{na}\right)^3 \frac{(n-l-1)!}{2n[(n+l)!]^3}\right\}^{1/2} e^{-r/na}\left(\frac{2r}{na}\right)^l L_{n-l-1}^{2l+1}\left(\frac{2r}{na}\right) Y_l^{m_l}(\theta,\phi)e^{-iE_n t} \tag{5.13}$$

The quantum numbers $n = 1,\ 2,\ \ldots$; $l = 0,\ 1,\ \ldots,\ n-1$; and $m_l = -l,\ -l+1,\ \ldots,\ l-1,\ l$ label, respectively, the state energy, the total angular momentum, and the z-component of the total orbital angular momentum.

Note that for each n, the electron may have n different values of l, each of which can be projected to $2l+1$ different values of m_l. The nth energy level, then, can have n^2 distinct states:

$$\sum_{l=0}^{n-1}(2l+1) = n^2 \tag{5.14}$$

referred to as the degeneracy of the nth energy level.

5.2.2 The Hydrogen Spectrum

The principle quantum number identifies so-called stable states, in which the electron, although "orbiting," does not emit radiation, in contrast to the classical electromagnetic theory of accelerating charges. Transitions between stable orbits implies a transition between energy levels. With hydrogen, as with any atom, this energy transition is mediated, and thus measured indirectly, via the emission or absorption of light,

$$E = \frac{2\pi}{\lambda} = E_{n_1} - E_{n_2} \tag{5.15}$$

which is the energy difference between initial and final states, n_1 and n_2.

The wavelengths of light associated with all such transitions between atomic hydrogen's discrete energy levels create radiation spectra given by the Rydberg formula:

$$\frac{1}{\lambda} = R_\infty\left(\frac{1}{n_1^2} - \frac{1}{n_2^2}\right) \tag{5.16}$$

with the Rydberg constant,

$$R_\infty = \frac{me^4}{64\pi^3} = 2 \text{ eV} = 10^7 \text{ m}^{-1} = 10^{-3} \text{ Å}^{-1} \tag{5.17}$$

and $n_1 < n_2$ are (integer) principle quantum numbers.

R_∞ follows directly from the determination of the principle energy levels in solving the radial Schrödinger equation, which assumed the mass number of the nucleus $M \gg m$ the electron mass number. Better agreement with experiment results from using the reduced mass

$$\mu = \frac{mM}{M+m} = \frac{m}{1+\frac{m}{M}} = \frac{M}{1+\frac{M}{m}} \tag{5.18}$$

Applying this correction to the Rydberg constant, $m \to \mu$ gives the Rydberg constant for hydrogen.

$$R_H = \frac{R_\infty}{1+\frac{m}{M}}$$

Since, for hydrogen, $\frac{M}{m} \approx 2000$ (and bigger for other atoms), the correction factor is 0.9995 or more, approaching 1.

Table 5.1: Hydrogen spectra

n_1	n_2	Spectral Series Name	Spectrum Range	Convergence Wavelength
1	$2 \to \infty$	Lyman	ultraviolet	91 nm
2	$3 \to \infty$	Balmer	visible	365 nm
3	$4 \to \infty$	Paschen	infrared	820 nm
4	$5 \to \infty$	Brackett	far infrared	1458 nm
5	$6 \to \infty$	Pfund	far infrared	2278 nm
6	$7 \to \infty$	Humphreys	far infrared	3281 nm

Figure 5.1: Graphical representations of hydrogen spectra

5.2.3 Hydrogenic Atoms

Atoms, stripped of all but one electron, behave just like hydrogen except that the nuclear charge $Z \neq 1$ and the reduced mass number take into account the larger nuclear mass number:

$$\frac{1}{\lambda} = R_\infty Z^2 \left(\frac{1}{n_1} - \frac{1}{n_2^2} \right)$$

5.2.4 μ- and π-Mesic Atoms

Both pions (mesons containing up and down quarks) and muons (leptons, like electons, only heavier) have negative charge states and can therefore form hydrogenic atoms with bare nuclei. The mass numbers of these particles are several hundred times larger than that of the electron, and so the resulting orbits are much smaller, perhaps even within the nuclear charge distribution.

5.3 The Zeeman Effect

5.3.1 Classical Orbital Angular Momentum

A particle of mass number m in a central force experiences no torque

$$\boldsymbol{\tau} = \frac{d\mathbf{L}}{dt} = 0 \tag{5.19}$$

so the angular momentum $\mathbf{L} = m\mathbf{v} \times \mathbf{r}$ of its elliptical orbit is constant in both magnitude and direction. Consequently, $L_z = |\mathbf{L}| \cos\theta$, where $0 \leq \theta \leq 180°$, will also be constant, regardless of axis orientation. $|\mathbf{L}|$ depends on the eccentricity ($\epsilon = \sqrt{a^2 - b^2}/a$) of the ellipse, such that for $\epsilon = 0$ (a circle), $L = mva = a\sqrt{-2mE}$, while for $\epsilon \approx 1$ nearly a straight line $L = 0$. E is the total energy, constant, as well, in a central force, and depends only on the value of the major axis, $2a$, $E \propto 1/2a$, not the eccentricity or instantaneous position.

5.4 Classical Magnetic Dipole Moment

An electron in circular orbit, equivalent to a current $I = e\nu$, where e is the electron charge and ν is the orbital frequency, produces a magnetic dipole with moment

$$\boldsymbol{\mu} = \mathbf{I} \times \mathbf{A} \tag{5.20}$$

where $\mathbf{A}$ is the (vector) area of the loop. For circular motion, where $v = r\omega = 2\pi r\nu$,

$$|\mathbf{L}| = mvr = m(2\pi r\nu)r = 2m\nu\pi r^2 = \frac{2m}{e}|\boldsymbol{\mu}| \tag{5.21}$$

Thus,

$$\boldsymbol{\mu} = -\frac{e}{2m}\mathbf{L} \tag{5.22}$$

the directions being opposite due the the electron's negative charge.

In an external magnetic field $\mathbf{B}$, the dipole experiences a torque

$$\boldsymbol{\tau} = \boldsymbol{\mu} \times \mathbf{B} \tag{5.23}$$

so that $\boldsymbol{\mu}$ and $\mathbf{B}$ tend to align. Integration of the torque with respect to angular position yields the potential energy change

$$U_B = -\boldsymbol{\mu} \cdot \mathbf{B} = \frac{e}{2m}\mathbf{L} \cdot \mathbf{B} \tag{5.24}$$

Arranging the reference frame so that the z-axis is parallel to $\mathbf{B}$,

$$U_B = \frac{e}{2m}L_z|\mathbf{B}| \tag{5.25}$$

5.4.1 Quantization of Orbital Angular Momentum

Applying an external magnetic field to discharging atoms splits spectral lines, the frequency shift being directly proportional to the magnitude of the applied field. This indicates the existence of discrete energy levels in addition to those of the principle quantum states. Because the splitting is discrete, is seems that both magnitude and direction of orbital angular momentum are quantized. In the case of magnitude,

$$|\mathbf{L}| = \sqrt{l(l+1)} \tag{5.26}$$

where l is the orbital angular momentum quantum number, ranging from $l = 0,\ 1,\ 2, \ldots,\ n-1$, for principal quantum number n.

Additionally, the direction of $\mathbf{L}$ is oriented in such a fashion that its z-component (the component parallel to $\mathbf{B}$) is quantized:

$$L_z = m_l \tag{5.27}$$

where m is the magnetic quantum number, ranging from $m_l = -l,\ -(l-1), \ldots,\ 0,\ \ldots,\ l-2,\ l-1,\ l$. Note that for $l \neq 0$, $L_z < |\mathbf{L}|$.

Because $U_B = \frac{e}{2m}L_z B$ and L_z is quantized, then the total energy is quantized

$$E = E_n + U_B = E_n + \frac{e}{2m}L_z B = E_n + m_l \frac{e}{2m}B \tag{5.28}$$

where E_n is the discrete energy level when $\mathbf{B} = 0$. $\frac{e}{2m}$ is called the Bohr magneton, μ_B.

The result is that an external magnetic field splits the total energy into $2l + 1$ equally-spaced energy levels, leading to additional discrete lines upon discharge.

The most common transitions, known as electric dipole transitions, follow the selection rules

$$\Delta l = \pm 1 \text{ and } \Delta m_l = \pm 1 \text{ or } 0. \tag{5.29}$$

Thus, three lines will be seen

$$\Delta E = 0 \text{ and } \Delta E = \pm \frac{e}{2m}B \tag{5.30}$$

Note the proportionality of the shift to the field strength. This result is known as the "normal" Zeeman effect. Other transitions occur, but are much weaker. For example, the electron has its own, intrinsic, angular momentum, which contributes to further splitting, due to what is known as the "anomalous" Zeeman effect.

5.5 Electron Spin

Spin **S** is the name given to intrinsic angular momentum. It's magnitude, in analogy with orbital angular momentum, is given by

$$|\mathbf{S}| = \sqrt{s(s+1)} \tag{5.31}$$

with z-component

$$S_z = m_s \tag{5.32}$$

where $m_s = -s,\ -(s-1),\ \ldots,\ 0,\ \ldots,\ s-1,\ s$.

The intrinsic angular momentum also gives rise to a magnetic moment

$$\boldsymbol{\mu}_s = -g_s \frac{e}{2m}\mathbf{S} \tag{5.33}$$

where g_s is the dimensionaless gyromagnetic ratio. Note,

$$g_s = \frac{|\boldsymbol{\mu}_s|/|\mathbf{S}|}{|\boldsymbol{\mu}|/|\mathbf{L}|} \tag{5.34}$$

Experiment shows that $g_s \approx 2$, indicating that the intrinsic magnetic moment to angular momentum ratio is about twice as large as the same ratio with respect to orbital angular momentum.

The existence of this intrinsic spin was demonstrated in an experiment performed by Stern and Gerlach. The resulting split in the distribution results from a net deflecting force of an inhomogeneous magnetic field exerted on each magnetic moment $\boldsymbol{\mu}_s$ of $F_z = \mu_{sz}\frac{dB}{dz}$.

The potential energy of a charged particle with magnetic moment $\boldsymbol{\mu}_s$ in an inhomogeneous magnetic field **B** is

$$U_B = -\boldsymbol{\mu}_B \cdot \mathbf{B} = -\mu_{sx}B_x - \mu_{sy}B_y - \mu_{sz}B_z \tag{5.35}$$

Arranging the reference frame so that $B_y = 0$, then B_x and B_z depend only on x and z (not y)

$$\mathbf{F}_B = -\nabla U_B = \frac{\partial}{\partial x}(\mu_{sx}B_x + \mu_{sz}B_z)\hat{\imath} + \frac{\partial}{\partial z}(\mu_{sx}B_x + \mu_{sz}B_z)\hat{k} \tag{5.36}$$

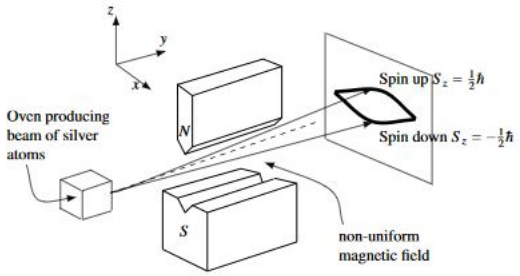

Figure 5.2: Stern-Gerlach apparatus

In a Stern-Gerlach experiment $\partial B_z/\partial x = \partial B_x/\partial z = 0$, and, in fact, $B_x \approx 0$ integrating along the beam axis (undulating motion), while $\partial B_x/\partial x \ll 1$, so:

$$\mathbf{F}_B = F_z = \mu_{sz}\frac{\partial B_z}{\partial z} \tag{5.37}$$

One might expect, if there weren't spin, to find a smear up and down, but instead, two clusters, above and below the center line, were found.

5.6 Fine Structure

Spectal lines associated with principle quantum numbers resolve into closely spaced pairs, triplets, etc., due to two effects.

5.6.1 Relativistic Correction

Schrödinger's equation is derived from the classical expression for kinetic energy in terms of momentum: $p^2/2m \to -i\hbar/2m\nabla^2$.

A Taylor expansion of the expression

$$E^2 = p^2 + m^2 \tag{5.38}$$

substituted into

$$K = E - m \tag{5.39}$$

yields the second-order correction

$$\Delta E \approx -\frac{p^4}{8m^3} \tag{5.40}$$

5.6.2 Spin-Orbit Coupling

From the electron's frame of reference, the nucleus appears to orbit with the same angular velocity as the electron does when measured in the nuclear reference frame. This nuclear orbit, the equivalent of a current loop, gives rise to a magnetic field, which interacts with the electron's magnetic moment. Because this magnetic moment is proportional to the spin, and because the orbit-induced magnetic field is proportional to the angular momentum of the orbit, the interaction is referred to as spin-orbit coupling. A potential energy arises

$$U \propto \mathbf{L} \cdot \mathbf{S} \propto \boldsymbol{\mu}_s \cdot \mathbf{B} \tag{5.41}$$

which results in two modifications to electron motion: Larmor and Thomas precession.

5.6.3 Total Angular Momentum

The total angular momentum, $\mathbf{J}$, is the vector sum of the orbital and spin angular momenta:

$$\mathbf{J} = \mathbf{L} + \mathbf{S} \tag{5.42}$$

$$J^2 = L^2 + S^2 + 2\mathbf{L} \cdot \mathbf{S} \tag{5.43}$$

$$J^2 = j(j+1) \quad L^2 = l(l+1) \quad S^2 = s(s+1) \tag{5.44}$$

$$|\mathbf{L} \cdot \mathbf{S}| = \frac{1}{2}[j(j+1) - l(l+1) - s(s+1)] \tag{5.45}$$

$$\Delta E_{so} \propto j(j+1) - l(l+1) - s(s+1) \tag{5.46}$$

the energy splitting to to spin-orbit coupling.

Possible values for j are $j = |l - s|,\ |l - s| + 1,\ \ldots,\ l + s - 1,\ l + s$, where l and s are, respectively, the orbital and spin quantum numbers. For hydrogen-like atoms, $s = 1/2$, so

$$j = \begin{cases} l + s,\ l - s & l > 0 \\ s & l = 0 \end{cases} \tag{5.47}$$

As with orbital and spin angular momentum, the z-direction of $\mathbf{J}$ is quantized when defined physically

$$J_z = m_j \tag{5.48}$$

where $m_j = -j,\ -j + 1,\ \ldots,\ j - 1,\ j$.

Combining both relativistic and spin-orbit corrections:

$$\Delta E_{fs} = -\alpha^4 m \frac{1}{4n^4} \left(\frac{2n}{j + \frac{1}{2}} - \frac{3}{2} \right) \tag{5.49}$$

This correction is $\alpha^2 < 10^{-4}$ smaller than the principle energies, and negative. Note that, as $l = 0, \ldots, n - 1$, $j = \frac{1}{2}, \ldots, n - \frac{1}{2}$, the nth principle energy level splits into n sublevels.

5.7 Hyperfine Splitting

The spin of the nucleus also creates a magnetic field, interacting with both the electron's orbit (nuclear spin-orbit interaction) and its spin (spin-spin), together leading to so-called hyperfine splitting. Note that the nucleus is a compound object and its mass is large, so its dipole momentum is small and a bit more complicated to calculate:

$$\boldsymbol{\mu}_p = \gamma_p \frac{e}{m_p} \mathbf{S}_p \tag{5.50}$$

where $\gamma_p \approx 2.8$. Thus,

$$\Delta E_{hf} = \left(\frac{m}{m_p} \right) \alpha^4 m \frac{\gamma_p}{2n^3} \frac{\pm 1}{(f + \frac{1}{2})(l + \frac{1}{2})}, \quad \text{for } f = j \pm \frac{1}{2} \tag{5.51}$$

where $f = j + s_p$, the total angular momentum quantum number (orbital plus both spins).

Due to the ratio of masses, hyperfine splitting is about 1000 times smaller than fine structure splitting and, depending on spin direction, raises or lowers the energy.

5.8 Lamb Shift

Because fine structure splitting ends up depending on j and not explicitly on l, states with different l but same j should be degenerate. It turns out that they are not, due to the explicitly QFT effects of vacuum polarization (spontaneous electon-positron production around the nucleus), which screens the nuclear charge; electron mass renormalization (that is, the ground state-energy of the electromagnetic field due to the nuclear charge is non-zero: so-called vacuum fluctuations in the field affect the electron's energy), and anomolous magnetic moments (modifications, known as radiative corrections to the magnetic dipole moment result in g_s not being exactly 2).

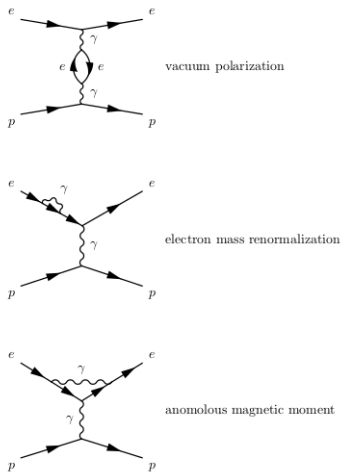

Figure 5.3: Feynman diagrams of vacuum polarization processes that result in Lamb energy shifts

$$\Delta E_{\text{Lamb}} = \alpha^5 m \frac{k(n,0)}{4n^3}, \quad \text{for } l = 0 \tag{5.52}$$

where $k(n,0) \approx 13$, but varying with n from 12.7 ($n = 1$) to 13.2 ($n \to \infty$).

$$\Delta E_{\text{Lamb}} = \alpha^5 m \frac{1}{4n^3} \left[k(n,l) \pm \frac{1}{\pi(j+\frac{1}{2})(l+\frac{1}{2})} \right], \quad \text{for } l \neq 0 \text{ and } j = l \pm \frac{1}{2} \tag{5.53}$$

where $k(n,l) < 0.05$.

Clearly, this is a small effect, especially when $l \neq 0$, about 0.1 of fine structure when $l = 0$, and positive.

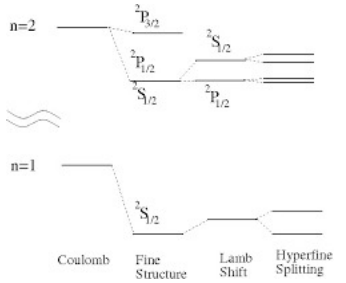

Figure 5.4: Spectrum shifts due to the various effects described

5.9 Many-Electron Atoms

5.9.1 The Pauli Exclusion Principle

No two electrons can have the same set of quantum numbers $(n,\ l,\ m_l,\ m_s)$. That is, two electrons cannot simultaneously occupy the same state.

5.9.2 A Single Particle in a One-Dimensional Box

Consider a particle of mass number m moving in a one-dimensional, infinitely deep "box" of length a. The energy is quantized

$$E_n = \frac{n^2}{2ma^2}$$

where n is a positive integer. If the particle is, say, an electron, with intrinsic spin, then its state is specified by two quantum numbers $(n,\ m_s)$.

5.9.3 More Than One Particle in a One-Dimensional Box

If the box contains two electrons, then, in the lowest energy (ground) state of the system, the primary quantum number of both is $n = 1$. But the two will not have the same pair of quantum numbers. One will have spin up $(1,\ +\frac{1}{2})$, the other will have spin down $(1,\ -\frac{1}{2})$. A third electron could not, according to Pauli, also have $n = 1$. In the ground state, it would have $n = 2$, as would a fourth electron, one with up-spin, the other with down-spin. A fifth electron in the ground state would have $n = 3$, and so forth. Thus, the Pauli exclusion principle implies that the energy of a multi-particle spin-1/2 system is higher than it would be if all particles would be at $n = 1$.

Excited states may exist, in which one or another electron is not occupying the lowest possible energy configuration, and photon emission occurs when an excited state relaxes to the ground state.

What happens when a magnetic field interacts with the spin of three non-interacting particles in the ground state of an infinite square well?

$$E = E_n - \boldsymbol{\mu} \cdot \mathbf{B} = E_n - \mu_{sz} B = E_n + m_s \frac{e\hbar}{m} B \tag{5.54}$$

If the particles are spin-1/2, for example, the spin of third particle in the $n = 2$ state could be either up or down when no magnetic field is present, but must be down $(m_s = -1/2)$ for the system to remain in the ground state with an external magnetic field (why?).

5.9.4 Spectroscopic Notation for Electron Configurations

Assuming an independent particle model, in which individual electrons move independently in the nuclear field and the average field of other electrons, electron states are described by the quantum numbers n, l, m_l, m_s.

Electrons with the same n are said to occupy the same electron shell, which, for some purposes, are designated

n value:	1	2	3	4	...
symbol:	K	L	M	N	...

Although they may occupy the same shell, electrons with a given n may occupy different subshells or orbits, designated by l. For a given n, $l = 0,\ \ldots,\ n - 1$, and each corresponding state is designated

l value:	0	1	2	3	4	5	...
symbol:	s	p	d	f	g	h	...

A particular orbit is then defined by the pair $(n,\ l)$, and the convention is to symbolize this orbit by nl, with n given by its value and l given by its symbol. The number of electrons in an orbit is given by a superscript, and a configuration is designated by a sequence of orbits. The five-electron configuration of boron in its ground state, for example, is given by $1s^2 2s^2 2p^1$. Thus, in the L $(n = 2)$ shell of ground-state boron, 2 electrons occupy the s subshell and 1 electron occupies the p subshell.

5.9.5 The Atomic Shell Model

The Pauli exclusion principle implies that the maximum number of electrons in a subshell can be determined from the values of m_l and m_s. There are $2l + 1$ values of m_l for each l and $2S + 1 = 2$ values of m_s for each S, which is $1/2$ for electrons. Then the maximum number of electrons in a subshell is $2(2l + 1)$:

l value:	0	1	2	3
subshell symbol:	s	p	d	f
maximum number:	2	6	10	14

5.9.6 Spectroscopic Notation for Atomic States

Atomic states are specified by the quantum numbers related to total orbital angular momentum, total spin angular momentum, and total angular momentum, L, S, J. L values are designated

L value:	0	1	2	3	4	5	...
symbol:	S	P	D	F	G	H	...

Atomic state designation is by total orbital angular momentum, L, pre-superscripted by $2S + 1$ and post-subscripted by J, so, for ground-state boron, where $L = 1$, $S = 1/2$, $J = 1/2$, the notation is ${}^2P_{1/2}$.

5.9.7 LS Coupling

As in the case of hydrogenic atoms, residual Coulomb interactions, spin-orbit interactions, and spin-spin interactions complicate the simple model. Given

$$\mathbf{L} = \sum_i \mathbf{L}_i \tag{5.55}$$

$$\mathbf{S} = \sum_i \mathbf{S}_i \tag{5.56}$$

where the vector sum is over all electrons, the total angular momentum

$$\mathbf{J} = \mathbf{L} + \mathbf{S} \tag{5.57}$$

Each vector is quantized with magnitude

$$|\mathbf{L}|^2 = l(l+1)\hbar^2 \tag{5.58}$$

$$|\mathbf{S}|^2 = s(s+1)\hbar^2 \tag{5.59}$$

$$|\mathbf{J}|^2 = j(j+1)\hbar^2 \tag{5.60}$$

The quantization implies, therefore, that the total angular momentum quantum number j, again, has the values $j = l + s,\ l + s - 1,\ l + s - 2,\ \ldots,\ |l - s|$. The z-components are also quantized

$$L_z = M_l \tag{5.61}$$
$$S_z = M_s \tag{5.62}$$
$$J_z = M_j \tag{5.63}$$

where

$$M_l = \sum_i (m_l)_i = -l,\ -l + 1,\ \ldots,\ l - 1,\ l \tag{5.64}$$
$$M_s = \sum_i (m_s)_i = -s,\ -s + 1,\ \ldots,\ s - 1,\ s \tag{5.65}$$
$$M_j = M_l + M_s = -j,\ -j + 1,\ \ldots,\ j - 1,\ j \tag{5.66}$$

so, l, s, and j can be inferred from M_l, M_s, and M_j.

What is the relationship between the total electron magnetic moment and the total angular momentum?

$$\boldsymbol{\mu} = \boldsymbol{\mu}_L + \boldsymbol{\mu}_S = -\frac{e}{2m}\mathbf{L} - 2\frac{e}{2m}\mathbf{S} = -\frac{e}{2m}(\mathbf{L} + 2\mathbf{S}) \tag{5.67}$$

And,

$$\mathbf{J} = \mathbf{L} + \mathbf{S} \tag{5.68}$$

Further, since

$$\frac{|\boldsymbol{\mu}_L|}{|\mathbf{L}|} = \frac{1}{2}\frac{|\boldsymbol{\mu}_S|}{|\mathbf{S}|} \tag{5.69}$$

the triangles indicated by the vector equations are not similar, and so the resultants are not (anti-)parallel.

Thus, $\mu \nparallel \mathbf{J}$.

Then, what is the projection of the total magnetic momentum $\boldsymbol{\mu}$ on the total angular momentum $\mathbf{J}$?

Using Equation 5.67,

$$\mu_J = \frac{\boldsymbol{\mu}\cdot\mathbf{J}}{|\mathbf{J}|} = -\frac{e}{2m}\left[\frac{|\mathbf{L}|^2 + 2|\mathbf{S}|^2 + 3\mathbf{L}\cdot\mathbf{S}}{|\mathbf{J}|}\right] \tag{5.70}$$
$$= -\frac{e}{2m}\left[\frac{|\mathbf{L}|^2 + 2|\mathbf{S}|^2 + \frac{3}{2}(|\mathbf{J}|^2 - |\mathbf{L}|^2 - |\mathbf{S}|^2)}{|\mathbf{J}|}\right] \tag{5.71}$$
$$= -\frac{e}{2m}\left[\frac{|\mathbf{J}|^2 + \frac{1}{2}(|\mathbf{J}|^2 + |\mathbf{S}|^2 - |\mathbf{L}|^2)}{|\mathbf{J}|}\right] \tag{5.72}$$
$$= -\frac{e}{2m}|\mathbf{J}|\left[1 + \frac{|\mathbf{J}|^2 + |\mathbf{S}|^2 - |\mathbf{L}|^2}{2|\mathbf{J}|^2}\right] \tag{5.73}$$
$$= -\frac{e}{2m}\sqrt{j(j+1)}\left[1 + \frac{j(j+1) + s(s+1) - l(l+1)}{2j(j+1)}\right] \tag{5.74}$$
$$= -\frac{e}{2m}\sqrt{j(j+1)}g \tag{5.75}$$

where the Landé g-factor

$$g \equiv 1 + \frac{j(j+1) + s(s+1) - l(l+1)}{2j(j+1)} \tag{5.76}$$

A g-factor characterizes the magnetic moment and angular momentum of a quantum. It is essentially a dimensionless proportionality constant that relates a magnetic moment to its associated angular momentum. It is a measure of the relative energy splittings in weak magnetic fields.

5.9.8 Atomic Excited States

Electric dipole transitions from excited atoms are governed by the selection rules: $\Delta J = 0,\ \pm 1$, although $J = 0 \to J = 0$ is not allowed; $\Delta L = 0,\ \pm 1$, although if the transition involves just one electron, $\Delta L \neq 0$; $\Delta S = 0$; and $\Delta M_J = 0,\ \pm 1$, although if $\Delta J = 0$, $M_j = 0 \to M_j = 0$ is not allowed. Other, weaker transitions may occur, as well.

5.9.9 Anomolous Zeeman Effect

Semiclassically, the normal Zeeman effect is seen as the atomic magnetic moment $\boldsymbol{\mu}$ precessing about an external magnetic field $\mathbf{B}$. The stronger the field, the faster the precession and the greater the split. If the $\mathbf{L} \cdot \mathbf{S}$ interaction is stronger than the interaction of either $\mathbf{L}$ or $\mathbf{S}$ with $\mathbf{B}$, then $\mathbf{L}$ and $\mathbf{S}$ precess rapidly about $\mathbf{J}$, such that $\boldsymbol{\mu}$ precesses more rapidly about $\mathbf{J}$ than about $\mathbf{B}$, giving rise to the anomolous Zeeman effect, whose strength depends on the component of $\boldsymbol{\mu}$ along $\mathbf{J}$, producing more than three spectral lines.

Chapter 6

Nuclear Physics

6.1 Introduction

No theory of the nucleus exists, unlike the case, for example, of the hydrogenic atom. Spectroscopy makes clear that nuclear energy levels exist, indicating the quantum-mechanical nature of nuclear phenomena. Despite the development of a field theory (QCD) for the strong (nuclear) interaction, the many-body complications inherent in the nucleus have precluded a satsifactory application of it to nuclei. A number of models, each describing a limited range of properties, some perhaps employing approximations to QCD, have been developed.

The characteristic energies of atomic phenomena are on the order of eV. For nuclei, they are on the order of MeV. Atoms are therefore easily excited, and readily combine into molecules and crystals. Nuclei, on the other hand, excite only in very special circumstances.

6.2 Basic Properties of Nuclear Ground States

6.2.1 Structure

Nuclei are composed of nucleons: protons and neutrons. Protons have exactly the same magnitude of charge as electrons, but with opposite sign, and a mass about 1800 times larger. Neutrons are very slightly more massive than protons and have no net charge.

The number of protons in a nucleus is identified with the atomic number, Z, while the number of neutrons, N, is the difference between the mass and atomic numbers, $N = A - Z$. Equivalently, the atomic number is the sum of the numbers of protons and neutrons, $A = Z + N$.

Nuclear structure is summarized symbolically as

$$^{A}_{Z}X \tag{6.1}$$

where X is the chemical symbol for an element.

About 80% of the roughly 1500 known nuclei are unstable. In nuclei with small A, $N \approx Z$. As A increases, nuclear stability requires N to increase at a greater rate than Z, because the repulsive Coulomb force between protons pushes them farther and farther apart. Proton matter is less dense than neutron matter, so that as A increases, there are more neutrons than protons per nuclear volume.

Isotopes are nuclei with the same number of protons, Z. Isotones have the same number of neutrons, N. Isobars have the same mass number, A. Isomers have the same number of protons Z and same mass number A.

6.2.2 Mass

Nuclear masses are conventionally expressed in *unified mass* units, $u = \frac{m_{^{12}_6C}}{12} = 1.660539 \times 10^{-27}$ kg, or $1\ u = 931.48$ MeV. In these units, the proton mass, $m_p = 1.007277\ u$, the neutron mass, $m_n = 1008665\ u$, and the electron mass, $m_e = 0.0005486\ u$. Notice that carbon's atomic mass is less than the sum of its constituent protons (6), neutrons (6), and electrons (12), a manifestation of the relativistic equivalence of mass and energy (in this case binding, or potential, energy).

The natural mixing of isotopes in any sample renders chemical determinations of atomic wights uncertain. Mass spectrometry, which measures the mass-to-charge ratio, is perhaps the most accurate method to determine nuclear masses.

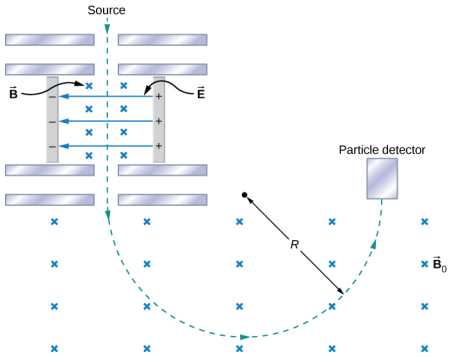

Figure 6.1: Mass spectrometer or velocity selector

Mass spectrometry works as follows:

1. Ionize the element or compound (with electrical discharge or evaporation from a hot filament).
2. Accelerate the ions in an electric field to a uniform kinetic energy and collimate.
3. Select velocities using crossed electric and magnetic fields ($qE_{\text{vs}} = qvB_{\text{vs}} \Rightarrow v = \frac{E_{\text{vs}}}{B_{\text{vs}}}$) and pass only undeflected particles.
4. Record positions of particles interacting with a detector after they curve in a uniform magnetic field:

$$\begin{aligned} qvB &= \frac{mv^2}{r} \\ r &= \frac{m}{q}\frac{v}{B} \\ \frac{m}{q} &= \frac{rBB_{\text{vs}}}{E_{\text{vs}}} \end{aligned} \tag{6.2}$$

Note that this technique results in atomic (or molecular) masses, rather than nuclei masses.

In this way, mass spectrometry can determine the relative abundance of each isotope of an element. The term natural abundance refers to the fractional distribution of an element's isotopes resulting from natural processes on, say, a planet. Atomic weight is the average mass of all an element's isotopes weighted by the abundance. Isotope abundance varies among planets, and even by location on a planet, but, on a short time scale, remains relatively constant. The natural abundance is determined by the creation probability in nucleosynthesis, production rates from natural radioactivity, and the relative stability of the various isotopes.

6.2.3 Charge

Isotopes of an element are nearly indistiguishable chemically. We conclude that the nuclear charge determines the gross properties of an element. The nuclear charge is positive, and its magnitude is Z times the charge magnitude of an electron, where Z, is, to the limit of experiment ($< 10^{-15}$), an integer.

6.2.4 Strong Nuclear Force

All nuclei, then, are positively charged: all–other than hydrogen–contain more than one proton. How can there then be nuclei? Shouldn't Coulomb repulsion make multi-proton nuclei impossible?

The Coulomb interaction falls off as the square of the separation between charged partcles, but extends to infinity.

An interaction, referred to as the *strong* or *strong nuclear* interaction, keeps nuclei together. It must be attractive within nuclei and at least 100 times stronger than the Coulomb interaction (because there are stable atoms with around 100 protons). Not apparent outside the nucleus, the interaction should become infinitesimal beyond a distance of around a nuclear diameter. On the other hand, protons don't swallow one another in the nucleus, so this intra-nuclear interaction must be repulsive at distances smaller than a nucleon radius.

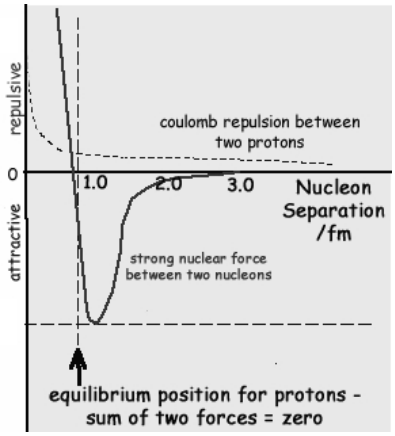

Figure 6.2: One model of the strong nuclear force as a function of nucleon separation; the Coulomb force is indicated, as well

Within nuclei, this interaction must occur not only between protons, but between neutrons and between protons and neutrons as well. Such a many-body problem is difficult to solve explicitly. The curve represents

one of many phenomenological models trying to account for experimental results.

The curve shows that the nuclear force has short range, its strength rapidly decreasing with particle separation. At distances greater than $1 - 2$ fm, it becomes insignificant; within the nuclear volume, it holds protons together despite the repulsive Coulomb force. It appears to be independent of electric charge: neutron-neutron, neutron-proton, and proton-proton nuclear interactions are approximately equally strong. It is the only fundamental interaction that saturates, which it does in the case that a nucleon is completely surrounded by other nucleons; nucleons located beyond the surrounding nucleons do not interact with the surrounded nucleon.

The nuclear force tightly binds nucleons. Given the dual attractive-repulsive form of the force, the nucleons must be in very close proximity, seeming to stick to one another as if under the influence of a "contact" potenitial. It is, in fact, useful in describing some nuclear behaviors to model nucleons as constituents of an incompressible fluid whose motions are correlated with those of all neighboring constituents. However, it can be just as useful in interpretting nuclear behavior to assume that constituent nucleons move completely independently, albeit in an apparently constant potential formed by the attraction of nearest, in-contact, neighbors. Surface nucleons have fewer neighbors, and are thus less tightly bound. All this suggests that nuclei tend to be spherically shaped.

6.2.5 Binding Energy

Because of the energy required to hold nucleons together, the nuclear mass $M_{nuc} = A - Zm_e$ is less than the sum of the component nucleon masses.

$$E_{\text{binding}} = Zm_p + Nm_N - M_{nuc} \tag{6.3}$$

Binding energy, E_{binding} is the manifestation of the potential well nucleons experience in a nucleus. This energy is released in formation, typically as photons, and it is the threhold energy for breaking a stable nucleus into its constituent nucleons. If $E_{\text{binding}} < 0$, the nucleus is unstable and will spontaneously disintegrate.

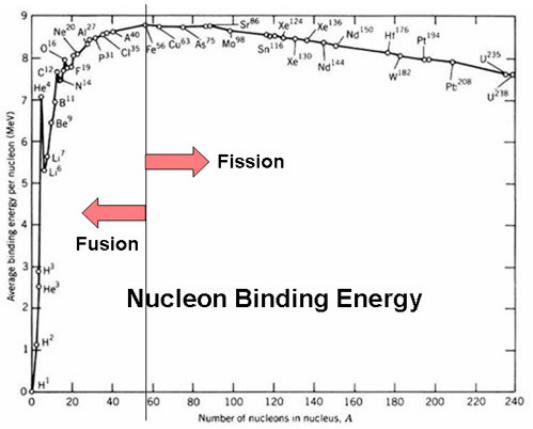

Figure 6.3: Binding energy per nucleon as a function of atomic mass

If each nucleon attracted every other nucleons equally, the binding energy per nucleon would increase with A. That it does not is in part because the nuclear interaction's range is short and saturates.

Binding energy increases–rapidly–with increasing $A < 60$. In this range, in fact, the fusion of nuclei is energeticaly favorable. Conversely, for $A > 60$, fission is energeticaly favorable. Other factors (to be discussed) prevent everything in the universe from becoming iron, cobalt, nickle, and copper.

Even numbers correlate with stability. Stable nuclei tend to have both even Z and N. Two nucleons of the same species can pair tightly in a particularly strong attraction, significantly increasing the total nuclear binding energy.

The binding energy per nucleon is between a thousand and a million times greater than the electron binding energy in an atom, which is of the order of electron volts for the valence electron and of the order of keV for inner electrons.

6.2.6 Nuclear Radius

The boundaries of nuclei are indefinite. For example, electron scattering experiments find a range of cross-sections. Taking the mean of these, and modeling nuclei as spheres of positive charge, the root mean square of the radius is calculated, since the nuclear cross-section is proportional to the square of the radius.

An upper limit on the size of the nucleus can be given by the head-on repulsion of a low-mass projectile by a high-mass nucleus. In the famous scattering experiments by Hans Geiger and Ernst Marsden, under the supervision of Ernst Rutherford (1910), a collimated beam of alpha (α) radiation [helium nuclei ($Z = 2$)] was aimed at a very thin sheet of gold (Au; $Z = 79$). The α particles of such a beam have a well-defined kinetic energy, ranging from roughly 5 MeV from decays of ^{226}Ra to approximately 7 MeV from decays of ^{214}Po. That even a small number ($\sim 10^{-4}$) of them scattered essentially straight back to their source meant that they were encountering a tiny but massive object. Because there was no indication of anything breaking apart, the scattering must have been elastic and most likely due to electrostatic repulsion. The interpretation is that, as they they approach Au nuclei, the kinetic energy of the alpha particles transforms into potential energy. At some distance from the nuclei, the direction of motion is reversed and the particles accelerate back the way they came. This distance of closest approach, b, can be estimated using energy conservation:

$$\begin{aligned} K_\alpha &= \frac{q_\alpha q_{\mathrm{Au}}}{b_{\mathrm{Au}}} \\ b_{\mathrm{Au}} &= \frac{q_\alpha q_{\mathrm{Au}}}{K_\alpha} \end{aligned} \tag{6.4}$$

Plugging in all the known quantities, $b_{\mathrm{Au}} \approx 3 \times 10^{-14}$ m $= 30$ fm. Similar experimental results were achieved with silver (Ag; $Z = 47$) foil, for which calculation gives $b_{\mathrm{Ag}} \approx 2 \times 10^{-14}$ m $= 20$ fm.

To measure the radius, rather than estimate its upper limit, requires probes that reach the nuclear surface, that is, probes with more kinetic energy.

The de Broglie wavelength of an 100-MeV electron, for example, is around 2 fm. If a beam of these is sent through a thin foil, a circular diffraction pattern forms on the screen behind.

The scattering amplitude:

$$\begin{aligned} F(\mathbf{k}_i, \mathbf{k}_f) &\propto \left\langle e^{i\mathbf{k}_f \cdot \mathbf{x}} \right| V(\mathbf{x} \left| e^{i\mathbf{k}_i \cdot \mathbf{x}} \right\rangle \\ &= \int d\mathbf{x} V(\mathbf{x}) e^{i(\mathbf{k}_i - \mathbf{k}_f)\cdot \mathbf{x}} \\ &= \int d\mathbf{x} V(\mathbf{x}) e^{i\mathbf{q}\cdot \mathbf{x}} \equiv F(\mathbf{q}) \end{aligned} \tag{6.5}$$

where $\mathbf{q} = \mathbf{k}_i - \mathbf{k}_f$ is the momentum transfer. Note that the scattering amplitude is the Fourier transform of the potential.

A Coulomb-like, radially symmetric potential with a fixed center has the form

$$V(\mathbf{x}) = -Z\alpha \int d\mathbf{x}' \frac{\rho_p(\mathbf{x}')}{|\mathbf{x} - \mathbf{x}'|} \tag{6.6}$$

where $\alpha = \frac{e^2}{4\pi}$ and $\rho_p(\mathbf{x}')$ is the proton number density such that

$$1 = \int d\mathbf{x}' \rho_p(\mathbf{x}') \tag{6.7}$$

is the normalization condition.

Then

$$F(\mathbf{q}) \propto -Z\alpha \int d\mathbf{x} \int d\mathbf{x}' \frac{\rho_p(\mathbf{x}')}{|\mathbf{x} - \mathbf{x}'|} e^{i\mathbf{q}\cdot\mathbf{x}} \tag{6.8}$$

and we set $F(0) = 1$ (no effect when no momentum transfer).

The result takes the form

$$F(\mathbf{q}) \propto -Z\alpha \int d\mathbf{x} \rho_p(\mathbf{x}) e^{i\mathbf{q}\cdot\mathbf{x}} \tag{6.9}$$

The (charged) scattering amplitude is the Fourier transform of the charge distribution.

If the charge distribution is indeed spherical, then, switching to spherical polar coordinates and choosing the reference frame such that $\mathbf{q} = q\hat{z}$ and $\rho_p(\mathbf{x}) = \rho_p(r)$

$$F(\mathbf{q}) \propto \int_0^{2\pi} d\phi \int_0^{\infty} r^2 dr \rho_p(r) \int_0^{\pi} \sin\theta d\theta e^{iqr\cos\theta} \tag{6.10}$$

$$= \frac{4\pi}{q} \int_0^{\infty} r dr \rho_p(r) \sin qr \tag{6.11}$$

Scattering from a spherical or circular obstruction creates a circular interference pattern just like diffraction through a circular aperture. The intensity distribution of this pattern is given by the squared modulus of the Fourier transform of a circular aperture of radius a:

$$I(\theta) = I_0 \left(\frac{2J_1(ka\sin\theta)}{ka\sin\theta} \right)^2 \tag{6.12}$$

where I_0 is the maximum intensity of the pattern at the (Airy) disc center, J_1 is the Bessel function of the first kind of order one, $k = \frac{2\pi}{\lambda}$ is the wavenumber, and θ is the angle between the axis of the circular aperture and the radius of interest in the pattern.

The zeros of $J_1(x)$ are approximately 3.8317, 7.0156, 10.1735, 13.3237, 16.4706, etc. The first minimum (dark ring) of the diffraction pattern occurs where $ka\sin\theta = 3.8317\ldots$, or

$$\sin\theta \approx \frac{3.83}{ka} = \frac{3.83\lambda}{2\pi a} = 1.22\frac{\lambda}{2a} = 0.61\frac{\lambda}{a} \tag{6.13}$$

A uniform charge distribution, such as

$$\rho_p(r) \propto \frac{\Theta(R-r)}{\frac{4}{3}\pi R^3} \tag{6.14}$$

would yield an interference pattern:

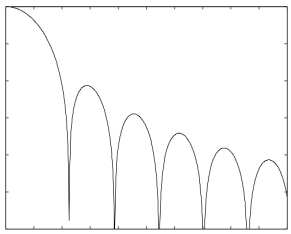

Figure 6.4: Interference pattern resulting from a circular charge distribution of uniform density

The lobes correspond to the shape of the nucleus, while the minima are characteristic of the edges. The sharp edge to the distribution yields minima of zero. Experiments do not yield zeroes, indicating "fuzzier" edges.

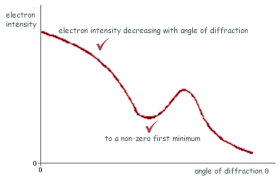

(a) Electron diffraction pattern

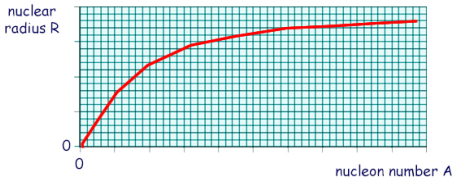

(b) Nuclear radius as a function of atomic number

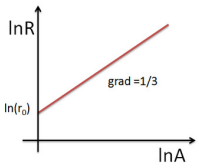

(c) $\ln Rvs \ln A$

Figure 6.5: Determining nuclear radii

Such measurements over a range of atomic numbers can be summarized empirically by

$$R = r_0 A^{1/3} \tag{6.15}$$

6.2.7 Density

Different types of radius measurements give different results, in part because each measures a different thing. Electron scatter probes the Coulomb charge radius. Neutron scattering probes the strong or nuclear force radius. Spectroscopy measures corrections due to finite nuclear size of Schrödinger wave equation predictions, which assume a point nucleus. Charge distribution studies give $r_0 \approx 1.2$ fm, while mass radius calculations

$$R = \sqrt{\frac{Zr_p^2 + Nr_N^2}{A}} \tag{6.16}$$

gives $r_0 \approx 1.4$ fm.

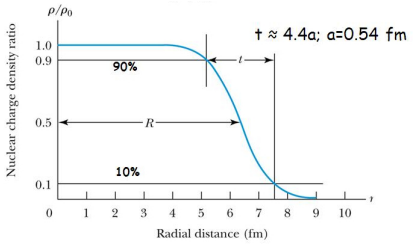

Figure 6.6: Nuclear charge density versus radial distance

Taken together, these results imply a tail in nuclear density distribution rather than a sharp edge, approximated reasonably well by the Woods-Saxon formula:

$$\rho(r) = \frac{\rho(0)}{1 + e^{(r-R)/a}} \tag{6.17}$$

where R is the width at half max, and a represents the so-called skin thickness, t,

$$t = 4a \ln 3 \tag{6.18}$$

Note that the core nuclear mass density is approximately the same in all nuclei.

$$\rho = \frac{m_N A}{\frac{4}{3}\pi R^3} = \frac{m_N A}{\frac{4}{3}\pi r_0^3 A} = \frac{m_N}{\frac{4}{3}\pi r_0^3} \tag{6.19}$$

independent of Z and A.

This gives a density of around 2×10^{17} kg/m^3, about 10^{12} times that of the core of the sun. The mass of a teaspoon (5 cm^3) of nuclear matter is about 10^{12} kg (a few billion tons).

6.2.8 Nuclear Angular Momentum

Spin

As indicated by, for example, the hyperfine structure of atomic spectral lines, nuclei possess spin angular momentum and magnetic moments.

Nucleons are fermions, spin-$\frac{1}{2}$ particles, and so subject to the Pauli Exclusion Principle: no two nucleons of the same species may be described by the same set of quantum numbers.

Therefore, analogously to the "stacking" of electrons in atoms, nucleons, in forming a nucleus, occupy subshells of increasingly energetic quantum shells. As is the case of orbital electrons, no more than two nucleons of a given species, with opposite spin, can occupy a given subshell. In distinction from the atomic case, the potential in this case is due only to other constituent nucleons.

This process is constrained by the empirical facts that a purely neutronic bound state is impeded by the Pauli Exclusion (the only known counter example is the existence of neutron stars, in which the binding energy of the gravitational potential is sufficient to form uniform neutron matter), and a purely or even largely protonic bound state is impeded also by Coulomb repulsion. While low-mass nuclei are formed stably when the numbers of protons and neutrons are about equal, stable formation of more massive nuclei require additional neutrons to separate protons.

A pair of neutrons will not bind, but only barely. A proton and a neutron will bind (deuteron), but only barely. Deuteron physics is somewhat complex. Its spin and total angular momentum are each 1, but its orbital angular momentum is in a superposed state [96% S ($L = 0$); 4% D ($L = 2$)], and its electric quadrupole moment is non-zero (it is not spherical), all related to the binding interaction having a non-central component. An alpha particle is tightly bound, but there are no stable $A = 5$ nuclei. The half-life of ${}^{5}_{2}$He is 7.9×10^{-22} s, while that of ${}^{5}_{3}$Li is about 3×10^{-22} s. In both cases, the odd nucleon has time for only a few nuclear transits before escaping.

Total Nuclear Spin

Total nuclear spin, denoted $\mathbf{I} = \mathbf{L} + \mathbf{S}$, can take integer or half-integer values, the result, as is that of the total magnetic moment, from the vector addition of intrinsic spins and moments of the constituent particles. As we'll see when we discuss nuclear models, explaining measured values is a challenge. The total atomic spin is denoted $\mathbf{F} = \mathbf{I} + \mathbf{J}$.

Magnetic Moments

Nuclear magnetic dipole moments result from the intrinsic magnetic dipole moments of constituent protons and neutrons, and also from the motion of protons. The velocities of nucleons in a nucleus range between $\beta = 0.001 - 0.1$, and can be envisioned as thrashing around in close contact. If we consider them to be point-like,

$$\mu_l = |\boldsymbol{\mu}_L| = g_l l |\boldsymbol{\mu}_N| \tag{6.20}$$

where g_l is the gyromagnetic ratio, l is the orbital angular momentum quantum number, and μ_N is the nuclear magnetron. $g_l = 1$ for protons and 0 for neutrons.

$$|\boldsymbol{\mu_N}| = \frac{e}{2m_p} \approx 10^{-3} |\boldsymbol{\mu}_b| \tag{6.21}$$

Similarly for the spin angular momentum

$$\mu_s = |\boldsymbol{\mu}_S| = g_s s |\boldsymbol{\mu}_N| \tag{6.22}$$

There is no theory for nucleon g_s like QED is for g_s of the electron. The measured values are $g_s^p \approx 5.6$ and $g_s^N \approx -3.8$. That g_s^p is quite different from 2 means that the proton is a compound object. That g_s^N is quite different from 0 means not only that the neuton is a compound object but also that it is comprised of charged objects distributed such that positive charge concentrates at the core and negative charge tends to the extremity.

The interaction of these dipole moments with the magnetic fields of atomic electrons results in atom energy level hyperfine splitting, depending on their relative orientation. Measurements of this splitting show that they are in some cases parallel and in other cases anti-parallel. When both A and Z of a nucleus are even, $\mu_N = 0$.

Quadrupole Moment

The existence of a (an electric) quadrupole moment indicates non-sphericity.

$$\mathcal{Q} = \frac{1}{e}\int_V (3z^2 - r^2)\rho(x,\ y,\ z)d\tau \tag{6.23}$$

where $r^2 = x^2 + y^2 + z^2$.

Consider, for example, a nucleus of Z protons (and $A - Z$ neutrons) as an ellipsoidal volume symmetric about one axis (call it the z-axis) so that the other axes x and y (semi-major/minor) are equal:

$$\frac{x^2 + y^2}{a^2} + \frac{z^2}{c^2} = 1 \tag{6.24}$$

within which the charge distribution is uniform $\rho(x, y, z) =$ constant. In this case, the volume of the ellipsoid is $V = \frac{4}{3}\pi a^2 c$, so

$$\rho(x, y, z) = \frac{Ze}{\frac{4}{3}\pi a^2 c} \tag{6.25}$$

Then, setting $R^2 = x^2 + y^2 \Rightarrow r^2 = R^2 + z^2$, and integrating in cylindrical coordinates (volume element $d\tau = RdRdzd\phi$),

$$\begin{aligned}
\mathcal{Q} &= 2\frac{1}{e}\frac{Ze}{\frac{4}{3}\pi a^2 c}\int_0^{2\pi}\int_0^{a}\int_0^{\frac{c}{a}\sqrt{a^2-R^2}} (2z^2 - R^2)RdRdzd\phi \\
&= \frac{3Z}{a^2 c}\int_0^{a}\int_0^{\frac{c}{a}\sqrt{a^2-R^2}} (2z^2 - R^2)RdRdz \\
&= \frac{2Z}{5}(c^2 - a^2)
\end{aligned} \tag{6.26}$$

Assume an average radius $\bar{R} = \sqrt[3]{a^2 c}$ and $c \approx a$, so that $c = \bar{R} \pm \delta R$, with $\delta R \ll \bar{R}$, then

$$a^2 = \frac{\bar{R}^3}{c} \approx \bar{R}^2\left(1 - \frac{\delta R}{\bar{R}}\right) \tag{6.27}$$

so that

$$c^2 - a^2 \approx \bar{R}^2\left\{\left[1 + 2\left(\frac{\delta R}{\bar{R}}\right)\right] - \left(1 - \frac{\delta R}{\bar{R}}\right)\right\} = 3\bar{R}^2\left(\frac{\delta R}{\bar{R}}\right) \Rightarrow \mathcal{Q} \approx \frac{6Z}{5}\bar{R}\delta R \tag{6.28}$$

One way to measure a nuclear electric quadrupole moment is via a technique called Mössbauer absorption spectroscopy. A pure sample of an element is immersed in a non-uniform electric field and exposed to a beam of gamma radiation emitted by the same isotope type as the sample. If the emitting and sampled nuclei were spherical, the nuclear transition energies would be exactly equal and resonant absorption would be observed with both materials at rest. The linear motor of a Mössbauer apparatus accelerates the source through a range of velocities, allowing a gamma ray energy scan via the Doppler effect. The intensity of gamma rays passing through the sample is recorded as a function of source velocity. At velocities corresponding to resonant energy levels of the sample, absorption increases, so the intensity drops, indicated by a dip in the spectrum.

Nuclei with $I > \frac{1}{2}$ appear non-spherical: their Mössbauer spectra exhibit, as dips, hyperfine splitting, removing the degeneracy among total spin projections I_z. The separation between dips indicates the magnitude and orientation of the nuclear charge distribution. If the quadrupole moment is found to be positive,

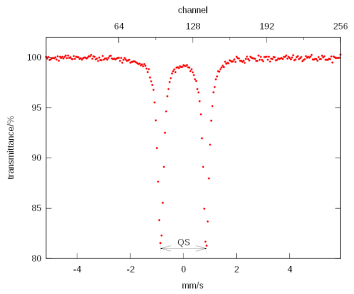

Figure 6.7: Sample Mössbauer absorption spectrum

then the ellipsoidal nucleus is prolate in the chosen field orientation. If it is negative, then the nucleus is oblate.

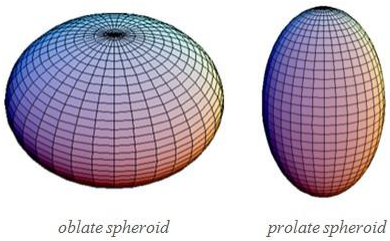

Figure 6.8: Oblate and prolate spheroids

What then is the relationship with I? Spinless nuclei have no total angular momentum vector that must maintain a fixed orientation in space, and so their orientation is a superposition of all possible orientations. Even if they were non-spherical, such nuclei would not exhibit hyperfine splitting in an oriented electric field due to the potential shifts averaging out. We'll see later that measurements of nuclear reactions can clarify the shape of $I = 0$ nuclei. As for $I = 1/2$ nuclei, they can assume only two orientations relative to an applied electric field. The interaction energies of the two orientations are equal, so the orientations are equally likely and the average energy split is zero, precluding the possibility of deducing non-sphericity in these kinds of measurements.

The rare earth elements (scadmium, yittrium, and the lanthanides) exhibit the largest $\mathcal{Q}$ values, the largest a prolate distribution in which c is 30% larger than a. On the other hand, $I = 0$ for more than half of all nuclei, and, even for $I > 1$ nuclei, the dimensions typically differ by no more than a few percent. For most purposes, then, the assumption of nuclear sphericity is an adequate approximation to the actual state.

6.3 Models

A successful model must be able to account for experimental results, for example, from scattering experiments. The scattering projectiles must have high kinetic energy, so that they can probe objects on the size of a nucleus, by $E = hc/\lambda$. As the nucleus occupies only 10^{-4} of an atom's volume, most projectiles pass through with their trajectory undeviated, but the distribution of scattering angles (differential cross-

sections: counts of particles scattering at specific angles) is evidence models have to describe, along with masses, stability, energy levels, and magnetic moments.

6.3.1 Liquid Drop Model

The liquid drop model is the oldest of still relevant nuclear models, and the most classical, but not completely so. It is premised on an analogy with an incompressible drop of liquid whose density is constant, and whose size and heat of vaporization (analogous to the binding energy) are proportional to its mass, or, equivalently, the number of its constituents. As we've seen, nuclear interior mass densities are approximately the same and nuclear binding energies are approximately proportional to their masses since $\Delta E/A \approx$ constant.

The liquid drop model pictures the nucleus as a sphere of uniform density which reduces to zero at its surface. By construction, the size (volume) of the nucleus is proportional to the number of nucleons, A, and so, consequently, density = mass/volume $\propto A/A =$ constant, as indicated by experiment. Furthermore, the surface area is therefore proportional to $A^{2/3}$, and the radius is proportional to $A^{1/3}$.

Because the nuclear interaction is attractive, a positive binding energy (positive work must be done to separate nucleons) due to it reduces the nuclear mass by an amount proportional to the number of nucleons, A, which, for an incompressible drop, is equivalent to the volume: $-a_V A$ ($a_V > 0$), where a_V, like the other proportionality constants to be introduced, must be determined empirically. Actually, alone of these constants, a_V can be estimated with QCD. This contribution assumes that every nucleon is surrounded by the same number of nucleons, which, of course, is not the case for those near the surface, which are, consequently, less tightly bound.

This "surface" effect increases the mass in proportion to the number of nucleons at the surface, $a_S A^{2/3}$.

The Coulomb energy between protons also decreases the binding energy (increasing the mass), by $E_C \propto Z^2/R = Z^2/r_0 A^{1/3} \propto Z^2/A^{1/3}$, and therefore increases the mass by $a_C Z^2 A^{-1/3}$.

Two quantum mechanical effects increase the mass, as well. An excess of protons over neutrons or neutrons over protons increases the mass in proportion to the excess or asymmetry, $a_A(N-Z)^2A^{-1} = a_A(A-2Z)^2A^{-1}$, due to the Pauli Exclusion Principle. Further, a so-called pairing energy, resulting from the tendency of neutrons or protons of opposite spin to group together, increases the mass as $a_P\delta(A,Z)A^{-1/2}$ (empirically; older versions of this model set the A-dependence $A^{-3/4}$) with the number of unpaired nucleons ($\delta(A,Z) = +1$ if both A and Z are even; 0 if A odd; and -1 if A is even but Z is odd).

Summing all these contributions results in a semi-empirical approximate mass formula

$$M = Zm_p + (A-Z)m_n - a_V A + a_S A^{2/3} + a_C Z^2 A^{-1/3} + a_A(A-2Z)^2A^{-1} + a_P\delta A^{-1/2} \tag{6.29}$$

The average binding energy per nucleon (not the energy required to remove a single nucleon) is then

$$\frac{\Delta E}{A} = \frac{[Zm_p + (A-Z)m_n - M]}{A} = a_V - a_S A^{-1/3} - a_C Z^2 A^{-4/3} - a_A(A-2Z)^2A^{-2} - a_P\delta A^{-3/2} \tag{6.30}$$

an approximately constant value (of 8 MeV) for large A, as we've seen.

6.3.2 Fermi Gas Model

Based on the free-electron gas model of conduction electrons in a metal, the Fermi gas model assumes that nucleons move in an attractive net potential of constant depth equal to the average interaction with other nucleons. The potential goes to zero within a distance equal to the range of nuclear forces. The net potential, then, approximates a three-dimensional finite square well of radius a little larger than the nuclear radius. The ground state minimizes the total energy without violating the Pauli Exclusion Principle.

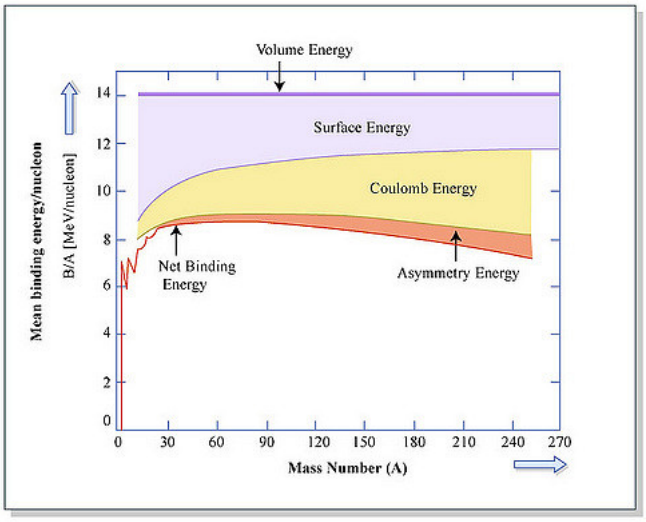

Figure 6.9: Contributions to the binding energy according to the liquid drop model (semi-emprical mass formula)

Since protons and neutrons are distinguishable, the Exclusion Principle treats them independently.

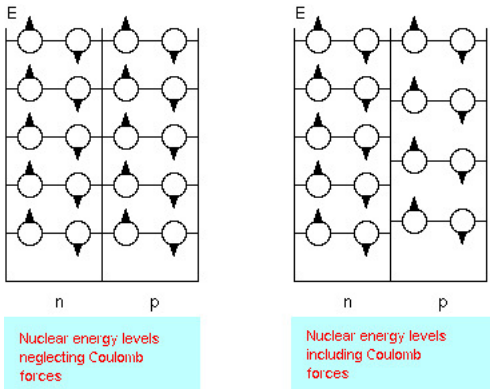

Figure 6.10: Neutron and proton energy levels in the Fermi gas model, without (left) and with (right) accounting for Coulomb repulsion

For a given value of A, at least for small A, the total energy of the nucleus is minimized if energy levels are filled with $Z = N$; otherwise, they'd occupy higher levels of energy. Through beta decay, a nucleus can adjust its N and Z values to approach $Z = N$, while maintaining $A = N + Z$. This idea is quantified in the asymmetry term of the semiempirical mass formula, $(Z - A/2)^2 A^{-1}$, which is minimized for $Z = A/2 = N$. Yet, stability requires $N > Z$ for large A, and the factor A^{-1} appearing in this term minimizes the contribution of the term, coinciding with the fact that the spacing between levels of a three-dimensional

potential well decrease with A. In sum, the asymmetry contribution decreases with A.

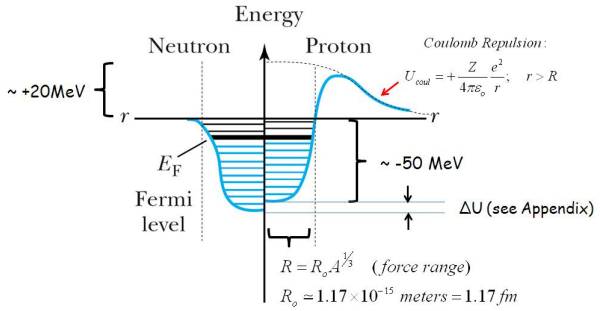

Figure 6.11: Nuclear fermi-energy levels; $\mathcal{E}_F \propto \rho^{2/3}$ (number density)

Because essentially every energetically accessible state is filled, the only possible collision is that in which two nucleons of the same type exchange quantum states, which, effectively, is not a collision. The few nucleons in partly filled degenerate states at the Fermi energy, can collide with one another, but this is a small fraction of the nuclear population. The conclusion of this picture is that, in a ground-state nucleus, nearly all nuclear constituents can move independently.

6.3.3 Shell Model

Considering the nucleus as a collection of individual nucleons in a potential well, as described in the Fermi Gas model, suggests inserting a potential into Schrödinger's equation to determine, for example, energy states. Evidence supporting such an approach is given by the existence of so-called magic number states, particularly stable nuclei with N or $Z = 2,\ 8,\ 20,\ 28,\ 50,\ 82,\ 125$. The nucleons that complete these "shells" have high binding energies, while the energies of the first excited states are larger than those of nuclei with similar, but not magic, nucleon counts.

This calls to mind the atomic shell model, and an analogous nuclear model has been constructed. This model pictures the short-range nuclear interaction not as a symmetrical central potential, but as a three-dimensional well, which acts as a restoring potential, like a three-dimensional harmonic oscillator, with potential energy of the form

$$U = \frac{1}{2}kR^2 = \frac{1}{2}m\omega^2 R^2 \tag{6.31}$$

and consequent energy levels

$$E_{n,l} = [2(n-1) + l]\omega \tag{6.32}$$

Here n, called the radial node quantum number, does not have the same meaning as n in the atomic case. Rather, it simply specifies the number of nodes of rR in the well, where rR is the product of the radial coordinate r with the radial dependence R of the eigenfunction. One implication of this is that the orbital angular momentum l is not limited by n. Note how increasing orbital angular momentum decreases the likelihood of $r = 0$, a sort of centrifugal effect.

Note also that $|rR|^2$ is proportial to the radial probability density.

In spectroscopic notation

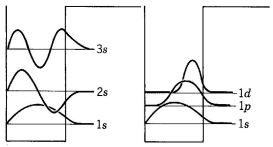

Figure 6.12: Nuclear wave functions in a shell model

value of l:	0	1	2	3	4	5	...
symbol:	s	p	d	f	g	h	...

The order (with respect to increasing energy) is shown by prefixing the value of n to the symbol for l.

It all works out pretty neatly, except that it doesn't get it right: there is no form for V(r) which leads even to the ordering of the nucleon energy levels required to explain the magic numbers.

To account for the observed magic number, a spin-orbit ($\mathbf{l} \cdot \mathbf{s}$) interaction must be included. Because $s = 1/2$, angular momentum states l are split into two orbitals, $i = l + \frac{1}{2}$ and $i = l - \frac{1}{2}$. The orbit is indicated symbolically by post-subscripting i. Each orbit contains a maximum of $2i + 1$ nucleons, and the Pauli exclusion principle excludes two nucleons with the same (n, l, i, m_i) quantum numbers. Shell closings correspond to the magic numbers. The relative energy splitting goes as

$$\mathbf{l} \cdot \mathbf{s} = \frac{1}{2}[i(i+1) - l(l+1) - s(s+1)] = \begin{cases} \frac{l}{2} & i = l + \frac{1}{2} \\ -\frac{l+1}{2} & i = l - \frac{1}{2} \end{cases} \tag{6.33}$$

The absolute energy splitting, $l + \frac{1}{2}$, increases with l. The energy of the $i = l + \frac{1}{2}$ orbit is lower than that of the $i = l - \frac{1}{2}$ orbit, a situation referred to as inverted.

The order in which the nuclear levels appear below the Fermi energy as the nuclear potential radius increases ($\propto A^{1/3}$) is given, at least for nuclei up to about $A = 184$, by the acrostic

spuds if pug dish of pig

that is,

spdsfpgdshfpig

and then applying the (inverted) spin-orbit splitting proportional to l.

Nucleons tend to pair up to form zero angular momentum states: even-even nuclei have zero total angular momentum, nuclei with odd numbers of protons or neutrons have total angular momentum and parity $[(-1)^l]$ due to the angular momentum of the last (odd) nucleon, while for odd-odd nuclei the parity is the product of those of the two odd nucleons, but the spin assignment is complicated.

This pairing interaction is a residual interaction not described by the shell-model net potential or the spin-orbit interaction. It amounts to a kind of collision, which reduces the energy of the system because they are close together. Being attractive, the coupling tends to be antiparallel: because nucleons are fermions, two of the same species must be described by an antisymmetric total eigenfunction, they are closer together if their spins are antiparallel and if their orbital angular momenta are also antiparallel, moving in opposite directions in the same orbit, as it were. This leads to the tendency for Z and N to be even and to the semiempirical mass formula's pairing term. This can lead to exceptions in ground state nuclear spin assignments and filling order.

This all works out quite nicely for energy levels and nuclear spins and parities. Because these are quantized, the assumptions underlying the pairing interaction do not have to be strictly met. This is not the case for multipole moments, whose magnitude need not be quantized.

6.3.4 The Collective Model

The collective model tries to combine features of the liquid drop and shell models, and by so doing provides a discription of multipole models. It does this by assuming nucleons in unfilled shells move independently but that the potential is not fixed, rather the nucleus undergoes shape deformations in accordance with correlated nuclear motions.

The deformations arise from the attractive interaction between the core and the independent nucleons, similar to tidal effects. As the independent nucleons move, so does the bulging, producing a magnetic dipole moment which can interact with an independently moving proton.

Since protons tend to populate the outer regions of the nucleus more than do neutrons, the tidal picture, due to both protons and neutrons in the unfilled shells, leads also to a description of the nuclear quadrupole moment discussed previously.

6.4 Decays and Reactions

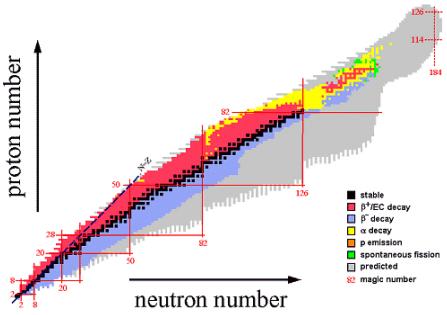

Figure 6.13: Nuclear stability curve

Some nuclei, in excited or ground states, undergo transformations, either through emission of massive particles [electrons (β^--decay), positrons (β^+-decay), or helium nuclei (α-decay)] or through emission of high-energy photons (γ-decay). All decay channels conserve charge, energy, linear and angular momentum, and nucleon number.

6.4.1 Radioactive Decay Law

A decay transformation results in a nucleus in a lower energy state (γ-decay) or a new nucleus (α- or β-decay). If, at $t = 0$ there are N_0 unstable parent nuclei, then there will be

$$N = N_0 e^{-\lambda t} \tag{6.34}$$

parent nuclei remaining at later time t. This is the radioactive decay law, a statistical rather than deterministic law: N is the expected number of surviving parents; Γ, called the decay or disintegration constant, characteristic of the parent and the process, is the inverse of the average or mean lifetime $\tau = 1/\Gamma$.

Another way to characterize the rapidity of the transformation is the half-life, also related to Γ:

$$\frac{1}{2} = e^{-\Gamma \tau_{1/2}} \Rightarrow \tau_{1/2} = \frac{\ln 2}{\Gamma} \tag{6.35}$$

and $\tau = \tau_{1/2}/\ln 2$.

The disintegration rate is also known as the activity:

$$\left|\frac{dN}{dt}\right| = \Gamma N_0 e^{-\Gamma t} = \Gamma N \tag{6.36}$$

As the number of parent nuclei decreases, the number of daughter nuclei increases, if stable: $N+N_D = N_0$. So,

$$N_D = N_0 - N = N_0(1 - e^{-\Gamma t}) \tag{6.37}$$

Typically, several related radioactive nuclei decay successively, so in nature one finds a standard mixture of nuclei. On the time scale of its lifetime, the parent population decreases exponentially, but, on the usually much shorter daughter lifetime time scale, the number of parents remains approximately constant, so the first daughter formation rate seems contant. Since they decay rapidly, the first daughter population is due entirely to parent decay rate, so the first daughter population remains constant. Similarly for the second daughters, and so forth: the populations of the parents and succeeding generations remain constant on time scales much shorter than the parent lifetime, approaching an equilibrium condition:

$$N_P\Gamma_P = N_{D1}\Gamma_{D1} = N_{D2}\Gamma_{D2} = \cdots \tag{6.38}$$

6.4.2 Alpha Decay

Alpha decay occurs commonly in nuclei with atomic number greater than $Z = 82$. It involves the emission of an α-particle–a helium nucleus–resulting in a different chemical element from the parent, one with an atomic mass reduced by four units and an atomic number reduced by two units.

$$^A_Z P \rightarrow ^{A-4}_{Z-2} D + ^4_2 He \tag{6.39}$$

The decay will occur spontaneously when the mass of the parent nucleus is greater than the mass of the daughter nucleus plus the mass of a helium nucleus. The total energy released in a decay, or the disintegration energy,

$$Q = M_{Z,A} - (M_{Z-2,A-4} + M_{2,4}) = M_P - (M_D + M_\alpha) \tag{6.40}$$

arises primarily from a reduction in the Coulomb energy of the nucleus when its charge Ze is reduced by charge $2e$. Energy conservation implies that

$$M_P = M_D + M_\alpha + K_D + K_\alpha \tag{6.41}$$

where K is kinetic energy. So Q is an invariant quantity, which, in the parent rest frame, is measured as

$$Q = K_D + K_\alpha \tag{6.42}$$

α-decay is a two body reaction, and momentum conservation along with energy conservation uniquely fixes the momentum and kinetic energy of the daughter nucleus and α-particle for a given parent nucleus.

Note that α-decay energies and lifetimes are inversely related (note log scale). The energies range from 8.9 MeV for $^{212}_{84}Po$ to 4.1 MeV for $^{232}_{90}Th$, perhaps a surprising small range and low values.

To explain, consider the $^{212}Po \rightarrow ^{208} Pb + ^4 He$ decay, and let's calculate the Coulomb repulsive potential when the two daughters are just touching. We approximate the lead nucleus and the α particle as uniformly charged spheres

$$V_0 = \frac{Z_{Pb}Z_{He}\alpha}{r'} \tag{6.43}$$

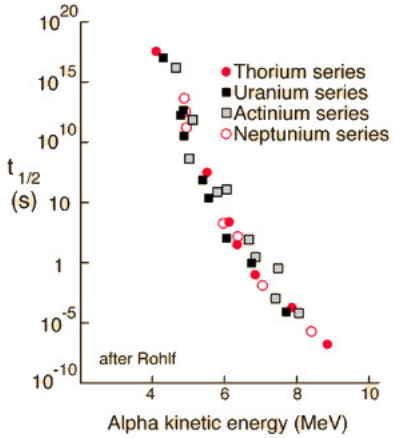

Figure 6.14: α-decay half-lives versus α-particles' kinetic energy

where $Z_{Pb} = 82$, $z_{He} = 2$, and $\alpha = 1/137$ is the fine structure constant. r' is the distance between the centers of the lead and helium nuclei. Recall that

$$R = r_0 A^{1/3} \tag{6.44}$$

where $r_0 \approx 1$ fm ≈ 5 GeV^{-1}, so $r' \approx 5 \times (4^{1/3} + 208^{1/3}) \approx 40$ Gev^{-1}. Plugging in all values, then, gives $V_0 \approx 0.03$ GeV $= 30$ MeV. Rutherford learned that the distance of closest approach of a 9 MeV α particle to a nucleus was 20 - 30 fm. The α particle feels the repulsive Coulomb potential increasing in inverse proportion to the distance between its center and that of the target nucleus. We just calculated that it would take 30 MeV of kinetic energy to reach the surface of the nucleus. Inside the surface it feels a rapid onset of the strong attractive nuclear potential, which soon dominates.

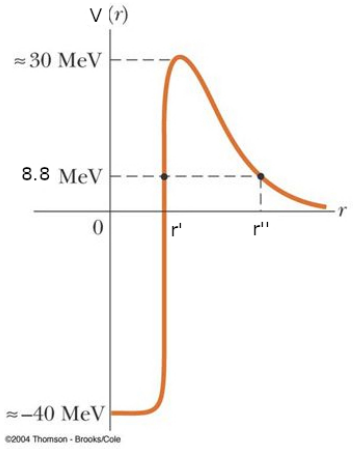

Figure 6.15: Coulomb barrier to α emission

So, why does the free α particle have less than 9 MeV of kinetic energy? To put the question another way, if a 9 MeV α particle is Coulomb repelled roughly 20-30 fm from the center of a 10 fm-radius nucleus, how does an α particle within the nucleus get out? The answer to these questions proved to be one of the early successes of quantum mechanics: barrier penetration (tunneling).

The quantum mechanical probability (flux) that a wave function can penetrate a potential barrier is given by the transmission coefficient:

$$T = \left[1 + \frac{\left(e^{\sqrt{2m(V_0-E)}a} - e^{-\sqrt{2m(V_0-E)}a}\right)^2}{16\frac{E}{V_0}\left(1-\frac{E}{V_0}\right)}\right]^{-1} \propto e^{-2\sqrt{2m(V_0-E)}a} \tag{6.45}$$

since $\sqrt{2m(V_0-E)}a \gg 1$.

This, of course, is the result for a rectangular barrier, but the Coulomb barrier can be modeled as a sum of rectangular barriers with decreasing heights, given by a Coulomb potential:

$$T \propto e^{-2\int_{r'}^{r''}\sqrt{2m(V(r)-E)}dr} \tag{6.46}$$

where now r' is the nuclear radius to the barrier maximum and r'' is the distance at which $V(r) < E$.

T is the instantaneous probability that an α particle with kinetic energy E trapped in a nuclear potential will penetrate a Coulomb barrier $V_0 > E$. We can imagine that such an α particle will be jostling around inside the nucleus and will periodically 'test' the barrier. The rate of such tests would depend on the particle's velocity and distance from the barrier:

$$N \approx \frac{v}{2r'} \tag{6.47}$$

This would give a decay rate (penetrations per second) of

$$\Gamma \approx \frac{v}{2r'}e^{-2\int_{r'}^{r''}\sqrt{2m(V(r)-E}dr} \tag{6.48}$$

and

$$\tau = \frac{1}{\Gamma} \tag{6.49}$$

V_0 and r' are roughly the same for $Z > 82$ nuclei, so the variation in Γ among the α emitters is primarily related to the α energy.

Now, $\tau(^{212}Po) \sim 10^{-6}$ s. How could there be any in nature? Short lifetime α emitters are in decay equilibrium families of lifetime parents. Such families are referred to as radioactive series, of which three can still be found in nature: $4n$ (Thorium; parent: $^{232}_{90}Th$, $\tau = 2.01 \times 10^{10}$ yr), $4n+2$ (Uranium; parent: $^{238}_{92}U$, $\tau = 6.52 \times 10^9$ yr), and $4n+3$ (Actium; parent: $^{235}_{92}U$, $\tau = 1.02 \times 10^9$ yr. The series names refer to the mass numbers of the elements in the series. For instance, the parent of the $4n+3$ series has $A = 235 = 4*58+3$. Since α decay is the only radioactive process that changes A, the A of all daughters in a series is a factor of 4 less than that of the parent.

What about $4n+1$ (Neptunium) series? It does exist, but the lifetime of the parent, $^{237}_{93}Np$, is only 3.25×10^6 yr, too short for any still to be present naturally. It can be produced artificially, and the radioactive series has been shown to follow, although unlike the others, which cascade to lead, this series cascades to ^{205}Tl (thalium). Note that ^{232}Th cascades to ^{208}Pb, ^{238}U cascades to ^{206}Pb, while ^{235}U cascades to ^{207}Pb.

6.4.3 Beta Decay

In the region of stability, plots of atomic masses $M_{Z,A}$ as a function of Z for fixed A are well described by the semi-empirical mass formula, except near magic numbers. If A is odd, the plot is a parabola; if A is even, there are two parabolas corresponding to the two possible signs of the semi-empirical mass formula's pairing term: a higher mass one when both Z and N are odd, and a lower mass on when both are even. These curves cross cut the stability curve, specifying how mass increases as Z varies from its most stable value at a given A. Clearly, for odd A, usually one, or at most two, values of Z are the most stable, while for even A, two or occasionally three values of Z are stable. Nuclei with other than the most stable Z for a given A, can become more stable by changing Z via one of three different β-decay processes: neutron-to-proton conversion with the release of an electron and an electron anti-neutrino, proton-to-neutron conversion with the release of a positron and an electron neutrino, and neutron-to-proton conversion with the capture of an inner-electron (usually a K electron) and the release of an electron neutrino. In each case, A remains unchanged, but Z changes by one unit, and a(n) (anti-)neutrino (ν) emerges as a decay product.

$$
\begin{aligned}
{}^{A}_{Z}P &\rightarrow {}^{A}_{Z+1}D + e^- + \overline{\nu} && (6.50)\\
{}^{A}_{Z}P &\rightarrow {}^{A}_{Z-1}D + e^+ + \nu && (6.51)\\
e^- + {}^{A}_{Z}P &\rightarrow {}^{A}_{Z-1}D + \nu && (6.52)
\end{aligned}
$$

α and β decays are competing processes for unstable nuclei. In both cases, the decay rates are directly related to the decay energy, as we've seen in the case of α decay. If an α decay would result in a nucleus far from the stability curve, it's energy would be small. But in this case, the β decay energy would relatively large, and consequently so will its rate. However, there are cases in which the rates are comparable, and so both processes occur with some comparable probability.

In β-decay, in terms of nuclear masses, and in the parent's rest frame,

$$M_P = M_D + m_e + K_{\text{total}} \tag{6.53}$$

so that

$$Q = K_{\text{total}} = (M_P - M_D - m_e) \tag{6.54}$$

We will see that this kinetic energy is not uniquely the electron's or positron's.

In inner electron capture, in terms of nuclear masses, and in the parent's rest frame,

$$M_P + m_e = M_D + K_{\text{total}} \tag{6.55}$$

so that

$$Q = K_{\text{total}} = M_P + m_e - M_D \tag{6.56}$$

is the kinetic energy of a mono-energetic neutrino, whose emission is followed by x-ray photons, characteristic of the *daughter* atom, as outer electrons fill vacated inner levels.

In terms of atomic masses, if $M(Z,A) > M_{Z+1,A}$, electron emission can occur. If $M_{Z,A} > M_{Z-1,A}$, then electron capture can occur. If $M_{Z,A} > M_{Z-1,A} + 2m_e$, positron emission can occur. But notice that in this circumstance, electron capture can also occur, while, on the other hand a range of atomic mass differences exists in which electron capture is possible but positron emission is energetically forbidden. In fact, atomic mass differences frequently fall in this range. As a result, the number of natural positron emitters is small.

In all these processes, the decay energy Q is typically less than 1 MeV, but can vary between a small fraction of 1 MeV to more than 10 MeV.

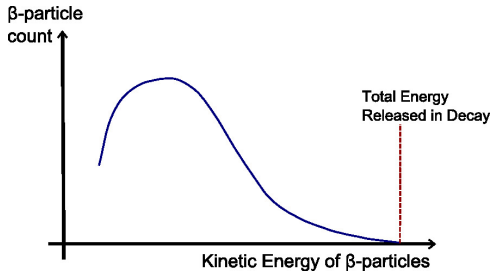

Figure 6.16: Kinetic energy spectrum of electons or positrons emitted in beta decay

Although people originally believed β decay to be a two-body process, the spectrum is clearly that of a three- (or more-) body process. This was eventually settled with the introduction of neutrinos.

6.4.4 Gamma Decay

If an excited nucleus relaxes to a lower energy state by emitting a photon, called a γ-ray, the atomic and mass numbers of the nucleus remain unchanged, and the photon has a definite energy corresponding to the discrete difference between energy levels:

$$h\nu = E_2 - E_1 \tag{6.57}$$

The frequencies (energies) of such photons are on average a thousand times higher than those of photons emitted in atomic transitions.

In ordinary cases, γ-decay occurs either after a β-decay leaves a daughter nucleus in an excited state, due to one or more selection rules preventing the energy-dependent tendency to transition to the ground state, or else following neutron capture.

The rate at which a given transition occurs is the inverse of the respective lifetime. It can range from around 10^{-8} to 10^{18} sec^{-1}. In natural units, the rate is the natural width (full width at half-max) of the excited state's energy distribution (a Breit-Wigner distribution). According to the energy-time uncertainty principle, if an excited state survives for the lifetime τ of the state, then its energy in the state can be specified only within an energy range Γ

$$\Gamma = \frac{1}{\tau} \tag{6.58}$$

Excited states are, thus, not perfectly sharp. Rather, they are spread over an energy range of width Γ. So, for example, an excited state with a typical lifetime of around 10^{-10} s has a width of about 10^{-5} eV, a very small fraction of the typical γ energy of around 1 MeV. Excited nuclei that γ-decay rarely are long-lived, but those that are are called isomers.

6.4.5 Nuclear Reactions

Nuclear reactions conserve total relativistic energy, linear momentum, angular momentum, charge, parity, and the number of nucleons. These should be obvious, except for the fact that beta decay does not conserve

parity. However, beta decay is not a nuclear reaction. It's the prototypical weak interaction, which does not conserve parity.

A reaction experiment is one in which a nucleus under study is bombarded with projectiles of known characteristics, and final products are investigated. In the typical experiment, only particles other than the residual nucleus are detected:

$$\text{Projectile} + \text{Target Nucleus} \rightarrow \text{Residual Nucleus} + \text{Detected Particle(s)}$$

where the total number of nucleons and charge are conserved. An abbreviated notation is commonly used for these reaction experiments:

$$\text{Target(Projectile, Detected Particle(s))Residual Nucleus}$$

Any stable nuclear particle can be a projectile or target. The number and type of emitted particles vary broadly. The residual nucleus will likely be stable if its Z-to-A ratio is approximately the same as that of the target nucleus. If this ratio is significantly smaller, the residual nucleus is usually radioactive, transforming via electron β decay. If this ratio is significantly larger, the residual nucleus is also radioactive, transforming via positron β decay or electron capture.

Nuclear reactors produce intense fluxes of neutrons, and are therefore used to produce radioactive electron-emitting tracers. Cyclotrons produce intense fluxes of charged particles, and are therefore used to produce sources of radioactive positron-emitting tracers or electron capturers.

Let's consider the example of a proton projectile. Unless its trajectory happens to be in the direction of the target nucleus's center, the Coulomb potential, or, if it gets close enough, the nuclear potential, will scatter it. Otherwise, it will probably collide with a nucleon part way through the nucleus, and, in a so-called direct interaction, either it or the struck nucleon, but not likely (1%) both, may escape immediately, carrying away most of the proton's energy. At least one of the two nucleons is likely to be reflected back into the nucleus at the nuclear surface, where the nuclear potential changes, as a light ray can be reflected at the boundary between different indices of refraction. An internally-reflected nucleon will likely collide with another nucleon, leading to a cascade of collisions. In this way, the energy of the reflected nucleon is distributed as vibrational excitations among many nucleons, a state referred to as a compound nucleus. No nucleon has sufficient excitation energy to escape the nuclear potential binding energy (8 MeV), but the collective vibrations may lead to a large enough fluctuation in the energy sharing to allow a nucleon to escape, assuming it is not internally reflected. Such fluctuations can lead to the "evaporation" of several nucleons, diminishing in the process the excitation energy of the compound nucleus. It will almost always be neutrons that evaporate, since protons must also overcome the Coulomb barrier. When the excitation energy falls below the neutron binding energy, the relatively slower process of γ decay eventually reduces the system to its ground state.

Classifying Nuclear Reactions

Scattering: The projectile and detected particle are the same

Elastic Scattering: The residual nucleus is left in its lowest or ground state

Inelastic Scattering: The residual nucleus is left in an excited state

Pickup: The projectile gains nucleons from the target

Stripping: The projectile loses nucleons to the target

Direct: The nucleon gained (lost) by the target enters (leaves) a shell without disturbing the target's other nucleons

Compound Nucleus: Target and projectile form a new nucleus in an excited state, which relaxes with a lifetime of around 10^{-16} s, much longer than the 10^{-21} s a traversal of the target by the projectile would take, so the subsequent transformation is independent of the formation of the compound nucleus.

Laboratory and Center-of-Mass Reference Frames

Consider this non-relativistically. If a projectile moves, in the laboratory frame, with velocity v_{proj}, then, in the center-of-mass (CM) frame,

$$v'_{proj} = v_{proj} - v_{CM} \tag{6.59}$$
$$v'_{targ} = v_{CM} \tag{6.60}$$

In the CM frame, $p_{tot} = 0$, so

$$\begin{aligned} m_{proj}v'_{proj} &= m_{targ}v'_{targ} \\ m_{proj}(v_{proj} - v_{CM}) &= m_{targ}v_{CM} \\ (m_{targ} + m_{proj})v_{CM} &= m_{proj}v_{proj} \end{aligned} \tag{6.61}$$

and $(m_{targ} + m_{proj})v_{CM}$ is the CM momentum in the laboratory frame. The transformation equations, then, are

$$v'_{targ} = \frac{m_{proj}}{m_{targ} + m_{proj}} v_{proj} \tag{6.62}$$
$$v'_{proj} = \frac{m_{targ}}{m_{targ} + m_{proj}} v_{proj} \tag{6.63}$$

6.4.6 Energy Relations

The energy released in a nuclear reaction

$$Q \equiv K_{\text{after}} - K_{\text{before}} = E_{0\ \text{before}} - E_{0\ \text{after}} \tag{6.64}$$

since $E = E_0 + K$ and energy is conserved. Exothermic or exoergic reactions, $Q > 0$, occur regardless of the kinetic energy of the initial particles. Endothermic or endoergic reactions, $Q < 0$ require the projectile kinetic energy to be above a certain threshold. If all particles are the same before and after the collision, and $Q = 0$, the reaction is elastic.

Consider a projectile a interacting with a target nucleus A at rest producing particle b and a residual nucleus B: $a + A \to b + B$. Relativistic energy will of course be conserved:

$$(K_a + m_a) + m_A = (K_b + m_b) + (K_B + m_B) \tag{6.65}$$

Then

$$Q = K_b + K_B - K_a = m_a + m_A - m_b - m_B \tag{6.66}$$

which shows that measuring an interaction's Q value offers information about the masses involved in the interaction, and can cross-check the results of mass spectrometry.

In principle, measuring K_a, K_b, and K_B would be sufficient, but it's often hard to measure K_B (being massive, there's little recoil and B is seldom free to investigate). But such nuclear physics interactions are typically sub-relativistic,

$$K = \frac{p^2}{2m} \tag{6.67}$$

and momentum is conserved,

$$\mathbf{p_a} = \mathbf{p_b} + \mathbf{p_B} \tag{6.68}$$

so

$$K_B = K_a \frac{m_a}{m_B} + K_b \frac{m_b}{m_B} - \frac{2}{m_B}\sqrt{m_a m_b K_a K_b}\cos\theta_{ab} \tag{6.69}$$

and

$$Q = K_b\left(1 + \frac{m_b}{m_B}\right) - K_a\left(1 - \frac{m_a}{m_B}\right) - \frac{2}{m_B}\sqrt{m_a m_b K_a K_b}\cos\theta_{ab} \tag{6.70}$$

where θ_{ab} is the angle between the directions of a and b.

6.4.7 Cross Sections

The probability that a projectile interacts with a nucleus in a given region of the target is called a cross section,

$$\sigma = \frac{\text{number of reactions per second per nucleus}}{\text{number of projectiles incident per second per area}} \tag{6.71}$$

the effective area per nucleus as "seen" by a projectile. It differs for different reactions and for different projectile energies (below threshold for an endothermic reaction, the cross section is zero). For a target of thickness t and n nuclei per unit volume, the number N_{sc} of particles scattered by N_0 incident projectiles is

$$N_{sc} = N_0(1 - e^{-n\sigma t}) \tag{6.72}$$

6.4.8 Fission

Bombarding uranium with neutrons produces elements in the middle of the periodic table, releasing, due to the reduction of Coulomb potential, around 200 MeV of energy in the form of the kinetic energy of the two fragments. Also emitted are two or three neutrons, which can induce remaining uranium nuclei to fission. Under certain conditions, a chain reaction can occur. If such a chain reaction could split all the nuclei in a block of uranium, the energy liberated would be $\sim 10^6$ times that liberated burning a block of coal or exploding a block of dynamite of the same mass, and because the time scale characterizing nuclear processes is much shorter than that characterizing atomic processes, the energy is released much more rapidly than in a chemical explosion.

The 200 MeV of released energy indicates that the fission potential well is around 200 MeV deep, implying that spontaneous splitting of uranium is unlikely. In fact, ^{238}U has a partial lifetime for fission of around 10^{16} years. What was just described is an example of induced fission, which is usually induced by the capture of a low-energy neutron. In a large-Z nucleus, the last neutron's binding energy $E_n \approx 6$ MeV. It may happen that the energy released in the capture is sufficient to exceed the fission barrier, or else it excites the nucleus into collective vibrations, similar to a compound nucleus, leading to periodic elongations, some of which may be sufficient for fission.

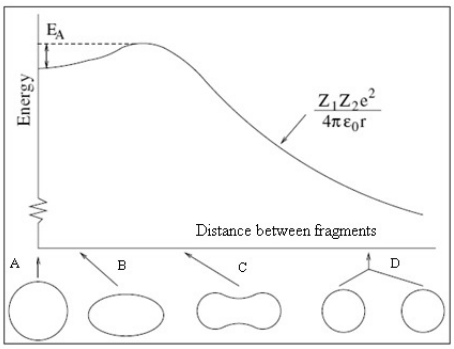

Figure 6.17: Potential energy curve as a function of distance between fragments when fission occurs

Such behavior exemplifies the collective motions expected in the liquid drop model, which, in turn, is the basis for the collective model.

A fission chain reaction can occur because each fission produces two or three neutrons. A fission rarely splits the parent in half. Rather, while both daughters approximately retain the Z:N ratio of the parent, one daughter normally has Z and N near the magic numbers 50 and 82, presumably to optimize energy. This, however, leaves both nuclei with excess neutrons relative to their atomic mass numbers. Beta decay accounts for most of the subsequent transformations toward the stability curve, despite it being a relatively slow, weak process. In the interim, the excited, unstable nuclei can evaporate one or more of the excess neutrons. A nucleus can still have excess neutrons after a β decay, and one of these can subsequently evaporate, a process referred to as delayed neutron emission.

In a fission reactor, surrounding the fissile material (uranium) with a low nuclear mass material moderate the kinetic energies of released neutrons by providing as scattering medium. This increases the likelihood that one or another of these neutrons is captured by another uranium atom, inducing the next fission. Smaller energies mean longer de Broglie wavelengths, and the cross section for neutron capture is directly related to this wavelength, rather than the size of the nucleus. To sustain a chain reaction, this cross section must be large enough to ensure that the probability is greater than or equal to 1 that one of the two or three neutrons from each fission will be captured. At reactor startup, the probability is tuned to be slightly bigger than 1 before gradually being reduced to 1 when equilibrium is attained. Such control is accomplished by interleaving rods with very large neutron capture cross sections between the uranium-moderator blocks. Control is made easier by the fact that some neutron emission is delayed.

The kinetic energies of all daughters are in part carried away by entropy absorbed in reactor parts. The entropy-transported kinetic energy boils a liquid which drives the turbines of electric generators.

6.4.9 Fusion

Fusion is the forming of a single nucleus from two nuclei. This will occur when the two nuclei have small A, and the A of resulting the nucleus is no more than 60, where the binding energy per nucleon is a maximum. In terms of the semi-empirical mass formula, fusing increases stability because it reduces the surface area relative to volume of low-mass nuclei, increasing the binding energy per nucleon more than the decrease from greater Coulomb energy, which isn't all that much because Z remains small.

Despite its favorable energetics, the cross section for such a transformation is miniscule at ordinary energies and not much bigger at significantly higher energies.

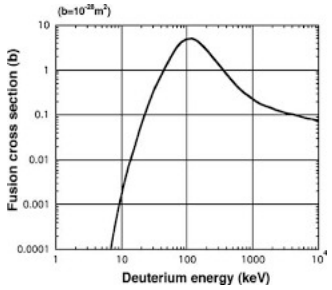

Figure 6.18: Cross section of Deuterium-Deuterium fusion as a function of Deuterium energy

Thermal fusion does occur in stars. The random kinetic energy at the sun's interior, where temperatures are $\sim 10^7$ K, is only around 10^3 eV, so fusion proceeds there at an extremely slow rate. The large quantity of energy produced by the sun is due to its size, not the tiny fusion reaction rate. Fusion in the stars results not only in a broad spectrum of electromagnetic radiation, but also the primordial production of all the elements from helium to iron.

Stars are believed to form from interstellar hydrogen (90%) and helium (10%) of extremely low density (1 atom/cm^3), both of which were created in the early universe as it began to cool, but before its rapid expansion period.

During the universe's initial high energy density/high temperature period, particles and radiation were in equilibrium:

$$
\begin{aligned}
n &\to p + e + \bar{\nu} \\
\bar{\nu} + p &\to n + \bar{e} \\
p + n &\to p + n + \gamma \\
e + \bar{e} &\to \gamma + \gamma \\
\gamma &\to e + \bar{e}
\end{aligned}
$$

During cooling prior to rapid expansion (inflation), the first nuclei and atoms formed:

$$
\begin{aligned}
&p + e \rightarrow {}^1_1 H + \gamma \\
&{}^1_1 H + n \rightarrow {}^2_1 H + \gamma \\
&{}^2_1 H + {}^2_1 H \rightarrow \begin{cases} {}^3_2 He + n \\ {}^3_1 H + {}^1_1 H \end{cases} \\
&{}^3_2 He + n \rightarrow {}^3_1 H + {}^1_1 H \\
&{}^3_1 H + {}^2_1 H \rightarrow {}^4_2 He + n
\end{aligned}
$$

The standard model of star formation begins with an upward density fluctuation in the diffuse interstallar medium. As a result, gas and dust begin to cluster, which, if sufficiently large, can, as a result of mutual gravitational attraction, stabilize and accrete, increasing the gravitational attraction. Interior pressure and temperature consequently increase. As the temperature approaches roughly 10^5 K, hydrogen atoms ionize, creating a plasma of protons and electrons. At $T \approx 10^7$ K, proton kinetic energy is just sufficient to penetrate one another's Coulomb barriers.

$$p + p \rightarrow d + \bar{e} + \nu + K(0.42 \text{ MeV})$$

Involving both electromagnetic penetration and weak decay, this process is very slow. The diproton state is highly unstable due to the Pauli exclusion principle, which forces the two protons to have anti-aligned spins, leading to large spin-spin interactions, in addition to large asymmetry and pairing contributions to the mass, all resulting in negative binding energy. Further, the temperature is insufficient for protons to fuse with helium and its two protons, but when, eventually, a sufficient number of deuterons are present, their fusion with protons to form helium involves only the strong nuclear force, and so readily proceeds. All of this comprises the so-called proton-proton cycle:

$$
\begin{aligned}
&p + p \rightarrow d + \bar{e} + \nu + K(0.42 \text{ MeV}) \\
&p + p \rightarrow d + \bar{e} + \nu + K(0.42 \text{ MeV}) \\
&d + p \rightarrow {}^3He + \gamma + K(5.49 \text{ MeV}) \\
&d + p \rightarrow {}^3He + \gamma + K(5.49 \text{ MeV}) \\
&{}^3He + {}^3He \rightarrow {}^4He + p + p + K(12.86 \text{ MeV}) \\
&e + \bar{e} \rightarrow \gamma + \gamma + K(1.02 \text{ MeV}) \\
&e + \bar{e} \rightarrow \gamma + \gamma + K(1.02 \text{ MeV})
\end{aligned}
$$

The proton-proton cycle liberates 26.72 MeV of energy. The two neutrinos carry away about 0.3 MeV. The rest is goes into random kinetic energy of core constituents, along with further gravitational contraction.

Because the $A = 5$ nuclear state is unstable, fusing individual nucleons to helium will not proceed to higher A nuclei. When the core density of primordial and proton-proton cycle helium is sufficiently high, carbon can form as follows

$${}^4He + {}^4He + {}^4He \rightarrow {}^8Be + {}^4He \rightarrow {}^{12}C + \gamma + K(7.28 \text{ MeV})$$

but only if the beryllium-helium fusion occurs before the ${}^8Be$ splits back into two helium nuclei within about 10^{-15} sec. As unlikely as this seems, an excited ${}^{12}C$ state at about 7.65 MeV, which happens to be the sum

of the kinetic energies of the three helium nuclei and the Q value when the core temperature reaches about 10^8 K, allows a resonance reaction, so the cross section becomes large enough for it to take place.

With increasing carbon density at the core, the carbon cycle replaces the proton-proton cycle as the primary energy source. Carbon, reappearing at the end of the cycle, acts as a catalyst in the fusion of four protons into helium, releasing along the way photons, positrons, and neutrinos.

$$
\begin{aligned}
&{}^{12}C + p \rightarrow {}^{13}N + \gamma + K(1.93 \text{ MeV}) \\
&{}^{13}N \rightarrow {}^{13}C + \bar{e} + \nu + K(1.20 \text{ MeV}) \\
&{}^{13}C + p \rightarrow {}^{14}N + \gamma + K(7.55 \text{ MeV}) \\
&{}^{14}N + p \rightarrow {}^{15}O + \gamma + K(7.29 \text{ MeV}) \\
&{}^{15}O \rightarrow {}^{15}N + \bar{e} + \nu + K(1.73 \text{ MeV}) \\
&{}^{15}N + p \rightarrow {}^{12}C + {}^{4}He + K(4.96 \text{ MeV}) \\
&e + \bar{e} \rightarrow \gamma + \gamma + K(1.02 \text{ MeV}) \\
&e + \bar{e} \rightarrow \gamma + \gamma + K(1.02 \text{ MeV})
\end{aligned}
$$

The carbon cycle also liberates 26.72 MeV of energy, but these neutrinos carry away 1.4 MeV. Since no step in the carbon cycle is as slow as the proton-proton fusion at the beginning of the proton-proton cycle, the former process proceeds much more rapidly than the latter.

While some carbon is forming in the sun, it has not yet entered the carbon cycle. A star with twice the mass of the sun's would rapidly reach the higher, critical temperature.

As the density and temperature of the core increases, heavier elements are formed by successive fusing of helium: ${}^{16}_{8}O$, ${}^{20}_{10}Ne$, ${}^{24}_{12}Mg$. When the core temperature reaches around 10^9 K, these nuclei fuse to form even A nuclei up to ${}^{56}_{26}Fe$.

Outside the core, where it's cooler, the proton-proton cycle continues. Even-A nuclei straying into this region can fuse with protons to produce odd-A nuclei. For example,

$$
\begin{aligned}
{}^{20}_{10}Ne + p &\rightarrow {}^{21}_{11}Na + \gamma \\
{}^{21}_{11}Na &\rightarrow {}^{21}_{10}Ne + \bar{e} + \nu
\end{aligned}
$$

Such odd-A nuclei can fuse with helium and release neutrons

$$
{}^{21}_{10}Ne + {}^{4}_{2}He \rightarrow {}^{24}_{12}Mg + n
$$

Because the maximum binding energy per nucleon is realized at $A \approx 60$, and therefore Coulomb repulsion no longer favors nucleus capture, iron is about the heaviest element to be formed by fusion. Neutron capture, however, which proceeds by the strong nuclear force, will occur, since it releases abou 6 MeV of binding energy. Thus, through a series of neutron captures and subsequent β decays, so as to keep the Z/A ratio along the stability curve, nuclei can be formed, beginning with ${}^{56}_{26}Fe$, up to ${}^{209}_{83}Bi$. Abundances of such atoms, as discerned from spectral measurements, cosmic ray and meterorite analyses, and the composition of Earth, are inversely related to their neutron capture cross sections, when these are averaged over the neutrons' high thermal energy distribution. Except as filled shells affect neutron affinity and binding energies, neutron capture cross sections tend to increase–so abundances decrease–with A.

Because the half-life of $^{210}_{83}Bi$ to α-decay is only 5 days, too little time for additional neutron capture, given the relative dearth of neutrons, $^{209}_{83}Bi$ is the end of the neutron capture series. But when the temperature of the core begins to fall due to lack of fusion fuel, a precipitous gravitational collapse leads to an explosion producing an enormous neutron flux, which likely leads to such a rapid succession of neutron captures that elements heavier than $^{209}_{83}Bi$ form.

Chapter 7

Relativistic Kinematics

7.1 Covariant Notation

Consider space-time coordinates as a four-dimensional vector or four-vector (also called a Lorentz vector):

$$x^{\mu} = \begin{pmatrix} t \\ x \\ y \\ z \end{pmatrix} \tag{7.1}$$

The superscript $\mu = 0, 1, 2, 3$ designates this as a contravariant vector. The equivalent covariant vector has a subscript.

The magnitude squared of a four-vector is an invariant

$$x^2 \equiv \sum_{\mu,\nu} g_{\mu\nu} x^{\mu} x^{\nu} = t^2 - x^2 - y^2 - z^2 \tag{7.2}$$

where $g_{\mu\nu}$ is the covariant metric tensor of special relativity:

$$g_{\mu\nu} = \mathrm{diag}(1, -1, -1, -1) \equiv \begin{pmatrix} 1 & 0 & 0 & 0 \\ 0 & -1 & 0 & 0 \\ 0 & 0 & -1 & 0 \\ 0 & 0 & 0 & -1 \end{pmatrix} \tag{7.3}$$

The notation of Equation 7.2 can be simplified further by adopting the Einstein summation convention, or contraction, which drops the summation signs in lieu of implicit summation over pairs of co- and contravariant indices.

$$x^2 = g_{\mu\nu} x^{\mu} x^{\nu} \tag{7.4}$$

The covariant metric tensor transforms a contravariant vector into a covariant vector

$$x_{\mu} = g_{\mu\nu} x^{\nu} \tag{7.5}$$

and the contravariant metric tensor transforms a covariant vector into a contravariant vector

$$x^\mu = g^{\mu\nu} x_\nu \tag{7.6}$$

Thus, Equation 7.4 will usually be written

$$x^2 = x_\mu x^\mu \tag{7.7}$$

7.2 Four-Momentum

In particle physics, this notation is most often used with the energy-momentum four-dimensional, or four-momentum, vector

$$p^\mu = \begin{pmatrix} E \\ p_x \\ p_y \\ p_z \end{pmatrix} \tag{7.8}$$

The squared magnitude of this four-vector is the squared invariant mass

$$m^2 = p^2 = E^2 - |\mathbf{p}|^2 \tag{7.9}$$

Here, $E = \gamma m$ and $|\mathbf{p}| = \beta\gamma m$, where $\gamma = \sqrt{\frac{1}{1-\beta^2}}$ and $\beta = \frac{v}{c}$ is the speed relative to the speed of light.

7.3 Lorentz Transformations

Special relativity is based on the axiom that the squared four-vectors just presented are Lorentz scalars, that is, they are invariant under Lorentz transformations, in which the Lorentz vectors themselves transform as

$$x^\mu \to x^{\mu'} = \Lambda^\mu_\nu x^\nu \tag{7.10}$$

in the contravariant case. In the covariant case,

$$x_\mu \to x'_\mu = \Lambda^\nu_\mu x_\nu \tag{7.11}$$

Typically, Λ is a boost along some axis. Choosing the x-axis, for example, and boosting along it $-\beta$, such that a particle with velocity β along x in the lab frame is at rest in the boosted frame,

$$\Lambda^\mu_\nu = \begin{pmatrix} \gamma & -\beta\gamma & 0 & 0 \\ -\beta\gamma & \gamma & 0 & 0 \\ 0 & 0 & 1 & 0 \\ 0 & 0 & 0 & 1 \end{pmatrix} \tag{7.12}$$

Higher-rank tensors (a scalar is a rank-zero tensor, a vector is a rank-one tensor) are boosted along each rank:

$$A^{\mu\nu} \to A^{\mu\nu'} = \Lambda^\mu_\rho \Lambda^\nu_\sigma A^{\rho\sigma} \tag{7.13}$$

Note that from Equations 7.10 and 7.11 that $\Lambda^\mu_\nu \neq \Lambda^\nu_\mu$. Rather,

$$\Lambda^{\nu}_{\mu} = g_{\mu\rho}\Lambda^{\rho}_{\sigma}g^{\sigma\nu} \tag{7.14}$$

Also note that the matric tensor is a rank one tensor, and so transforms

$$g^{\mu\nu} = \Lambda^{\mu}_{\rho}\Lambda^{\nu}_{\sigma}g^{\rho\sigma} \tag{7.15}$$

This condition defines the Lorentz group, the possible Lorentz transformations.

7.4 Collisions

In relativistic kinematics, the total four-momentum is conserved. In the center of mass (CM) frame, the magnitude of the total momentum is zero, but not the total energy.

Remember the difference between conserved and invariant quantities: a conserved quantity is one that is the same value before and after an interaction; an invariant quantity has the same value in all inertial systems. Energy is conserved in all interactions, but not invariant in different frames; mass is invariant in different frames, but not conserved in interactions.

See Griffiths, chapter 3, for examples.

Suggestions for solving problems in relativistic kinematics:

1. Use the invariant $m^2 = E^2 - p^2$ when you know a particle's momentum and need to know its energy, and vice versa.
2. Use $p/E = \beta$ if you want to determine the velocity knowing the momentum and energy.
3. Exploit the invariance of the square of the energy-momentum 4-vector, $p^2 = m^2$.
4. Try the CM frame if you're frustrated by the lab frame.

Chapter 8

Symmetries, Conservation Laws, and Group Theory

8.1 Introduction

By symmetry is meant an operation that can (at least in principle) be performed on a system which leaves the system invariant, such that the system after the operation is indistinguishable from the system before the operation. Symmetries are associated with conservation laws by Noether's Theorem, and are described mathematically by group theory.

8.2 Groups

A group, G, is a set of elements, $A,\ B,\ C, \ldots$, and an operator, $\bullet$, that satisfy the following axioms:

closure: If A and B are elements of G, then so is $A \bullet B$

associativity: If A, B, and C are elements of G, then $A \bullet (B \bullet C) = (A \bullet B) \bullet C$

identity: There exists an element, I, of G such that for every element of G, $A \bullet I = I \bullet A = A$

inverse: For every element of G, there exists an inverse $A \bullet A^{-1} = A^{-1} \bullet A = I$

The equilateral triangle, for example, is unaffected by a (counter-)clockwise rotation $(R_-)R_+$ through $\frac{2\pi}{3}$ radians, rotations about a bisector of any vertex, $R_A,\ R_B,\ R_C$, or by doing nothing, I. Note that, for example, $R_+^2 = R_+ \bullet R_+ = R_-$. We can call this the equilateral triangle group.

If any two group elements A and B commute, $A \bullet B = B \bullet A$, the group is referred to as abelian, otherwise as non-abelian.

A function f that perserves group structure, that is, $f(B) \bullet f(B) = f(A \bullet B)$ is referred to as a group homomorphism, implying that f maps G onto another group. If there exists a function g that reverses the mapping, $g(f(A)) = A$, for all elements of G, then f is referred to as a group isomorphism.

Table 8.1: Equilateral triangle group operations (group table)

	I	R_+	R_-	R_A	R_B	R_C
I	I	R_+	R_-	R_A	R_B	R_C
R_+	R_+	R_-	I	R_C	R_A	R_B
R_-	R_-	I	R_+	R_B	R_C	R_A
R_A	R_A	R_C	R_B	I	R_+	R_-
R_B	R_B	R_A	R_C	R_-	I	R_+
R_C	R_C	R_B	R_A	R_+	R_-	I

Groups can be represented by groups of matrices. That is, matrix M_A corresponds to element A for all elements, and if $A \bullet B = C$, then $M_A M_B = M_C$. The representation is not necessarily faithful, in the sense that any number of elements may be represented by the same matrix, that is, the group of matrices is homomorphic, but not necessarily isomorphic.

If G is a group of matrices, it represents itself, and is in fact the fundamental representation. Generally, matrices of various dimensions will also represent G. Additional representations can be constructed by combining irreducible ones that can be decomposed into block diagonal form, but these are not counted. Only the irreducible ones are of concern to physics.

8.3 Continuous Symmetries

The equilateral triangle group is an example of a finite group (it contains a finite number of elements), but there are also infinite groups (consider the circle rather than the equilateral triangle).

8.3.1 $SO(2)$

Special orthogonal transformations in two dimensions are represented by the group $SO(2)$. Orthogonal means that the transformation matrices are square with determinants of 1 or -1, satisfy $O^T O = O O^T = I$ or, equivalently, $O^T = O^{-1}$, and whose rows and columns are orthogonal unit vectors, while sums of products across rows or columns are zero. Orthogonality implies that the magnitude of the transformed vectors is left invariant. Special means that the determinants of the matrices equal 1, which implies that only rotations–not reflections–are allowed.

A fundamental representation of this group is the 2×2 rotation matrix

$$O_\alpha = \begin{pmatrix} \cos\alpha & \sin\alpha \\ -\sin\alpha & \cos\alpha \end{pmatrix} \tag{8.1}$$

describing clockwise rotations of angle α.

This is an abelian group, so a finite rotation can be thought of as a product of n rotations each of angle α/n,

$$O_\alpha = (O_{\alpha/n})^n \tag{8.2}$$

Keeping this in mind, let $n \to \infty$, so that α/n is small enough to take only the first terms in the Taylor expansions of the the trigonometric functions

$$O_\alpha = \lim_{n\to\infty} \begin{pmatrix} 1 & \alpha/n \\ -\alpha/n & 1 \end{pmatrix}^n \equiv \lim_{n\to\infty} \left(I - i\frac{\alpha}{n}J\right)^n \tag{8.3}$$

where, again, I is the identity matrix (here, 2×2), and

$$J \equiv \begin{pmatrix} 0 & i \\ -i & 0 \end{pmatrix} \tag{8.4}$$

Recalling that $e^A = \lim_{n\to\infty}(1 + A/n)^n$,

$$O_\alpha = e^{-i\alpha J} \tag{8.5}$$

J is called the generator of this representation of $SO(2)$: all rotations can be generated begining with J.

$SO(2)$ can be conceptualized therefore as describing rotations in the complex plane, products of $e^{i\alpha}$ for real α. Such transformations leave the magnitude of complex numbers invariant. This is actually the definition of the group of unitary transformations in one, complex dimension, $U(1)$, signifying that $U(1)$ and $SO(2)$ are isomorphic to one another.

8.3.2 $SO(3)$

Rotations in three dimensions are described by the group $SO(3)$. The Cartesian axes may be taken as the axes of rotation

$$R_{\alpha_x} = \begin{pmatrix} 1 & 0 & 0 \\ 0 & \cos\alpha_x & \sin\alpha_x \\ 0 & -\sin\alpha_x & \cos\alpha_x \end{pmatrix} \quad R_{\alpha_y} = \begin{pmatrix} \cos\alpha_y & 0 & -\sin\alpha_y \\ 0 & 1 & 0 \\ \sin\alpha_y & 0 & \cos\alpha_y \end{pmatrix} \quad R_{\alpha_z} = \begin{pmatrix} \cos\alpha_z & \sin\alpha_z & 0 \\ -\sin\alpha_z & \cos\alpha_z & 0 \\ 0 & 0 & 1 \end{pmatrix} \tag{8.6}$$

Using the same approach as with $SO(2)$, an arbitrary rotation

$$R = e^{-i\boldsymbol{\alpha}\cdot\mathbf{J}} \tag{8.7}$$

where

$$\boldsymbol{\alpha} = (\alpha_x,\ \alpha_y,\ \alpha_z) \tag{8.8}$$

are the rotation angles about the axes and

$$J_x = \begin{pmatrix} 0 & 0 & 0 \\ 0 & 0 & i \\ 0 & -i & 0 \end{pmatrix} \quad J_y = \begin{pmatrix} 0 & 0 & -i \\ 0 & 0 & 0 \\ i & 0 & 0 \end{pmatrix} \quad J_z = \begin{pmatrix} 0 & i & 0 \\ -i & 0 & 0 \\ 0 & 0 & 0 \end{pmatrix} \tag{8.9}$$

are the generators for the rotation matrices.

Arbitrary $S0(3)$ rotations, unlike $SO(2)$ rotations, are non-abelian:

$$[J_k, J_l] = 2i\sum_m \varepsilon_{klm} J_m \tag{8.10}$$

where ε_{klm} is the completely antisymmetric, rank 3, unit tensor: $\varepsilon_{klm} = -\varepsilon_{lkm} = 1$, and similarly with other permutations, while $\varepsilon_{kkl} = 0$, and similarly with any repeated indices. The commutation relations of Equation 8.10 consititue the $SO(3)$ Lie algebra, a linear algebra that underlies the group properties.

8.3.3 $SU(2)$

The conjugate transpose (Hermitian conjugate) of a unitary matrix is equal to its inverse, $U^\dagger U = UU^\dagger = I$. Special unitary matrices have determinant 1. They have the form

$$U = \begin{pmatrix} r_0 - ir_3 & -r_2 - ir_1 \\ r_2 - ir_1 & r_0 + ir_3 \end{pmatrix} \tag{8.11}$$

where r_i are real.

The unitary condition is satisfied if $r_0^2 + r_1^2 + r_2^2 + r_3^2 = 1$, which also satisfies the unit determinant condition. Therefore,

$$r_0 = \sqrt{1 - (r_1^2 + r_2^2 + r_3^2)} \tag{8.12}$$

which in the infinitessimal limit of $d\mathbf{r} = (dr_1,\ dr_2,\ dr_3)$, and to first order, $r_0 = 1$, so

$$U = I - id\mathbf{r} \cdot \boldsymbol{\sigma} \tag{8.13}$$

where $\boldsymbol{\sigma} = (\sigma_1,\ \sigma_2,\ \sigma_3)$ are the Hermitian Pauli matrices

$$\sigma_1 = \begin{pmatrix} 0 & 1 \\ 1 & 0 \end{pmatrix} \quad \sigma_2 = \begin{pmatrix} 0 & -i \\ i & 0 \end{pmatrix} \quad \sigma_3 = \begin{pmatrix} 1 & 0 \\ 0 & -1 \end{pmatrix} \tag{8.14}$$

which satisfy the commutation relations

$$[\sigma_k, \sigma_l] = 2i \sum_m \varepsilon_{klm} \sigma_m \tag{8.15}$$

The Pauli matrices as written here are normalized such that

$$\mathrm{Tr}(\sigma_k \sigma_l) = 2\delta_{kl} \tag{8.16}$$

Notice that σ_2 is the generator of $SO(2)$, and the commutation relations are the same as those for $SO(3)$. While the three differ globally, they are equivalent locally.

8.3.4 $SU(3)$

$SU(3)$ is the three-dimensional equivalent of $SU(2)$. A general $n \times n$ complex matrix has $2n^2$ free parameters. A unitarity constraint reduces that to n^2. The determinant-1 requirement reduces the number of free parameters by 1. So, $SU(n)$ matrices have $n^2 - 1$ free parameters. While $SU(2)$, therefore, has 3 free parameters and, hence, 3 group generators (the Pauli matrices), $SU(3)$ has 8 free parameters and generators, which are usually the Gell-Mann matrices

$$\lambda_1 = \begin{pmatrix} 0 & 1 & 0 \\ 1 & 0 & 0 \\ 0 & 0 & 0 \end{pmatrix} \quad \lambda_2 = \begin{pmatrix} 0 & -i & 0 \\ i & 0 & 0 \\ 0 & 0 & 0 \end{pmatrix} \quad \lambda_3 = \begin{pmatrix} 1 & 0 & 0 \\ 0 & -1 & 0 \\ 0 & 0 & 0 \end{pmatrix}$$
$$\lambda_4 = \begin{pmatrix} 0 & 0 & 1 \\ 0 & 0 & 0 \\ 1 & 0 & 0 \end{pmatrix} \quad \lambda_5 = \begin{pmatrix} 0 & 0 & -i \\ 0 & 0 & 0 \\ i & 0 & 0 \end{pmatrix} \quad \lambda_6 = \begin{pmatrix} 0 & 0 & 0 \\ 0 & 0 & 1 \\ 0 & 1 & 0 \end{pmatrix} \tag{8.17}$$
$$\lambda_7 = \begin{pmatrix} 0 & 0 & 0 \\ 0 & 0 & -i \\ 0 & i & 0 \end{pmatrix} \quad \lambda_8 = \tfrac{1}{\sqrt{3}} \begin{pmatrix} 1 & 0 & 0 \\ 0 & 1 & 0 \\ 0 & 0 & -2 \end{pmatrix}$$

The commutation relations between these are

$$[\frac{\lambda_k}{2}, \frac{\lambda_l}{2}] = i \sum_m f_{klm} \frac{\lambda_m}{2} \tag{8.18}$$

where f_{klm} are structure constants antisymmetric under the exchange of two indices and

$$f_{123} = 1 \quad f_{458} = f_{678} = \frac{\sqrt{3}}{2} \quad f_{147} = f_{165} = f_{246} = f_{257} = f_{345} = f_{376} = \frac{1}{2} \tag{8.19}$$

The normalization of the Gell-Mann matrices as written here is, like that of the Pauli matrices

$$\mathrm{Tr}(\lambda_k \lambda_l) = 2\delta_{kl} \tag{8.20}$$

Chapter 9

Standard Model

9.1 Introduction

On the fundamental level, matter is made of three types of elementary particles: quarks, leptons, and mediators.

Table 9.1: Quarks

quark	mass [MeV]	charge	D	U	S	C	B	T
d	2	$-1/3$	-1	0	0	0	0	0
u	5	$2/3$	0	1	0	0	0	0
s	100	$-1/3$	0	0	-1	0	0	0
c	1200	$2/3$	0	0	0	1	0	0
b	4200	$-1/3$	0	0	0	0	-1	0
t	174000	$2/3$	0	0	0	0	0	1

Table 9.2: Leptons

lepton	mass [MeV]	charge	L_e	L_μ	L_τ
e	0.511	-1	1	0	0
ν_e	$< 2 \times 10^{-6}$	0	1	0	0
μ	106	-1	0	1	0
ν_μ	< 0.2	0	0	1	0
τ	177	-1	0	0	1
ν_τ	< 18	0	0	0	1

Each lepton and quark pairs with an anti-lepton and anti-quark, with opposite quantum number signs. Each quark and anti-quark has three different colors (strong charge), and there are eight sorts of gluon. And then there's the Higgs boson. In some counting schemes, that's 61 different particles.

Table 9.3: Mediators

Mediator	Charge	Mass [MeV]	Lifetime [s]
gluon	0	0	∞
photon	0	0	∞
$W^{\pm}$	± 1	80420	3.11×10^{-25}
Z^0	0	91190	2.64×10^{-25}
graviton	0	0	∞

We know of four kinds of interactions among these particles (although not every particle engages in each kind of interaction; in fact, the kind of interactions a given particle engages in is one of the distinctions among the particles): strong, electromagnetic, weak, and gravitational. In quantum field theory, each interaction involves a field and a mediator.

Table 9.4: Interactions

Interaction	Relative Strength	Theory	Mediator
Strong	10	QCD	gluon
Electromagnetic	10^{-2}	QED	photon
Weak	$\sim 10^{-13}$	QFD	$W^{\pm}$, Z^0
Gravitational	10^{-42}	GR	graviton

Particle physics does not take gravitation into account. On the scale of of the interactions at accessible energies (and distances), it is much too weak to make an impact.

Here we present a qualitative overview of the remaining three interactions. Much of the presentation depends on interpretting Feynman diagrams. Recall that, in the convention we are using, time flows from left to right. Other than that, nothing empirical is represented.

Feynman diagrams are shorthand for a quantity calculable by following rules for interpreting them. To analyze a process, all diagrams that can contribute to that process should be identified (drawn). This amounts to creating every possible way that the inbound external lines can result in the outbound external lines, regardless of the number of internal lines and vertices. Each diagram is evaluated by following Feynman rules, which enforce momentum and energy conservation at each vertex–and therefore for the entire diagram. The results of these evaluations are summed, and this sum represents the physical process represented by the external lines.

It turns out that the number of such diagrams is infinite. What may, or may not save the day, depending on the interaction, is that each vertex in a diagram contributes a multiplicative factor, related to the strength of the interaction. If the factor is significantly less than 1, the contribution from additional vertices decreases with number, so the number of diagrams that need to be considered to evaluate the process depends on the precision required, and may not be very many.

9.2 Quantum Electrodynamics (QED)

All electromagnetic phenomena are reducible to a charged particle emitting or absorbing a photon.

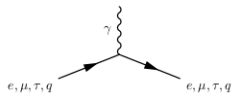

Figure 9.1: All QED interactions are built from this QED primitive

More complicated processes are combinations of this primitive vertex, for example Møller scattering (Coulomb repulsion).

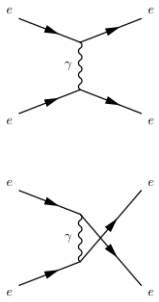

Figure 9.2: Møller scattering (Coulomb repulsion)

Both diagrams must be included in the analysis.

Topological reconfiguring of a Feynman diagram (usually) results in a diagram of another physical process. Rotating or twisting the Møller scattering diagram yields Bhabha scattering (Coulomb attraction).

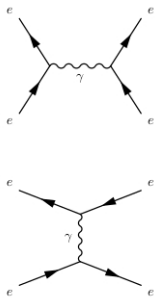

Figure 9.3: Bhabha scattering (Coulomb attraction)

A particle line pointing backward in time represents the corresponding antiparticle. Again, both diagrams must be included in the analysis.

Møller and Bhabha scattering are related by *crossing symmetry*. The occurrence of reaction

$$A + B \to C + D \tag{9.1}$$

implies that reactions expressed by moving one constituent of such a viable reaction to the other side of process are dynamically possible and will occur if they are kinematically possible. That is, assuming no conservation law is violated, the following reactions will also occur:

$$A \to \bar{B} + C + D \tag{9.2}$$
$$A + \bar{C} \to \bar{B} + D \tag{9.3}$$
$$\bar{C} + \bar{D} \to \bar{A} + \bar{B} \tag{9.4}$$

Notice that moving a constituent to the other side of the process requires transforming it into it opposite: particle → anti-particle; anti-particle → particle. The reverse reaction $C + D \to A + B$ may be allowed due to the detailed balance principle rather than crossing symmetry.

Calculations involving crossing symmetry-related diagrams are nearly identical. From this point of view, they are essentially distinct physical manifestations of the same process.

Thus, Compton scattering, pair-production, and pair-annihilation are roughly indistinquishable theoretically, albeit clearly different empirically.

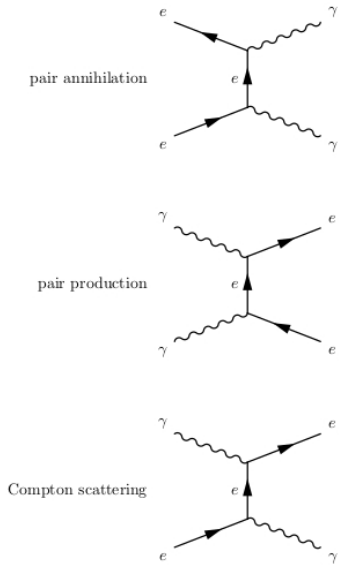

Figure 9.4: Photon interaction processes: Top: Pair annihilation $e^- + e^+ \to \gamma + \gamma$; Middle: Pair production $\gamma + \gamma \to e^- + e^+$; Bottom: Compton scattering $\gamma + e^- \to \gamma + e^-$

Additional vertices require adding primitive vertices. Here are additional diagrams for Møller scattering (Coulomb repulsion)

Internal lines do not manifest. The particles they represent are referred to as virtual particles; they cannot be observed. External lines exhibit the physically observable process; internal lines describe the underlying mechanism.

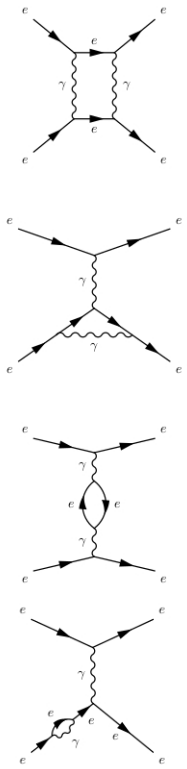

Figure 9.5: Higher-order Møller scattering diagrams

Each vertex contributes the multiplicative factor $\alpha = 1/137$, and so, with each additional vertex, the contribution to the total amplitude is reduced by this factor, and the contribution to the probability is roughly this factor squared.

It should be noted that α is not a constant at short distances (or as seen by probes of higher energy), but increases the nearer the source charge. This occurs because the vacuum, whose lowest energy state is not zero, behaves like a dielectric, producing virtual e^+e^- pairs, which shield a "bare" charge by polarizing the region around it.

The effect is calculated with so-called loop diagrams.

Each loop is an e^+e^- pair, with the appropriate side of the loop drawn to the bare charge. This so-called vacuum polarization partially screens the charge, reducing the field.

At distances less than around the electron Compton wavelength, $\lambda_c = 1/m = 2.43 \times 10^{-10}$ cm, the effective charge increases. Obviously, this isn't what we measure as the unit charge. The effect is seen with high-energy scattering, and is only exhibited on the macroscopic scale by the Lamb shift in atomic spectra.

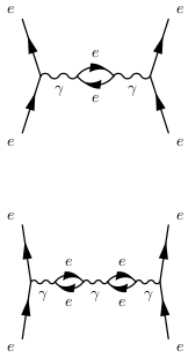

Figure 9.6: Loop diagrams showing virtual pairs

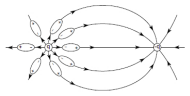

Figure 9.7: Vacuum polarization

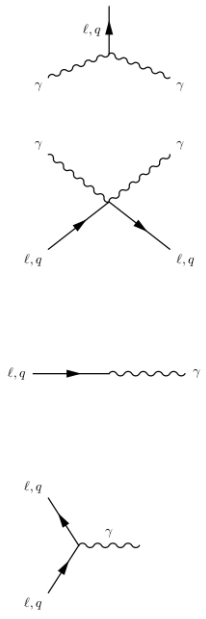

Figure 9.8: Processes forbidden under QED due to violation of one or another conservation law

Note that some diagrams are impossible under electrodynamics:

9.3 Quantum Chromodynamics (QCD)

All strong interactions are reducible to gluon emission or absorption.

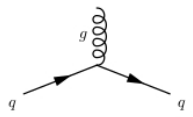

Figure 9.9: An example of a QCD primitive

The basic strong interaction binding two quarks thus is mediated by exchanging gluons.

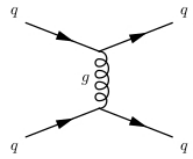

Figure 9.10: Quark binding

While it takes only one number to describe electric charge, it takes three symbols to describe strong charge, referred to as color. At a quark-quark-gluon vertex, the flavor won't change, but the color may. As color is always conserved, the gluon that mediates the change must carry color (unlike the photon, which carries no electric charge).

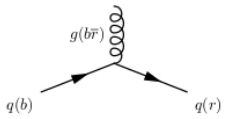

Figure 9.11: Color exchange via a gluon

Gluons carry one color and one anti-color. Given three colors, one might expect 9 combinations, but (think $SU(3)$ and its $n^2 - 1 = 8$ generators) there are only 8.

Since gluons carry color, they, unlike the neutral photon, can couple directly to one another, either three or four at a time. (The symmetry group of QED, $U(1)$, is abelian, while that of QCD, $SU(3)$, is not.)

This obviously makes QCD more complicated than QED, but it's not the only reason. Whereas in QED, each vertex includes a factor of $\alpha = 1/137$, limiting the number of vertices that will contribute to a QED process, the typical QCD vertex includes a factor $\alpha_s > 1$. That is, each additional vertex increases the contribution of a diagram to the sum.

This factor, though, is not a constant, for the same reason that α is not a constant: vacuum polarization. The effect is that α_s is large at the scale of the nucleus, but small at distances less than the size of a proton. This is referred to as asymptotic freedom: at short distances, quarks behave as free particles.

It results from a competition between virtual quark loops and gluon loops (there are no photon loops, since there are no photon-photon interactions), that is, between quark polarization, which increases α_s, and

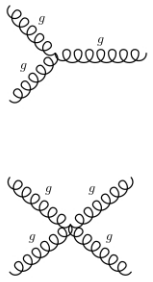

Figure 9.12: Gluon-only vertices

gluon polarization, which decreases it. The outcome depends on the number f of quark flavors versus the number n of colors as

$$a = 2f - 11n \tag{9.5}$$

which equals -21 for 6 flavors and 3 colors. Since $a < 0$, α_s decreases at short distances.

Free quarks and gluons are never seen, they are confined in colorless configurations of mesons (quark-anti-quark pairs) and baryons (quark triplets). Quark confinement and the empirical manifestations of only colorless combinations is more difficult to explain than asymptotic freedom. They are long-range effects, where $\alpha_s > 1$, so perturbation theory and the Feynman method fail. Qualitatively, one assumes that in separating, the quark-gluon potential increase until it exceeds the threshold for the formation of quarks and gluons, and the state chooses the lower energy path: the potential snaps, as it were, and colorless objects form.

9.4 Quantum Flavor Dynamics (Weak Interactions)

The weak interaction, of which there is a neutral version and a charged version, is the only fundamental interaction (ignoring gravity) affecting all fundamental fermions. Weak interactions are reducible to $W^{\pm}$ or Z^0 vector boson emission or absorption.

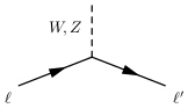

Figure 9.13: Weak interaction primitive

9.4.1 Neutral Currents

Neutral weak processes leave the charges of the interacting particles unchanged. Also unchanged are flavor, baryon number, and lepton numbers. Energy, momentum, and spin may be transferred. Here are some examples of weak neutral processes:

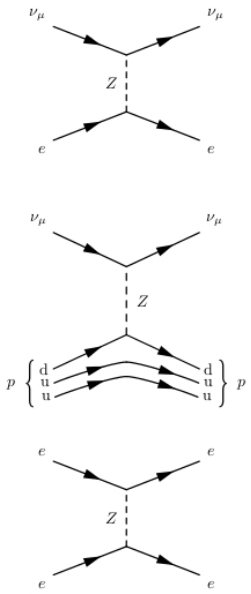

Figure 9.14: Weak neutral processes: Top: electron-neutrino scattering; Middle: proton-neutrino scattering; Bottom: electron-electron scattering

Note that any process mediated by a photon can be mediated by a Z^0 (but not vice versa). Its very small effect on such processes can measured in $e^- + e^+ \rightarrow \mu^- + \mu^+$ Bhabha scattering and parity (mirror symmetry) violation in atomic, electromagnetic processes. Mainly, though, neutral currents are involved in interactions involving neutrino scattering.

9.4.2 Charged Currents

Charged currents alone change flavor; only weak charged interactions produce flavor transformations.

Leptons

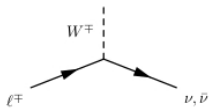

Figure 9.15: A(n) (anti-)lepton transformed into a(n) (anti-)neutrino via $W^\pm$ exchange

When a lepton is converted into a neutrino through the absorption or emission of a W, the family is not changed: the standard model (for now) conserves lepton family.

Neutrino-muon scattering is very unlikely, and expecting to do this experimentally would be foolhardy, but a topological twist of the diagram yields the cleanest charged weak transition, muon decay.

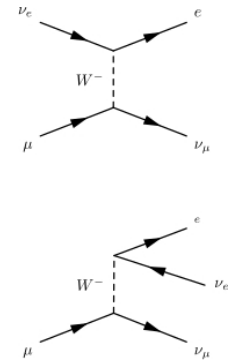

Figure 9.16: Muon transformation into an electron, a muon neutrino, and an electron anti-neutrino

Quarks

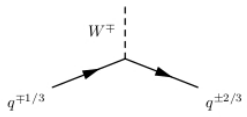

Figure 9.17: Quark flavor transition via $W^\pm$ exchange

A common charged weak transition is the *semileptonic* process in which a d-quark converts to an u-quark with the other vertex being a transition between charged and neutral leptons.

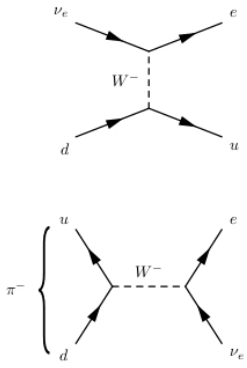

Figure 9.18: Semileptonic transition via $W^\pm$ exchange

The bare quark reaction in the top diagram will never occur due to quark confinement, but charged neutrino scattering off a quarks in a proton or neutron can occur, albeit with quite small probability. On the other hand, pion decay, as diagrammed at the bottom, is common. More common still, for reasons we may get to discuss, is the muon current instead of the electron current. The diagram looks the same.

Another common semileptonic transition is neutron decay. Topologically twisting the neutrino-quark scattering diagram yields a diagram analogous to the muon decay diagram, but some additional (spectator) quarks

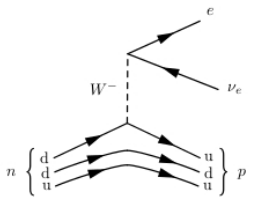

Figure 9.19: Neutron decay via $W^{\pm}$ exchange

Charged weak interactions can also result in purely hadronic transitions, but the rate due to $W^{\pm}$ exchange is overwhelmed by the strong (QCD) process (the strong coupling constant is about 10^{14} times larger than the weak coupling constant [refer to Table 9.4]).

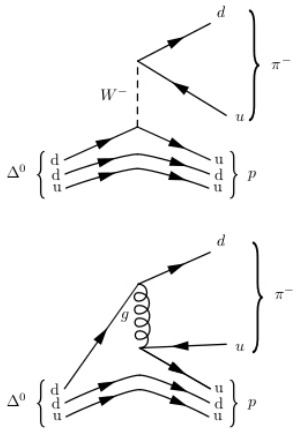

Figure 9.20: Hadronic transitions via weak and strong interactions

While weak charged transitions between quarks, as with leptons, change flavor, such change, unlike that in the leptonic case, may be intergenerational, though they are more likely to stay within family.

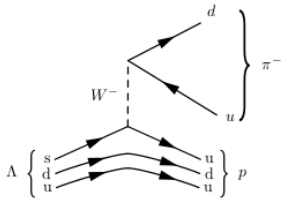

(a) $\Lambda\ (sdu) \rightarrow p\ (udu) + \pi^-$

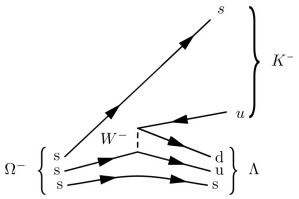

(b) $\Omega^-\ (sss) \rightarrow \Lambda(sdu) + K^-$

Figure 9.21: Weak charge transitions between quarks

How is it that lepton transitions conserve family number, while quark transistions do not? The Standard Model answers this question by postulating that the charged weak interaction couples not to the quarks which couple to the strong interaction (and have mass through the Higgs), but to linear combinations of these, mixed by the Cabibbo-Kobayashi-Maskawa (CKM) matrix:

$$\begin{pmatrix} d' \\ s' \\ b' \end{pmatrix} = \begin{pmatrix} V_{ud} & V_{us} & V_{ub} \\ V_{cd} & V_{cs} & V_{cb} \\ V_{td} & V_{ts} & V_{tb} \end{pmatrix} \begin{pmatrix} d \\ s \\ b \end{pmatrix} \tag{9.6}$$

That is, as far as the weak interaction is concerned, the families are

$$\begin{pmatrix} u \\ d' \end{pmatrix} \quad \begin{pmatrix} c \\ s' \end{pmatrix} \quad \begin{pmatrix} t \\ b' \end{pmatrix} \tag{9.7}$$

rather than

$$\begin{pmatrix} u \\ d \end{pmatrix} \quad \begin{pmatrix} c \\ s \end{pmatrix} \quad \begin{pmatrix} t \\ b \end{pmatrix} \tag{9.8}$$

and 'weak' families are conserved.

The square of the matrix element gives the relative probability of the particular transition occuring. If the CKM matrix were a unit matrix, then $d' = d$, $s' = s$, and $b' = b$, and there'd be no transitions between (strong interaction) families. But, instead, nature has it that the matrix is unitary with (small) off diagonal elements:

$$\begin{pmatrix} 0.97446 & 0.22452 & 0.00365 \\ 0.22438 & 0.97359 & 0.04214 \\ 0.00896 & 0.04133 & 0.999105 \end{pmatrix} \tag{9.9}$$

where uncertanties are in the last two digits.

So, for example, $d' = V_{ud}d + V_{us}s + V_{ub}b = 0.97446d + 0.22452s + 0.00365b$, and, so, of all charged weak transitions involving the up-down' quark family, about 95% will be with the down quark, while about 5% will be with the strange quark, and a little over 0.001% will be with the bottom quark.

9.4.3 Self- and Electromagnetic Couplings

As is the case with gluons, $W^\pm$ and Z^0 couple to themselves and to one another, while $W^\pm$, being charged, also couple to the photon.

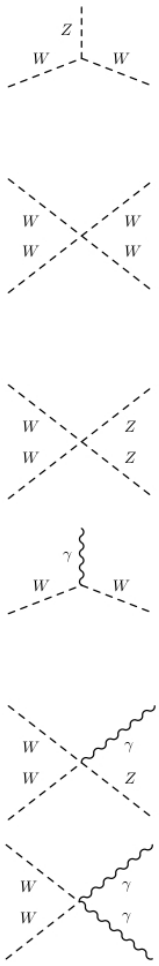

Figure 9.22: Self-coupling among electro-weak mediators

The non-abelian nature of the weak interaction leads to this result, but it's of little consequence empirically, as such contributions are surpressed by multiple orders of weak and electromagnetic coupling.

9.5 Transformations and Conservation Laws

The most universal pattern of particle behavior is that every one of them transforms into some number of other particles unless one or more conservation laws prevents them. Preventing such transitions could be that there are no less massive particles, leaving photons stable, or there are no less massive charged particles, leaving electrons stable. Baryon number conservation, assuming it holds, leaves protons, as the lightest baryon, stable, while lepton number conservation (perhaps) leaves the lightest neutrino stable. Similarly for positrons, anti-protons, and the lightest anti-neutrino.

Thus, aside from a handful of stable particles, everything else in this universe has a finite lifetime. Some are characterized by mean lifetimes, because they may transform in different ways, leading to branching fractions. Calculating lifetimes and branching fractions is one of the primary objectives of particle physics theory.

The different interactions are more or less charactized by these lifetimes, with the strong interaction being associated with the shortest lifetimes, around 10^{-23} s, and the weak interaction being associated with the longest lifetimes, ranging from around 10^{-13} s to 15 min, while the lifetimes associated with electromagnetic interactions are intermediate between these, roughly 10^{-16} s. In practice, particle physicists consider everything but strongly transforming states as stable: their lifetimes can be measured by track length or vertex displacement.

Strong interaction lifetimes are measured indirectly by reconstructing the mass of each state, measuring the spread of the distribution, and using the energy-time uncertainty principle to estimate the lifetime:

$$\tau = \Delta t \geq \frac{\hbar}{2\Delta m} \tag{9.10}$$

Obviously, the shorter the lifetime, the wider the mass distribution.

9.5.1 Conservation Laws

Which conservation laws are obeyed at the primitive vertices (and therefore in the reaction)?

1. Energy (all)
2. Momentum (all)
3. Angular momentum (all)
4. Charge (all)
5. Color (all: strong–zero in, zero out; others do not affect color)
6. Baryon number (all) The total number of quarks + antiquarks is the same before and after each interaction. Baryons (three quarks) have baryon number 1, anti-baryons (three anti-quarks) have baryon number -1, mesons (quark, anti-quark pairs) have baryon number 0, as do all leptons.
7. Lepton number (almost all) Leptons are not affected by the strong interaction, which therefore does not affect lepton number; an electromagnetic interaction changes no flavors; a weak interaction involving leptons has lepton in, lepton out, essentially always (except in the case of neutrinos) in the same family–lepton.
8. Flavor (strong, electromagnetic, and neutral weak only; charged weak changes)
9. OZI [Okubo, Zweig, Iizuka] (relevant only to strong interactions) If initial state particles connect to final-state particles only by gluon lines in a Feynman diagram, the process is suppressed

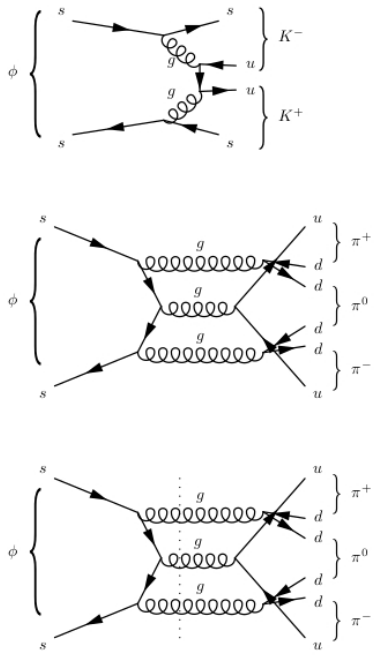

Figure 9.23: An example of OZI suppression: the three-pion modes, though kinematically favorable, are suppressed relative to the two-kaon mode

Chapter 10

Gauge Theories

A gauge theory is a field theory, such as quantum electrodynamics or general relativity, whose Lagrangian is invariant under certain local transformations described by a Lie group, a continuous group whose elements are described by real parameters. The term gauge means a measurement. A general feature of these field theories is that the fundamental fields cannot be measured directly, however, an associated quantity, such as charge, energy, or velocity, can be. In these field theories, different configurations of the unobservable fields may yield identical observable quantities. Transformations between such field configurations are called gauge transformations, and the invariance of the measurable quantities under these transformations is called gauge invariance, sometimes called gauge symmetry, since invariance under transformation is considered a symmetry. Symmetries are described by groups, and the symmetry or gauge group of these symmetries is of the form of a Lie group, associated with which is a Lie algebra of group generators, from which arises a (typically vector) field, called a gauge field. Such fields are included in the Lagrangian to ensure gauge invariance. When quantized, the quantum (quanta) of the field(s) is (are) referred to as a gauge boson.

All the fundamental interactions in nature are described by gauge theories. Consider, first, classical electromagnetism. The indefiniteness of the scalar potential V is what is known as a global gauge symmetry, since no physical effect can be measured by changing the value of V everywhere by the same amount. This global symmetry assures global charge conservation: the total charge in the universe is a constant.

Maxwell noticed that Ampere's Law in differential form,

$$\boldsymbol{\nabla} \times \mathbf{B} = \mathbf{j} \tag{10.1}$$

where $\mathbf{B}$ is the magnetic field, and $\mathbf{j}$ is current per unit area, is not consistent with the continuity equation

$$\boldsymbol{\nabla} \cdot \mathbf{j} = -\frac{\partial \rho}{\partial t} \tag{10.2}$$

when ρ, the charge density, varies in time, since the divergence of a curl vanishes:

$$\boldsymbol{\nabla} \cdot (\boldsymbol{\nabla} \times \mathbf{B}) = 0 = \boldsymbol{\nabla} \cdot \mathbf{j} \tag{10.3}$$

Maxwell's modification of Ampere's Law

$$\boldsymbol{\nabla} \times \mathbf{B} = \mathbf{j} + \frac{\partial \mathbf{E}}{\partial t} \tag{10.4}$$

satisfies the continuity equation due to Gaus's Law.

$$\boldsymbol{\nabla} \cdot \mathbf{E} = \rho \tag{10.5}$$

It further insures local charge conservation since the continuity equation states that net charge can be neither created nor destroyed in an arbitrarily small volume. Converting global charge conservation to local charge conservation required coupling electric and magnetic fields.

Maxwell's introduction of another field into Ampere's Law is equivalent to introducing a vector potential $\mathbf{A}$ to accompany the scalar potential V, whose indefiniteness leads to global charge conservation, in which the electric field is the negative gradient of V. To get local charge conservation, the vector potential $\mathbf{A}$ is related to $\mathbf{B}$,

$$\mathbf{B} = \boldsymbol{\nabla} \times \mathbf{A} \tag{10.6}$$

which leads, from Faraday's equation,

$$\boldsymbol{\nabla} \times \mathbf{E} = -\frac{\partial \mathbf{B}}{\partial t} \tag{10.7}$$

to

$$\mathbf{E} = -\boldsymbol{\nabla} V - \frac{\partial \mathbf{A}}{\partial t} \tag{10.8}$$

This is now a local gauge symmetry, because $\mathbf{A}$ and V do not uniquely determine $\mathbf{E}$ and $\mathbf{B}$. For example, if, for some arbitrary twice-differentiable function f that depends only on position and time, $V \rightarrow V - \frac{\partial f}{\partial t}$, then, if $\mathbf{A} \rightarrow \mathbf{A} + \boldsymbol{\nabla} f$, the electric and magnetic fields remain unchanged. Local gauge invariance results in the equations determining the electric and magnetic fields, the only physical observables, remaining unchanged despite arbitrary, but correlated, changes in $\mathbf{A}$ and V. This correlation is important: V can be locally, not just globally, varied, because a compensating change can be made in A.

Conversely, local invariance forces a relationship between potentials and therefore fields. The field equations can then be derived from Lorentz invariance. This is more or less the approach to developing gauge theories, like those comprising the standard model: A global symmetry is turned into a local symmetry by the addition of one or more new fields, and from the resulting relations the field equations are obtained.

As an aside, this is the origin of general relativity. The addition of the gravitational field turns special relativity's global space-time transformations into local ones.

Quantum mechanically, it is not the indeterminancy of the absolute magnitude of V, but the impossibility of measuring the absolute phase of the wave function that is the global symmetry.

The expectation value $< u >$ of an operator $\hat{U}$, the physical observable, is given by

$$< u >= \int_{-\infty}^{+\infty} \Psi^{\dagger}(\mathbf{x}, t) \hat{U} \Psi(\mathbf{x}, t) d\mathbf{x} \tag{10.9}$$

This is invariant under the global transformation $\Psi(\mathbf{x}, t) \rightarrow e^{i\theta} \Psi(\mathbf{x}, t)$, when θ is a scalar. Local phase invariance requires a phase with space and time dependence, $\theta(\mathbf{x}, t)$. The derivatives in Schrödinger's free-particle equation are not invariant under such a local transformation.

For electromagnetism, the charge would be involved, so to go from global to local invariance means $Q\theta \rightarrow Q\theta(\mathbf{x}, t)$. Again, to preserve electromagnetic fields, introducing A along with V and making correlated gauge transformations on them, will satisfy the Schrödinger equation, which will thus be gauge invariant, but it will no longer be the free-particle equation. Electromagnetic fields will be included.

The Hamiltonian, in terms of $\mathbf{A}$ and V, which leads to the Lorentz force equation of motion

$$\mathbf{F} = Q\mathbf{E} + Q\mathbf{v} \times \mathbf{B} \tag{10.10}$$

is

$$H = \frac{1}{2m}(\mathbf{p} - Q\mathbf{A})^2 + QV \tag{10.11}$$

With the usual prescription for quantum mechanics, the Hamiltonian becomes the Schrödinger equation:

$$\left[\frac{1}{2m}(-i\hbar\boldsymbol{\nabla} - Q\mathbf{A})^2 + QV\right]\Psi(\mathrm{x}.t) = i\hbar\frac{\partial\Psi(\mathbf{x},t)}{\partial t} \tag{10.12}$$

Thus, gauge invariance results from substituting $\boldsymbol{\nabla} - iQ\mathbf{A}$ for $\boldsymbol{\nabla}$ and $\frac{\partial}{\partial t} + \frac{iQV}{\hbar}$ for $\frac{\partial}{\partial t}$ of the free-particle Schrödinger equation. That is, turning the free-particle Schrödinger equation into a local gauge invariant equation containing the electromagnetic field requires inserting $Q\mathbf{A}$ in the spatial derivatives and QV in the time derivative. Very similar derivative substitutions result in the compensating fields of the other gauge theories.

In summary, to set up a gauge theory, identify a global gauge symmetry which can be expressed by a transformation, convert it to a local symmetry by insisting the transformation depend on space and time coordinates and contain something equivalent to a charge, and compensate for the local transformation by adding new fields which can be inserted into the field-free wave equation by a suitable substitution of derivatives.

This works when relativity is incorporated. In quantum electrodynamics, the vector potential $\mathbf{A}$ becomes the wave function of the photon. When, for example, an electron, emits a photon, the phase of its wave function changes. However, when the photon is reabsorbed by the same or a different electron, there is a compensating phase change. The photon emission and absorption correlates the phase changes, maintaining the overall symmetry because the electrons are indistinguishable. This process is directly equivalent in the non-relativistic case to the simultaneous phase and gauge transformations.

Chapter 11

Quantum Electrodynamics

11.1 Non-Relativistic Quantum Mechanics

The position representation of the Schrödinger equation acting on the wave function $\psi(\mathbf{x})$ arises from the subsitutions (with $\hbar = 1$) $E \to i\frac{\partial}{\partial t}$ and $\mathbf{p} \to -i\boldsymbol{\nabla}$ into the classical Hamiltonian.

$$H = \frac{|\mathbf{p}|^2}{2m} + V(\mathbf{x}) \to i\frac{\partial}{\partial t}\psi(\mathbf{x}) = \left(-\frac{|\boldsymbol{\nabla}|^2}{2m} + V(x)\right)\psi(\mathbf{x}) \tag{11.1}$$

Assuming $\psi(\mathbf{x})$ satisfies this equation, the complex conjugate of the entire expression may be multiplied by $\psi(\mathbf{x})$ and subtracted from the original expression multiplied by $\psi^*(\mathbf{x})$:

$$i\left(\psi^*(\mathbf{x})\frac{\partial}{\partial t}\psi(\mathbf{x}) + \psi(\mathbf{x})\frac{\partial}{\partial t}\psi^*(\mathbf{x})\right) = -\frac{1}{2m}\left(\psi^*(\mathbf{x})|\boldsymbol{\nabla}|^2\psi(\mathbf{x}) - \psi(\mathbf{x})|\boldsymbol{\nabla}|^2\psi^*(\mathbf{x})\right) \tag{11.2}$$

which is equivalent to

$$i\frac{\partial}{\partial t}|\psi(\mathbf{x})|^2 = -\frac{1}{2m}\boldsymbol{\nabla}\cdot(\psi^*(\mathbf{x})\boldsymbol{\nabla}\psi(\mathbf{x}) - \psi(\mathbf{x})\boldsymbol{\nabla}\psi^*(\mathbf{x})) \tag{11.3}$$

Comparing this to the continuity equation

$$\frac{\partial}{\partial t}\rho(\mathrm{x}) + \boldsymbol{\nabla}\cdot\mathbf{j}(\mathbf{x}) = 0 \tag{11.4}$$

we can associate

$$|\psi(\mathbf{x})|^2 = \rho(\mathbf{x}) \tag{11.5}$$

and

$$-\frac{i}{2m}(\psi^*(\mathbf{x})\boldsymbol{\nabla}\psi(\mathbf{x}) - \psi(\mathbf{x})\boldsymbol{\nabla}\psi^*(\mathbf{x})) = \mathbf{j}(\mathbf{x}) \tag{11.6}$$

Seeing that the density is positive definite justifies Max Born's statistical interpretation of the wave function, for which he was awarded the Nobel Prize in 1954, to wit, $\psi^*\psi$ is a probability density.

11.2 Relativistic Quantum Mechanics

Following the same procedure, but starting with the relativistic energy-momentum relation

$$p_\mu p^\mu = m^2 = E^2 - |\mathbf{p}|^2 \tag{11.7}$$

instead of the classical Hamiltonian, leads to the Klein-Gordon equation, a quantized version of the relativistic energy-momentum relation:

$$\left(\frac{\partial^2}{\partial t^2} - |\boldsymbol{\nabla}|^2 + m^2\right)\phi(x) = (\partial_\mu \partial^\mu + m^2)\phi(x) \equiv (\Box + m^2)\phi(x) = 0 \tag{11.8}$$

where x is the space-time 4-vector, ϕ a wave function, and $\Box \equiv \partial_\mu \partial^\mu$.

A plane wave solution works for free particles, just as in the non-relativistic case

$$\phi(x) = Ne^{-ip_\mu x^\mu} = Ne^{-i(Et - \mathbf{p}\cdot\mathbf{x})} \tag{11.9}$$

where N is a normalization constant and E and $\mathbf{p}$ satisfy the relativistic energy-momentum relation. But interpretting this in terms of this relation is problematic, for $E = \pm\sqrt{|\mathbf{p}|^2 + m^2}$, and the negative solution can't be ignored, because a quantum system requires a complete set of states, but the positive energy states alone are not complete. The consequence is that energy levels are unbounded from below–there is no ground state–so it seems impossible to offer a sensible physical interpretation.

Moreover, let's, as in the non-relativistic case, take the complex conjugate of Equation 11.8 and multiply it by $\phi(x)$ while multiplying Equation 11.8 by $\phi^*(x)$. But now we have to subtract the two expressions, because the Klein-Gordon equation is second-order in space and time:

$$\frac{\partial}{\partial t}\left[i\left(\phi^* x \frac{\partial \phi(x)}{\partial t} - \phi(x)\frac{\partial \phi^*(x)}{\partial t}\right)\right] + \boldsymbol{\nabla}\cdot[-i(\phi^*(x)\boldsymbol{\nabla}\phi(x) - \phi(x)\boldsymbol{\nabla}\phi^*(x))] = 0 \tag{11.10}$$

Comparing with the continuity equation

$$i\left(\phi^*(x)\frac{\partial \phi(x)}{\partial t} - \phi(x)\frac{\partial \phi^*(x)}{\partial t}\right) = \rho(x) \tag{11.11}$$

and

$$-i(\phi^*(x)\boldsymbol{\nabla}\phi(x) - \phi(x)\boldsymbol{\nabla}\phi^*(x)) = \mathbf{j}(x) \tag{11.12}$$

or, in Lorentz-covariant form

$$\partial_\mu j^\mu(x) = 0 \tag{11.13}$$

where

$$j^\mu = i(\phi^*(x)\partial^\mu\phi(x) - \phi(x)\partial^\mu\phi^*(x) \tag{11.14}$$

Substituting the plane-wave, free-particle solution, Equation 11.9, into Equation 11.14,

$$j^\mu(x) = 2p^\mu|N|^2 \tag{11.15}$$

and, in particular

$$j^0 = \rho(x) = 2E|N|^2 \tag{11.16}$$

which implies that the interpretation of $\rho(x)$ as a probability density fails for negative energy solutions.

11.3 Feynman-Stückelberg Interpretation

Ernst Stückelberg proposed that negative energy modes be considered fields propagating backward in time. This led to a picture of associated particles and antiparticles having equal mass and spin but opposite charge, an ansatz that permitted a perturbation theory of processes involving these fields in the form of diagrams. Richard Feynman independently derived such diagrams in a particle formalism. They are now referred to as Feynman diagrams, in which external lines represent a particle propagating either backward or forward in time.

Rewriting the exponential of Equation 11.9

$$e^{-ip_\mu x^\mu} = e^{-i(-p_\mu)(-x^\mu)} \tag{11.17}$$

suggests that a negative-energy state can be considered a positive-energy state propagating backward in time or a positive anti-state propagating forward in time.

Further, multiplying the current 4-vector, Equation 11.15, by the electron charge, $-e$, allows it to be reinterpretted as an electric current

$$j^\mu(x) = -2ep^\mu|N|^2 = +2e(-p^\mu)|N|^2 \tag{11.18}$$

suggesting that the electric current is conserved in the free-particle plane wave solution for both positive- and negative- energy solutions.

The conserved probability interpretation of the continuity equation doesn't apply in relativistic quantum mechanics, in which particles and anti-particles can be created and annihilated.

11.4 Principle of Least Action

Because known spinless particles, for example, the pi mesons, are both unstable and interact strongly, the practical utility of the Klein-Gordon equation is limited. The principle of least action offers a more rigorous treatment in the context of quantum field theory, in which solutions for $\phi(x)$ include a quantum scalar or pseudoscalar field whose quanta are spinless particles.

Consider the action $S = \int_{t_0}^{t_1} dtL(q, \dot{q})$, where L is the Lagrangian, to be stationary under small, arbitrary changes of the generalized coordinate $q(t)$ at any time t:

$$\delta S = \int_{t_0}^{t_1} dt \left(\frac{\partial L}{\partial q}\delta q + \frac{\partial L}{\partial \dot{q}}\delta \dot{q} \right) = 0 \tag{11.19}$$

Integrating by parts after reordering derivatives

$$\int_{t_0}^{t_1} dt \left[\frac{\partial L}{\partial q} - \frac{d}{dt}\left(\frac{\partial L}{\partial \dot{q}} \right) \right] \delta q = 0 \tag{11.20}$$

Since the variations in q are arbitrary, the result is the Euler-Lagrange equation

$$\frac{\partial L}{\partial q} - \frac{d}{dt}\left(\frac{\partial L}{\partial \dot{q}} \right) = 0 \tag{11.21}$$

In field theory, L is obtained by integrating the Lagrangian density, or simply the Lagrangian, $\mathcal{L}(\phi(x), \partial_\mu\phi(x))$, where $\partial_\mu\phi \equiv \frac{\partial\phi}{\partial x^\mu}$, over four-dimensional space-time, so that the action is a four-dimensional integral, expressible in covariant form

$$\delta S = \int d^4x \left(\frac{\partial \mathcal{L}}{\partial \phi} \delta\phi(x) + \frac{\partial \mathcal{L}}{\partial(\partial_\mu \phi)} \delta\partial_\mu \phi(x) \right) = 0 \tag{11.22}$$

which yields the Euler-Lagrange equation for the field

$$\frac{\partial \mathcal{L}}{\partial \phi} - \partial_\mu \left(\frac{\partial \mathcal{L}}{\partial_\mu \phi} \right) = 0 \tag{11.23}$$

Choosing the Langrangian

$$\mathcal{L} = \frac{1}{2} \partial_\mu \phi \partial^\mu \phi - \frac{1}{2} m^2 \phi^2 \tag{11.24}$$

yields the Klein-Gordon equation.

In non-relativistic quantum mechanics, the physics cannot depend on a complex phase of ϕ. In relativistic quantum mechanics, or field theory, the field can be a real or complex scalar field.

Under an infinitesimal transformation

$$\phi \to \phi + i\alpha T \phi \tag{11.25}$$

where α is the parameter of the change and T is the generator of the group transformation. In the case of an infinitesimal phase change of magnitude α

$$\phi \to e^{i\alpha} \phi = i\alpha\phi \tag{11.26}$$

so $T = 1$.

The invariance of the action gives

$$\begin{aligned} \delta S &= i \int d^4x \left(\frac{\partial \mathcal{L}}{\partial \phi} \alpha\phi + \frac{\partial \mathcal{L}}{\partial(\partial_\mu \phi)} \partial_\mu(\alpha\phi) \right) \\ &= i \int d^4x \partial_\mu \left(\frac{\partial \mathcal{L}}{\partial(\partial_\mu \phi)} \alpha\phi \right) = 0 \end{aligned} \tag{11.27}$$

from which, given that the equality holds for all α,

$$j^\mu = i \left(\frac{\partial \mathcal{L}}{\partial(\partial_\mu \phi)} \phi \right) \tag{11.28}$$

is the conserved quantity Noether's theorem says must be associated with the symmetry of, in this case, phase invariance.

11.5 Perturbation Theory

Let's allow a small interaction affect the free particle

$$H = H_0 + V(\mathbf{x}, t) \tag{11.29}$$

where the unperturbed Hamiltonian, H_0, can be solved exactly

$$H_0\phi_n = E_n\phi_n \tag{11.30}$$

where

$$\int d^3x\phi_n^*(\mathrm{x})\phi_m(\mathrm{x}) = \delta_{nm} \tag{11.31}$$

The time evolution of the system is

$$\psi(\mathrm{x},t) = \sum_n a_n(t)\phi_n(\mathrm{x})e^{-iE_nt} \tag{11.32}$$

From here, one goes through the procedure of applying Schrödinger's equation and turning off the perturbation at large negative and positive times, so that the interaction occurs at a time t, to get the transition amplitude

$$T_{fi} = -i\int d^4x\phi_f^*(x)V(x)\phi_i(x) \tag{11.33}$$

where $\phi_n(x) \equiv \phi_n(\mathbf{x})e^{-iE_nt}$ is the covariant form of the wave function.

11.6 Classical Electrodynamics in Covariant Form

Maxwell's equations

$$\boldsymbol{\nabla}\cdot\mathbf{E} = \rho \tag{11.34}$$

$$\boldsymbol{\nabla}\times\mathbf{B} - \frac{\partial\mathbf{E}}{\partial t} = \mathbf{j} \tag{11.35}$$

$$\boldsymbol{\nabla}\cdot\mathbf{B} = 0 \tag{11.36}$$

$$\boldsymbol{\nabla}\times\mathbf{E} + \frac{\partial\mathbf{B}}{\partial t} = 0 \tag{11.37}$$

Equation 11.36 implies that $\mathbf{B}$ can be written

$$\mathbf{B} = \boldsymbol{\nabla}\times\mathbf{A} \tag{11.38}$$

where $\mathbf{A}$ is a vector potential, from which and Equation 11.37

$$\mathbf{E} = -\boldsymbol{\nabla}V - \frac{\partial\mathbf{A}}{\partial t} \tag{11.39}$$

where V is a scalar potential. Then Equation 11.35 can be written

$$\boldsymbol{\nabla}\times\mathbf{B} - \frac{\partial\mathbf{E}}{\partial t} = [-|\boldsymbol{\nabla}|^2\mathbf{A} + \boldsymbol{\nabla}(\boldsymbol{\nabla}\cdot\mathbf{A})] + \boldsymbol{\nabla}\frac{\partial V}{\partial t} + \frac{\partial^2\mathbf{A}}{\partial t^2} \tag{11.40}$$

from which

$$\Box\mathbf{A} + \boldsymbol{\nabla}\left[\boldsymbol{\nabla}\cdot\mathbf{A} + \frac{\partial V}{\partial t}\right] = \mathbf{j} \tag{11.41}$$

And Equation 11.34 becomes

$$\boldsymbol{\nabla}\cdot\mathbf{E} = -|\boldsymbol{\nabla}|^2\mathbf{V} - \frac{\partial}{\partial t}(\boldsymbol{\nabla}\cdot\mathbf{A}) \tag{11.42}$$

from which, after adding and subtraction $\frac{\partial^2 V}{\partial t^2}$,

$$\Box V - \frac{\partial}{\partial t}\left(\boldsymbol{\nabla}\cdot\mathbf{A} + \frac{\partial V}{\partial t}\right) = \rho \tag{11.43}$$

Defining

$$A^\mu = (V, \mathbf{A}) \tag{11.44}$$
$$j^\mu = (\rho, \mathbf{j}) \tag{11.45}$$

the two inhomogeneous differential equation, Equations 11.41 and 11.43, can be written in covariant form

$$\Box A^\mu - \partial^\mu(\partial_\nu A^\nu) = j^\mu \tag{11.46}$$

or, defining the electromagnetic field tensor

$$F_{\mu\nu} \equiv \partial_\mu A_\nu - \partial_\nu A_\mu \tag{11.47}$$

Equation 11.46 can be compactly written

$$\partial_\mu F^{\mu\nu} = j^\nu \tag{11.48}$$

The elements of $F_{\mu\nu}$ are $\mathbf{E}$ and $\mathbf{B}$, and so it contains all the physical information. Changes in $\mathbf{A}$ or V of the sort

$$A^\mu \to A^\mu + \partial^\mu f(\mathbf{x}, t) \tag{11.49}$$

where f is an arbitrary function of space and time, do not change the physics. Several choices for such a change to A^μ are standard.

The Lorentz condition, $\partial_\nu A^\nu = 0$, for example, gives, for Equation 11.48

$$\Box A^\mu = j^\mu \tag{11.50}$$

This freedom to vary the four-potential A^μ is known as gauge freedom, and the Lorentz condition is also known as the Lorentz gauge. Another gauge is the Coulomb gauge,

$$\boldsymbol{\nabla}\cdot\mathbf{A} = 0 \tag{11.51}$$

11.6.1 Covariant Derivative

For our purposes, a particle interaction with the electromagnetic field can be described as a transformation (known as minimal substitution)

$$p^\mu \to p^\mu + QA^\mu \tag{11.52}$$

Using the standard prescription, the Schrödinger equation becomes

$$\left(\frac{1}{2m}(-i\boldsymbol{\nabla} + Q\mathbf{A})^2 + QV\right)\psi(\mathbf{x},t) = i\frac{\partial\psi(\mathbf{x},t)}{\partial t} \tag{11.53}$$

A gauge transformation, Equation 11.49, should leave the form of Equation 11.53 invariant, which will be the case if the wave function simultaneously transforms

$$\psi(\mathbf{x},t) \to e^{-iQf(\mathbf{x},t)}\psi(\mathbf{x},t) \tag{11.54}$$

a space- and time-dependent, that is, local, phase transformation. Now, the $U(1)$ symmetry group corresponds to the circle group and can be represented by all possible phase transformation. Thus, QED is an (abelian) gauge theory with $U(1)$ group symmetry. As we'll see, the electromagnetic field is the gauge field mediating interactions between charged fermions.

Turning the argument around, requiring that Equation 11.54 leave the Schrödinger equation invariant leads to the minimal substitution, Equation 11.52, which, quantum mechanically, becomes

$$i\partial_\mu \to i\partial_\mu + QA_\mu \equiv iD_\mu \tag{11.55}$$

the covariant derivative.

11.7 Transition Amplitudes

Let's let Q be e, the charge of a proton, and define a potential V

$$V = -ie(\partial_\mu A^\mu + A^\mu\partial_\mu) - e^2A^2 \tag{11.56}$$

This is an operator, so the derivative acts on a wave function, not just on A^μ

$$V\psi = -ie(\partial_\mu A^\mu + A^\mu\partial_\mu)\psi - e^2A^2\psi$$

Since the charge e is small, we neglect the last term and consider the transition amplitude, Equation 11.33,

$$T_{fi} = -i\int d^4x\phi_f^*(x)V(x)\phi_i(x) = i\int d^4x\phi_f^*(x)(ie)(A^\mu\partial_\mu + \partial_\mu A^\mu)\phi_i(x) \tag{11.57}$$

Integrating the second term by parts, allowing the surface integral to vanish, leads to

$$T_{fi} = -i\int d^4x j^\mu_{fi}(x)A_\mu(x) \tag{11.58}$$

where

$$j^\mu_{fi}(x) = -ie[\phi_f^*(x)\partial^\mu\phi_i(x) - (\partial^\mu\phi_f^*(x))\phi_i(x)] \tag{11.59}$$

which appears similar to the Lorentz covariant form of the density-current four-vector, Equation 11.14, except that the wave function and its conjugate are different, the former is the initial state, the latter the final state, so rather than being the density-current four-vector of a system, this is the density-current four-vector of an interaction, in which, for example, the emission or absorption of a photon can affect a particle.

If we want to describe the interaction as between particles, rather than as an interaction between a particle and a general electromagnetic field, we need to identify the field source:

$$\Box A^\mu = j_{fi}^{\mu(2)} \tag{11.60}$$

now the current of the second particle, say, in the Lorentz gauge.

Consistent, then, with a scattering experiment, we consider only plane waves for the initial and final states, in which the incoming and outgoing particles are taken to be free.

$$j_{fi}^{\mu(2)}(x) = -e|N|^2(p_i^{(2)} + p_f^{(2)})^\mu e^{-i(p_i^{(2)} - p_f^{(2)})\cdot x} \tag{11.61}$$

so that

$$A^\mu(x) = -\frac{j_{fi}^{\mu(2)}(x)}{q^2} \tag{11.62}$$

where

$$q^\mu = (p_i^{(2)} - p_f^{(2)})^\mu \tag{11.63}$$

is the momentum transfer.

Thus,

$$\begin{aligned} T_{fi} &= -i\int d^4x j_{fi}^{\mu(1)}(x)\frac{-g_{\mu\nu}}{q^2}j_{fi}^{\mu(2)}(x) \\ &= |N|^4\int d^4x e^{-i(p_i^{(1)} - p_f^{(1)} + p_i^{(2)} - p_f^{(2)}\cdot x}\times \\ &\quad [ie(p_i^{(1)} + p_f^{(1)})^\mu]\frac{-g_{\mu\nu}}{q^2}[ie(p_i^{(2)} + p_f^{(2)})^\nu] \\ &= |N|^4(2\pi)^4\delta^4(p_i^{(1)} + p_i^{(2)} - p_f^{(1)} - p_f^{(2)})[ie(p_i^{(1)} + p_f^{(1)})^\mu]\frac{-g_{\mu\nu}}{q^2}[ie(p_i^{(2)} + p_f^{(2)})^\nu] \end{aligned} \tag{11.64}$$

Note that the $(2\pi)^4\delta^4()$ term, which effectively imposes four-momentum conservation, arises from integrating over the plane wave exponents. Note, too, that the result is completely symmetric with respect to the particles, as should be expected, so the tags are in some sense superfluous.

Define the so-called matrix element

$$-i\mathcal{M} = [ie(p_i^{(1)} + p_f^{(1)})^\mu]\frac{-g_{\mu\nu}}{q^2}[ie(p_i^{(2)} + p_f^{(2)})^\nu] \tag{11.65}$$

so that, in general, the transition amplitude can be written

$$T_{fi} = -i((2\pi)^4\delta^4(p_i^{(1)} + p_i^{(2)} - \sum_j p_j)|N|^4\mathcal{M} \tag{11.66}$$

11.8 The Feynman Calculus

Other than four-momentum conservation, guaranteed by the delta function, and the normalization, to ensure causality, all of the physics is in the matrix element, which contains the currents of the two particles (known as the couplings) and a term representing the magnetic field (which includes a momentum transfer: the difference between initial- and final-state four-momenta of each particle). This suggests the picture of an uncharged object, call it a photon, being emitted by one of the charged particles and absorbed by the other, in the process of which four-momentum is transferred. The term $\frac{-g_{\mu\nu}}{q^2}$ is called the photon propagator. This picture is realized as a Feynman diagram.

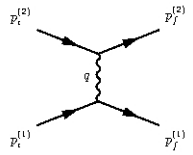

Figure 11.1: Feynman diagram of electrodynamics matrix element

Related to such diagrams is a set of rules (Feynman rules) for translating them into matrix elements.

1. A diagram consists of lines (external and internal) and vertices. The direction (in time) of a line indicates whether it represents a particle (forward, basically left-to-right), anti-particle (backward, basically right-to-left), or propagator (perpendicular, vertical).

2. Each vertex contributes a factor

$$(2\pi)^4\delta^4(\sum_j p_j)[ie(p_i + p_f)^\mu] \tag{11.67}$$

   where the delta function ensures four-momentum conservation at each vertex, p_j are *incoming* four-momenta, the arrows give the directions with respect to time of the four-momentum relative to the vertex in the coupling $e(p_i + p_f)^\mu$. Note that arrow direction is always continuous (in time) along a line.

3. Each internal line is a propagator, whose internal four-momentum transfer q^μ is integrated over. For a photon:

$$\int \frac{d^4q}{(2\pi)^4}\frac{-ig_{\mu\nu}}{q^2} \tag{11.68}$$

   Internal lines indicate virtual or off-shell particles.

4. Each diagram automatically includes $(2\pi)^4$ times a delta function that guarantees four-momentum conservation at each vertex. Integrating over this eliminates one degree of freedom.

5. The matrix element for a given process (for given initial and final states) generally corresponds to multiple diagrams, each contributing a term that needs to be summed.

11.9 Dirac Equation

Recall that the Klein-Gordon equation, $(\Box + m^2)\psi(x) = 0$, is for spin-0 particles. Free spin-1/2 particles are described by the Dirac equation:

$$(i\partial_\mu \gamma^\mu - m)\psi(x) = 0 \tag{11.69}$$

where γ^μ satisfy the anticommutation relation

$$\{\gamma^\mu, \gamma^\nu\} = \gamma^\mu\gamma^\nu + \gamma^\nu\gamma^\mu = 2Ig^{\mu\nu} \tag{11.70}$$

$\psi(x)$ must have four dimensions, represented by a column vector called a bi-spinor,

$$\psi \equiv \begin{pmatrix} \psi_A \\ \psi_B \end{pmatrix} \tag{11.71}$$

The simplest mathematical entity satisfying Equation 11.70 is a 4×4 matrix. Particle physicists typically choose the Björken-Drell convention, which has a 2×2 block formalism

$$\gamma^0 = \begin{pmatrix} 1 & 0 \\ 0 & -1 \end{pmatrix}, \quad \gamma^j = \begin{pmatrix} 0 & \sigma^j \\ -\sigma^j & 0 \end{pmatrix} \tag{11.72}$$

where 1 is the 2×2 identity matrix and σ^j are the Pauli matrices.

Considering a free-particle-at-rest plane wave solution, the Dirac equation can then be rewritten in two forms, one for each bi-spinor:

$$(i\frac{\partial}{\partial t} - m)\psi_A = 0 \tag{11.73}$$

$$(-i\frac{\partial}{\partial t} - m)\psi_B = 0 \tag{11.74}$$

with a positive energy (particle) solution for $\psi_A \propto e^{-imt}$ and a negative energy (anti-particle) solution for $\psi_B \propto e^{+imt}$.

The Pauli matrices are Hermitian: $\sigma^{j\dagger} = \sigma^j$. This implies that $\gamma^{0\dagger} = \gamma^0$ and $\gamma^{j\dagger} = -\gamma^j$. Using this and the anti-commutation relation,

$$\gamma^{\mu\dagger} = \gamma^0\gamma^\mu\gamma^0 \tag{11.75}$$

Taking the Hermitian conjugate of the Dirac equation

$$-i\partial_\mu\psi^\dagger(x)\gamma^{\mu\dagger} - m\psi^\dagger(x) = -i\partial_\mu\psi^\dagger(x)\gamma^0\gamma^\mu\gamma^0 - m\psi^\dagger(x) = 0 \tag{11.76}$$

We then define $\overline{\psi}(x) \equiv \psi^\dagger(x)\gamma^0$ so that multiplying the conjugate Dirac equation from the right by $-\gamma^0$

$$i\partial_\mu\overline{\psi}(x)\gamma^\mu + m\overline{\psi}(x) = 0 \tag{11.77}$$

Now, multiplying the Dirac equation on the left by $\overline{\psi}(x)$ and the conjugate equation on the right by $\psi(x)$, yields a continuity equation

$$i\partial_\mu(\overline{\psi}(x)\gamma^\mu\psi(x)) = 0 \tag{11.78}$$

It's interesting to note that the time component

$$\overline{\psi}(x)\gamma^0\psi(x) = \psi^\dagger(x)\psi(x) \tag{11.79}$$

looks like a solution that satisfies a probability interpretation, which couldn't be found with the Klein-Gordon equation. On the other hand, the antiparticle interpretation remains. Anyway, the continuity equation leads to a definition of a conserved (electric) current:

$$j_\mu = -e\overline{\psi}(x)\gamma_\mu\psi(x) \tag{11.80}$$

11.10 Spin-1/2 Particles

Consider a free-particle plane wave solution to the Dirac equation for non-zero momenta. ψ has four independent degrees of freedom, two for $E > 0$ and two for $E < 0$, where each pair corresponds to different spin states, so the bi-spinor can be separated into two spinors, ψ_A and ψ_B. Then, the plane-wave term is pulled out from two spinors u_A and u_B:

$$\psi(x) = \begin{pmatrix} u_A \\ u_B \end{pmatrix} e^{-ip\cdot x} \tag{11.81}$$

which leads to coupled equations

$$(\boldsymbol{\sigma}\cdot\mathbf{p})u_B = (E-m)u_A \tag{11.82}$$
$$(\boldsymbol{\sigma}\cdot\mathbf{p})u_A = (E+m)u_B \tag{11.83}$$

Looking just at the positive-energy $E > 0$ solutions, identify two independent spinors

$$u_A^{(1)} \equiv \chi^{(1)} = \begin{pmatrix} 1 \\ 0 \end{pmatrix} \quad u_A^{(2)} \equiv \chi^{(2)} = \begin{pmatrix} 0 \\ 1 \end{pmatrix} \tag{11.84}$$

Plugging this into Equation 11.83

$$u_B^{(1,2)} = \frac{(\boldsymbol{\sigma}\cdot\mathbf{p})}{E+m}u_A^{(1,2)} \tag{11.85}$$

And similarly for the negative energy $E < 0$ solutions, for which $u_B^{(1,2)} = \chi^{(1,2)}$, and Equation 11.82

$$u_A^{(1,2)} = \frac{-(\boldsymbol{\sigma}\cdot\mathbf{p})}{-E+m}u_B^{(1,2)} \tag{11.86}$$

The negative signs are there to indicate the physical four-momentum.

When performing calculations, the four solutions tend to be expressed

$$u^{(1)}(p) = N \begin{pmatrix} 1 \\ 0 \\ \frac{p_z}{E+m} \\ \frac{p_x+ip_y}{E+m} \end{pmatrix} \tag{11.87}$$

$$u^{(2)}(p) = N \begin{pmatrix} 0 \\ 1 \\ \frac{p_x-ipy}{E+m} \\ \frac{-p_z}{E+m} \end{pmatrix} \tag{11.88}$$

$$v^{(1)}(p) = u^{(4)}(-p) = N \begin{pmatrix} \frac{p_x-ip_y}{E+m} \\ \frac{-p_z}{E+m} \\ 0 \\ 1 \end{pmatrix} \tag{11.89}$$

$$v^{(2)}(p) = -u^{(3)}(-p) = N \begin{pmatrix} \frac{p_z}{E+m} \\ \frac{p_x+ip_y}{E+m} \\ 1 \\ 0 \end{pmatrix} \tag{11.90}$$

so that for particles

$$\psi(x) = ae^{-ip\cdot x}u \tag{11.91}$$

and for antiparticles

$$\psi(x) = ae^{ip\cdot x}v \tag{11.92}$$

11.10.1 Interacting Spin-1/2 Particles

Again employing the minimal substitution, $p^\mu \to p^\mu + eA^\mu$,

$$(i\partial_\mu\gamma^\mu - m)\psi(x) = (i\frac{\partial}{\partial t}\gamma^0 + i\boldsymbol{\nabla}\cdot\boldsymbol{\gamma} - m)\psi(x) = -eA_\mu\gamma^\mu\psi(x) \tag{11.93}$$

and left-multiplying by γ^0 leads to

$$i\frac{\partial}{\partial t}\psi(x) = (-i\boldsymbol{\nabla}\cdot\gamma^0\boldsymbol{\gamma} + \gamma^0 m)\psi(x) - eA_\mu\gamma^0\gamma^\mu\psi(x) \tag{11.94}$$

Since the right-hand side of this equation has the form $H = H_0 + V$, the term $-eA_\mu\gamma^0\gamma^\mu$ can be identified as the perturbing potential V, so, the transition amplitude is

$$T_{fi} = -i\int d^4x\psi^\dagger x(-eA_\mu\gamma^0\gamma^\mu)\psi_i(x) = -i\int d^4x j^\mu_{fi}(x)A_\mu(x) \tag{11.95}$$

where

$$j^\mu_{fi}(x) = -e\overline{\psi}_f(x)\gamma^\mu\psi_i(x) \tag{11.96}$$

11.10.2 Feynman Rules for Spin-1/2 Particles

1. Each photon propagator introduces the factor

$$\int \frac{d^4q}{(2\pi)^4} \frac{-ig_{\mu\nu}}{q^2} \tag{11.97}$$

while each fermion propagator introduces the factor

$$\int \frac{d^4q}{(2\pi)^4} \frac{i(\not{q} + m)}{q^2 - m^2} \tag{11.98}$$

where, in general, $\not{a} \equiv a_\mu \gamma^\mu$ for any a_μ

2. Each vertex introduces a factor

$$(2\pi)^4 \delta^4(\sum_j p_j) \times ie\gamma^\mu \tag{11.99}$$

where all four-momenta are assumed to point toward the vertex

3. Noting that both fermions and real photons can have external lines (recall that all four-momenta are assumed to point toward the vertex),

	incoming	outgoing
fermions	u	$\bar{u}$
antifermions	$\bar{v}$	v
photons	ε^μ	ε^{μ^*}

4. All contributing diagrams must be summed, but diagrams that differ only by exchanging identical fermions must have opposite signs, to satisfy the Pauli principle that wave function must be fully antisymmetric under the exchange of identical fermions

5. Integration over the delta functions reduce the number of momentum degrees of freedom; the final delta function is disgarding, leaving $-i\mathcal{M}$

11.11 Magnetic Moment of the Electron

Consider the interaction of an electron with an external magnetic field. Non-relativistic quantum mechanics posits an interaction term $\boldsymbol{\mu} \cdot \mathbf{B}$, where $\boldsymbol{\mu}$ is the magnetic moment of the electron, in the total Hamiltonian:

$$\boldsymbol{\mu} = g\mu_B \mathbf{S} \tag{11.100}$$

where $\mu_B = e/2m$ is the Bohr magneton, $\mathbf{S}$ is the spin vector of the electron

$$\mathbf{S} = \frac{1}{2}\boldsymbol{\sigma} \tag{11.101}$$

where $\boldsymbol{\sigma}$ are the Pauli matrices, and g is the Landé factor.

The term in the non-relativistic Hamiltonian can then be written

$$\frac{1}{2}g\mu_B\boldsymbol{\sigma}\cdot\mathbf{B} \tag{11.102}$$

which results, when $\mathbf{B}$ is static and weak, in Zeeman splitting.

Measurements show that $g \approx 2$. In fact, QED predicts the value in agreement with measurement to 9 decimal places.

By adding an electromagnetic field to the Dirac equation through minimal substitution,

$$\boldsymbol{\sigma}\cdot(\mathbf{p}+e\mathbf{A})u_B = (E+eA^0-m)u_A \tag{11.103}$$

$$\boldsymbol{\sigma}\cdot(\mathbf{p}+e\mathbf{A})u_A = (E+eA^0+m)u_B \tag{11.104}$$

And substituting u_B in the second equation for u_B in the first gives:

$$[\boldsymbol{\sigma}\cdot(\mathbf{p}+e\mathbf{A})]^2 u_A = [(E+eA^0)^2 - m^2]u_A \tag{11.105}$$

Noting that $\sigma^k\sigma^l = \delta^{kl} + i\varepsilon^{klm}\sigma^m$, and treating $\mathbf{p}$ as an operator (as it should be), leads to a simplification of the left-hand side of Equation 11.105:

$$\begin{aligned}
[\boldsymbol{\sigma}\cdot(\mathbf{p}+e\mathbf{A})]^2 &= \sigma^k\sigma^l[p^kp^l + e^2A^kA^l + e(p^kA^l + A^kp^l)] \\
&= (\delta^{kl} + i\varepsilon^{klm}\sigma^m)[p^kp^l + e^2A^kA^l + e(p^kA^l + A^kp^l)] \\
&= p^kp^k + e^2A^kA^k + e(p^kA^k + A^kp^k) + i(p^kA^l + A^kp^l)\varepsilon^{klm}\sigma^m \\
&= (\mathbf{p}+e\mathbf{A})^2 + e(\boldsymbol{\nabla}\times\mathbf{A})\cdot\boldsymbol{\sigma} \\
&= (\mathbf{p}+e\mathbf{A})^2 + e\boldsymbol{\sigma}\cdot\mathbf{B}
\end{aligned} \tag{11.106}$$

Taking the right-hand side only to first order (the non-relativistic limit, where $E - m \ll m$ and $A^0 \ll m$),

$$[(\mathbf{p}+e\mathbf{A})^2 + e\boldsymbol{\sigma}\cdot\mathbf{B}]u_A \approx 2m(E+eA^0-m)u_A \tag{11.107}$$

Rearranging into the form of the Schrödinger equation

$$(E-m)u_A = \left[\frac{(\mathbf{p}+e\mathbf{A})^2}{2m} - eA^0 + \frac{e}{2m}\boldsymbol{\sigma}\cdot\mathbf{B}\right]u_A \tag{11.108}$$

Notice that the last term represents the magnetic moment interaction with an external field, but explicitly demonstrating $g = 2$, because of our fudge. In fact, $g \neq 2$. The quantity computed and measured is the so-called anomolous magnetic moment:

$$a_e \equiv \frac{g_e - 2}{2} \tag{11.109}$$

A 1948 calculation due to Schwinger gives the result to first order:

$$a_e = \frac{\alpha}{2\pi} \approx 0.0011614 \tag{11.110}$$

Higher order, perturbative corrections (that is, diagrams with more photon vertices), give

$$a_e = 0.001159652181643(764) \tag{11.111}$$

It is measured at present to be

$$a_e = 0.00115965218073(28) \tag{11.112}$$

QED theory and experiment thus agree to more than 9 significant figures. The magnetic moment of the electron is the most accurately verified prediction in physics.